69-10

DEPARTMENT of OCEANOGRAPHY

SCHOOL of SCIENCE

OREGON STATE UNIVERSITY

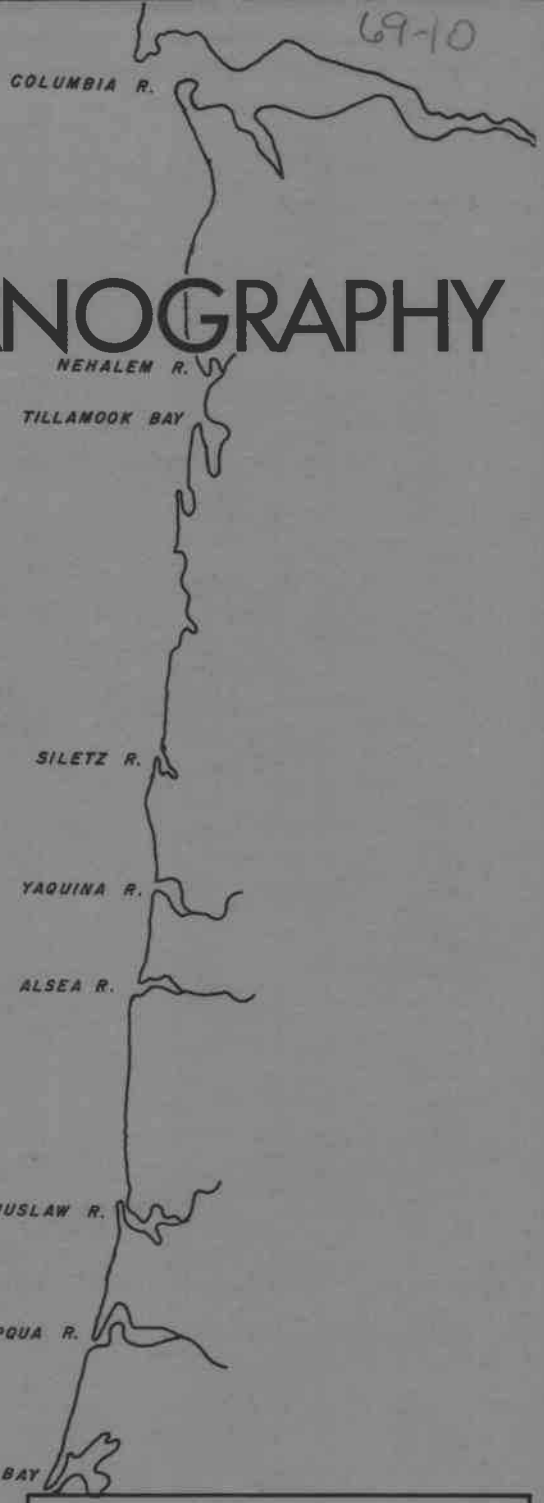

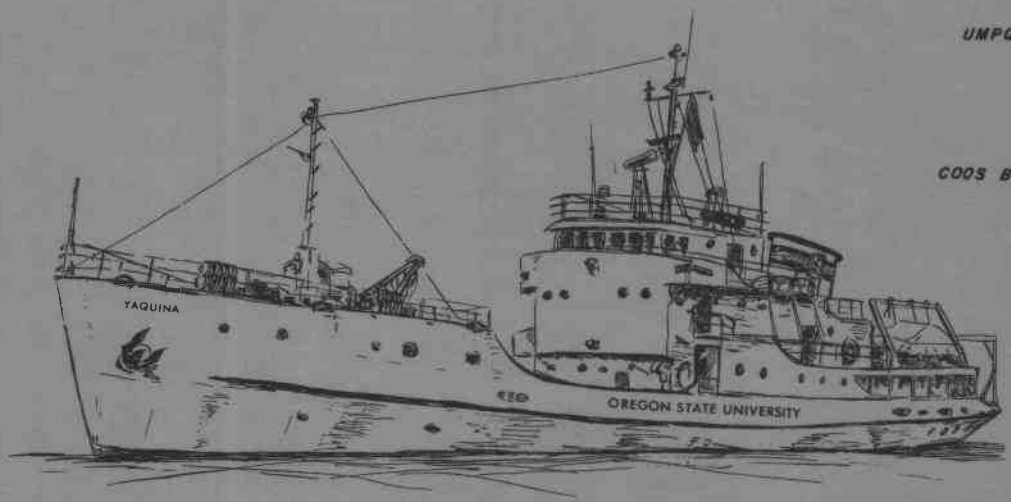

Dynamics of Single Point Ocean Moorings of a Buoy—A Numerical Model for Solution by Computer

A Progress Report
for
Office of Naval Research
Grant No. Nonr 1286(10)

by

John H. Nath
Visiting Associate Professor

Reference 69-10

July 1969

Department of Oceanography
School of Science
Oregon State University
Corvallis, Oregon 97331

DYNAMICS OF SINGLE POINT OCEAN MOORINGS OF A BUOY-- A NUMERICAL MODEL FOR SOLUTION BY COMPUTER

A Progress Report

for

Office of Naval Research
Grant No. Nonr 1286(10)

by

John H. Nath
Visiting Associate Professor

Reference 69-10

John V. Byrne
Chairman

July 1969

ABSTRACT

A numerical model was developed which predicts the dynamic response of a single mooring line and a buoy of forty feet diameter to sinusoidal waves, wind and current in all deep waters. All forces and reactions were considered to be in one plane.

The basic equations for the mooring line motion were obtained by considering a small element of the line in terms of the conservation of momentum and mass and the continuity of the line filament. The resulting partial differential equations were numerically integrated by first a transformation followed by application of the method of characteristics. A non-linear stress-strain diagram was used. The boundary conditions were that no motion occurred at the anchor except rotations and the motion of the upper end of the line was the same as the motion of the attachment point of the buoy.

The buoy was considered to be a rigid body and accelerations were determined from Newton's second law of motion. Recurrence formulas determined displacements and velocities.

A comparison with some prototype information was made. Transfer functions between wave spectra and line tension spectra were available for a mooring in 13,000 feet of water near Bermuda. The same transfer functions were developed with the numerical model and good agreement was achieved.

Frequency response curves for the moored buoy in pitch and heave were also obtained and the results show that one dimensional wave spectra obtained by double integration of the vertical acceleration of the buoy are valid.

ACKNOWLEDGEMENTS

Thanks are due to the Office of Naval Research for the funding of this work while the author was on sabbatical leave from the Department of Civil Engineering, Coloardo State University. Much encouragement and support was given by Mr. Robert Devereux of General Dynamics-Convair Division and the author owes thanks to that company for permission to publish some of the information in this report.

Dr. Wayne Burt and Dr. John Byrne of the Department of Oceanography, Oregon State University, helped significantly in administrative affairs and in providing an intellectual atmosphere which was conducive to the completion of this work.

The computer work was done at General Dynamics-Convair Division, San Diego, California because of the large storage capacity requirements of the program. Mr. Mike Felix and Miss Estelle Neuharth gave invaluable assistance in programming and in the tedious details of submitting runs.

The author also extends his sincere thanks to the cheerful, cooperative and competent assistance given to him by the secretarial force in the Department of Oceanography.

The publication of this report does not constitute approval by the U. S. Navy of the findings or the conclusions contained herein. It is published only for the exchange and stimulation of ideas.

TABLE OF CONTENTS

INTRODUCTION

In recent years oceanographers have attempted to measure various physical parameters of the ocean from moored buoys. Hence, the engineering design of buoys and buoy moorings has become increasingly important. The types of buoys and moorings are considerably varied, but the single large discus buoy with a single line mooring has been used with a high degree of success in deep ocean moorings. This report is about the dynamic response of such deep water single point moorings to ocean waves.

Until recently, the design of deep water moorings was based on a static analysis of the system, taking into account the forces of steady wind, ocean currents and gravity. If waves were considered, it was on a static basis dealing with a single large wave. However, in order to execute an economical engineering design, one needs to be able to predict buoy motion and mooring line motion and tensions as a result of oscillating wave forces.

In the summers of 1967 and 1968, the author conducted a study for the Convair Division of General Dynamics in San Diego, California, in which it was attempted to devise a numerical model of the buoy-mooring system which would predict system response to the dynamic forces of nature. During the 1968-69 academic year the study was continued at Oregon State University with the support of the Office of Naval Research while the author was on sabbatical leave from Colorado State University.

Literature Review

The mooring condition can be properly divided into two problems: 1) one of statics wherein one considers steady wind and current forces, and 2) one of dynamics where one considers the oscillating forces from the waves and the gusty wind. Throughout this report the first problem will be treated lightly as it is well documented by Nath and Felix (9). The foregoing reference shows how the static analysis is based on the work of Morrow and Chang (7). The problem of mooring line statics are also neatly reviewed by Berteaux (1).

Walton and Polachek (17) developed a digital computer solution for the response of an inelastic line in water when the motion of the ends are assumed. The buoy motion was assumed from knowledge of the wave form and the anchor end was assumed to be motionless. The continuous line was idealized to be a few concentrated masses and a matrix representation of the resulting non-linear equations of motion was formed. The line was assumed to be inelastic.

Paquette and Henderson (12) followed a procedure similar to that of Walton and Polachek. They assumed the buoy moved in an elipse which was four times higher than it was wide. The solution was developed for the analog computer. They did consider the line to be elastic, but they did not consider damping within the line. The solution was obtained for both steel and nylon lines but only a few wave forms were analyzed. They did not attempt to calculate frequency response

functions and they used a drag coefficient on the line of 1.8, which is higher than ordinarily used, in order to account for the additional drag due to line flutter. Some of their conclusions were that horizontal motion of the buoy had very little affect on line tension. For small scope, dynamic tension in the steel mooring cable was very serious. The synthetic fibres were not as subject to high dynamic tensions as steel fibres.

In some instances the response of a buoy system to steady state current is calculated, then a factor of safety of five or more is applied to account for dynamic conditions, fouling, fish bite, etc. Various other grossly approximate methods to account for the dynamics of the problem are utilized. One objective of this study is to determine the position of all parts of the mooring line and buoy at all times. Therefore, gross methods are not applicable.

A relatively new approach to the solution of problems dealing with mooring line dynamics was proposed by Wilson and Garbaccio (19). They studied the case of a large ocean vessel moored in deep water and subjected to harmonic waves. Simplifying assumptions were made, one of which was that the mooring line prevented the vessel from drifting, but no other motion of the ship was influenced. It was assumed that the vessel would be larger than 1000 tons. The numerical model was based on the method of characteristics and the boundary conditions were prescribed, or assumed, as follows: the line was assumed to be

tangent to the ocean floor at the anchor and the motion of the upper end of the line was assumed to follow a somewhat elliptical path as prescribed by the ship motion. A pseudo-dynamic solution was also developed wherein only the static solution was used in conjunction with the change in the effective water depth due to the passing of a wave. Fairly good agreement was obtained between both cases, but the magnitude of the water depth was not mentioned and it is felt that although the pseudo-dynamic solution may give reasonable results for relatively small water depths, it will be quite inadequate for large water depths.

An almost completely general approach was presented by Langer (5) for predicting the motions of a catenary in space. The term "catenary," as used in the report, refers to any purely flexible line that can resist tensile stresses only. The governing equations for a line subjected to any forcing systems were developed. However, the structural damping in the line was ignored and this omission was continued by Wilson and Garbaccio.

A new publication on the topic is by Reid (14), where the basic equations are reviewed in detail including important stress-strain relations for the mooring line. A general, three-dimensional vector approach is taken with specifics on the co-planar problem.

Purpose of this Research

The purpose of this research was to develop a numerical model of the dynamic action of a single point mooring of a large oceanographic buoy. In the future it is planned to use this model to study the influence on the system response from any of the important variables, such as scope, water depth and wave length, line type, atmospheric conditions and buoy size, shape and load. The initial goal has been accomplished and, in addition, a small amount of useful data was obtained which compares this work with prototype information.

Purpose and Scope of this Report

The purpose of this report is to document the development of the work which pertains mostly to the dynamic model. That is, not much space will be devoted to the static model. It is hoped that the procedures presented herein will be useful for developing solutions to related problems.

The work used for illustration is limited to considering a forty-feet diameter discus buoy moored with a single nylon line in 13,000 feet of water with an "in-place" scope of 1.31. However, the program has been tested favorably in nearly all water depths and for several scopes. Two programs were developed--one was based on a non-linear stress-strain diagram and did not include the damping factor due to the frictional action within the line, while the other did include the damping, but was based on a linear stress-strain diagram. Initial load stretch was

considered. Transfer functions were developed for the undamped case and compared with those determined from the Bermuda mooring of Buoy Bravo of General Dynamics-Convair (15).

THEORETICAL DEVELOPMENT

The forces of nature were applied to the mooring system in one plane. That is, it was assumed that wind, waves and current were all from the same direction. Consequently, the reaction motion of the mooring system was also in that vertical plane.

The static problem was solved first to determine the initial condition for the boundary value problem in dynamics. A sinusoidal wave was then applied to the system and at zero time the system was released from the static position and allowed to respond to the oscillatory forces. Thus the transitory condition was meaningless. The system was allowed to vibrate until steady state motion existed, when the program stopped. Thus the amplitudes of the steady state system response were obtained and compared with the wave amplitudes in order to determine transfer functions.

Motion of the Mooring Line

Problem in Statics

A set of integral equations were determined, as in Ref. 7, from considering the line to be in static equilibrium. These equations are:

$$T = T_B \exp\left[\int_{\theta_B}^{\theta} \frac{P \sin\theta - G}{P \cos\theta + F}\, d\theta\right] \tag{1}$$

$$s = T_B \int_{\theta_B}^{\theta} \frac{\exp\left[\int_{\theta_B}^{\theta} \frac{P \sin\theta - G}{P \cos\theta + F} \, d\theta\right]}{P \cos\theta + F} \, d\theta \tag{2}$$

$$\zeta = T_B \int_{\theta_B}^{\theta} \frac{\exp\left[\int_{\theta_B}^{\theta} \frac{P \sin\theta - G}{P \cos\theta + F} \, d\theta\right] \sin\theta}{P \cos\theta + F} \, d\theta \tag{3}$$

$$\xi = T_B \int_{\theta_B}^{\theta} \frac{\exp\left[\int_{\theta_B}^{\theta} \frac{P \sin\theta - G}{P \cos\theta + F}\right] \cos\theta}{P \cos\theta + F} \, d\theta \tag{4}$$

Wherein T is the line tension, B is a subscript denoting the bottom or anchor end of the line, θ is the angle the tangent of the line makes with the horizontal, s is the distance along the line from the anchor, ζ is the vertical coordinate of a point on the line from the ocean bottom, ξ is the horizontal coordinate of a point on the line from the anchor, P is the submerged weight of the line per foot, G is the tangential force acting on the line per foot and F represents the normal forces. Fig. (1) shows all the variables involved. The complete development of Eqs. (1) through (4) and the numerical procedures for their solution is given in Ref. 9. The computer program calculates the unstressed length of the line and accommodates large concentrated loads on the line.

The Equations of Dynamics

The equations of motion of the mooring line were developed with the approach taken by Langer (5) and reviewed briefly in Nath and Felix (8). In that development a few points were left unclear and some of them will be discussed here.

Consider a small element of the mooring line as shown in Fig. 2. The complete hydrodynamic forces acting on the line are designated as F and they will be discussed in detail in later sections. Such forces are considered to act only in a perpendicular direction because the longitudinal component of the hydrodynamic forces has a negligible influence on the action of the line. The other two forces acting on the element are the line tension, T, and the submerged weight, $g(\mu-\rho)ds$, where μ is the mass per foot of line and ρ is the mass of displaced water per foot of line. From Newton's second law of motion:

$$\Sigma \text{ Forces} = \frac{d}{dt}(mv) \tag{5}$$

wherein m is the total mass of the element and v is the instantaneous velocity vector of the motion of the element. The mass, m, is equal to $\mu\Delta s$ and will be assumed to be constant. The mass can increase or decrease with time from biological growth or corrosion, but such changes take place over a much longer time period than the periods of concern for wave dynamics. Therefore, Eq. (5) can be written:

$$\Sigma \text{ Forces} = m \frac{dv}{dt} \tag{6}$$

It will be necessary to obtain the perpendicular and parallel components of Eq. (6) and it is useful to note that, along the line:

$$\frac{d}{dt} = \frac{\partial}{\partial t} + v_{//} \frac{\partial}{\partial s} \tag{7}$$

Wherein $v_{//}$ is often the speed of an elastic wave along the line. Thus,

$$\Sigma \text{ Forces} = m \left(\frac{\partial v}{\partial t} + v_{//} \frac{\partial v}{\partial s} \right) \tag{8}$$

It will now be shown by dimensionless representation that the second term within the parentheses is negligible with respect to the first term. Let $v_{//}$ be the celerity of an elastic wave on the line and S_o and T_o be the corresponding wave length and period, and let $v = v_{//} v'$, $t = T_o t'$, $s = S_o s'$, where the prime denotes a dimensionless quantity. Then the part in parentheses of Eq. (8) becomes,

$$v_{//} \left(\frac{\partial v'}{T_o \partial t'} + \frac{v_{//} \partial v'}{s_o \partial s'} \right) \tag{9}$$

or,

$$\frac{v_{//}}{T_o} \left(\frac{\partial v'}{\partial t'} + \frac{\partial v'}{\partial s'} \right) \tag{10}$$

but,

$$\Delta t = o\left(\frac{\Delta s}{v_{//}}\right) \tag{11}$$

thus,

$$\frac{v_{//}}{T_o}\left(v_{//}\ \frac{\partial v'}{\partial s'} + \frac{\partial v'}{\partial s'}\right) \tag{12}$$

and since $v_{//} >> 1$ the second term in the parentheses can be neglected. Thus the required two components of Eq. (8) can be written,

$$\Sigma\,(\text{Forces})_{//} = m\left(\frac{\partial v}{\partial t}\right)_{//} \tag{13}$$

$$\Sigma\,(\text{Forces})_{\perp} = m\left(\frac{\partial v}{\partial t}\right)_{\perp} \tag{14}$$

Wherein the subscript $//$ denotes the parallel, or tangential, direction and $\perp$ denotes the perpendicular, or radial, direction.

The vector components acting on the line can be obtained as follows. Let V be any vector as shown in Fig. 3. Then the following relationships exist:

$$V_{//} = V_x \cos\theta + V_z \sin\theta \tag{15}$$

$$V_{\perp} = V_z \cos\theta - V_x \sin\theta \tag{16}$$

Since V is a vector, $\frac{\partial V}{\partial t}$ is a vector; therefore,

$$\left(\frac{\partial V}{\partial t}\right)_{\parallel} = \left(\frac{\partial V}{\partial t}\right)_x \cos\theta + \left(\frac{\partial V}{\partial t}\right)_z \sin\theta \tag{17}$$

$$\left(\frac{\partial V}{\partial t}\right)_{\parallel} = \frac{\partial V_x}{\partial t} \cos\theta + \frac{\partial V_z}{\partial t} \sin\theta \tag{18}$$

and

$$\left(\frac{\partial V}{\partial t}\right)_{\perp} = \left(\frac{\partial V}{\partial t}\right)_z \cos\theta - \left(\frac{\partial V}{\partial t}\right)_x \sin\theta \tag{19}$$

$$\left(\frac{\partial V}{\partial t}\right)_{\perp} = \frac{\partial V_z}{\partial t} \cos\theta - \frac{\partial V_x}{\partial t} \sin\theta \tag{20}$$

Now, taking the derivative of Eqs. (10, 11),

$$\frac{\partial V_{\parallel}}{\partial t} = \frac{\partial V_x}{\partial t} \cos\theta + \frac{\partial V_z}{\partial t} \sin\theta + (V_z \cos\theta - V_x \sin\theta) \frac{\partial \theta}{\partial t} \tag{21}$$

$$\frac{\partial V_{\perp}}{\partial t} = \frac{\partial V_z}{\partial t} \cos\theta - \frac{\partial V_x}{\partial t} \sin\theta - (V_x \cos\theta + V_z \sin\theta) \frac{\partial \theta}{\partial t} \tag{22}$$

Then by substitution,

$$\frac{\partial V_{\parallel}}{\partial t} = \left(\frac{\partial V}{\partial t}\right)_{\parallel} + V_{\perp} \frac{\partial \theta}{\partial t} \tag{23}$$

$$\frac{\partial V_{\perp}}{\partial t} = \left(\frac{\partial V}{\partial t}\right)_{\perp} - V_{\parallel} \frac{\partial \theta}{\partial t} \tag{24}$$

Similar relations are obtained when the differentiation is performed with respect to s. Thus, by rearrangement,

$$\left(\frac{\partial V}{\partial s}\right)_{\parallel} = \frac{\partial V_{\parallel}}{\partial s} - V_{\perp} \frac{\partial \theta}{\partial s} \tag{25}$$

$$\left(\frac{\partial V}{\partial s}\right)_{\perp} = \frac{\partial V_{\perp}}{\partial s} + V_{\parallel} \frac{\partial \theta}{\partial s} \tag{26}$$

Now, one can substitute any vector for V.

Let ϕ be a potential function such that its derivative along the line represents the rate of change of the unbalanced external forces. Then, substituting for m, the vector sum of Eqs. (13) and (14) can be expressed as,

$$\frac{\partial (\phi + T)}{\partial s} \Delta s = \Delta s \, \mu \frac{\partial v}{\partial t} \tag{27}$$

Then for Eq. (13), reversing,

$$\mu \left(\frac{\partial v}{\partial t}\right)_{\parallel} = \left(\frac{\partial T}{\partial s}\right)_{\parallel} + \left(\frac{\partial \phi}{\partial s}\right)_{\parallel} \tag{28}$$

or,

$$\mu\left(\frac{\partial v_{\parallel}}{\partial t} - v_{\perp} \frac{\partial \theta}{\partial t}\right) = \frac{\partial T_{\parallel}}{\partial s} - T_{\perp} \frac{\partial \theta}{\partial s} + \text{The sum of the external forces per foot in the parallel direction} \tag{29}$$

but T does not have a perpendicular component and the longitudinal forces are assumed to be only those due to gravity. It has been seen in past work that the perpendicular external forces are at least one order of magnitude greater than the longitudinal forces. Then, by rearrangement of Eq. (29),

$$\boxed{\frac{\partial v_{\parallel}}{\partial t} - v_{\perp} \frac{\partial \theta}{\partial t} - \frac{1}{\mu} \frac{\partial T}{\partial s} = -g\left(1 - \frac{1}{s.g.}\right) \sin\theta} \tag{30}$$

Eq. (30) is the equation of motion of the line in the parallel direction, wherein s. g. is the saturated specific gravity of the line. Similarly, the equation of motion in the perpendicular direction is:

$$\mu\left(\frac{\partial v_{\perp}}{\partial t} + v_{\parallel} \frac{\partial \theta}{\partial t}\right) = \frac{\partial T_{\perp}}{\partial s} + T_{\parallel} \frac{\partial \theta}{\partial s} + \text{The sum of the external forces per foot in the perpendicular direction} \tag{31}$$

or,

$$\boxed{\frac{\partial v_{\perp}}{\partial t} + v_{\parallel} \frac{\partial \theta}{\partial t} - \frac{T}{\mu} \frac{\partial \theta}{\partial s} = \frac{F_{\perp}}{\mu} - g \left(1 - \frac{1}{s.g.}\right) \cos\theta} \qquad (32)$$

In Eq. (32), $F_{\perp}$ represents the sum of all the external forces acting on the line in the perpendicular direction, excluding those due to gravity.

The conservation of mass concept supplies an independent equation. Consider a control volume that intersects the line at right angles with two planes a small distance apart, large enough in the transverse dimension so that the flow of the line mass into and out of the control volume takes place only through the two planes. Then the conservation of mass relation can be stated as,

$$\left[\frac{\partial(\mu v)}{\partial s}\right]_{\parallel} + \frac{\partial \mu}{\partial t} = \nu\ (s, t) \qquad (33)$$

wherein ν is the creation or destruction of mass, taken to be zero here. Thus,

$$\left(\mu \frac{\partial v}{\partial s} + v \frac{\partial \mu}{\partial s}\right)_{\parallel} + \frac{\partial \mu}{\partial t} = 0 \qquad (34)$$

By an order of magnitude analysis similar to that applied to Eq. (8), one can show that the second term within the parantheses is negligible with respect to the first term. Using this, plus Eq. (25), we have,

$$\boxed{\frac{\partial v}{\partial s} - v_{\perp} \frac{\partial \theta}{\partial s} + \frac{1}{\mu} \frac{\partial \mu}{\partial t} = 0} \tag{35}$$

The last governing equation is obtained by considering the line to be continuous, with a smooth curvature. From Eq. (16):

$$\left(\frac{\partial v}{\partial s}\right)_{\perp} = \frac{\partial v_z}{\partial s} \cos\theta - \frac{\partial v_x}{\partial s} \sin\theta \tag{36}$$

but, $v_z = \frac{\partial z}{\partial t}$ and $v_x = \frac{\partial x}{\partial t}$, so that

$$\left(\frac{\partial v}{\partial s}\right)_{\perp} = \left[\frac{\partial}{\partial t}\left(\frac{\partial z}{\partial s}\right)\right] \cos\theta - \left[\frac{\partial}{\partial t}\left(\frac{\partial x}{\partial s}\right)\right] \sin\theta \tag{37}$$

and, $\frac{\partial z}{\partial s} = \sin\theta$, $\frac{\partial x}{\partial s} = \cos\theta$, thus,

$$\left(\frac{\partial v}{\partial s}\right)_{\perp} = \cos^2\theta \frac{\partial \theta}{\partial t} + \sin^2\theta \frac{\partial \theta}{\partial t} \tag{38}$$

Then by simplifying Eq. (38) and expanding the lhs,

$$\boxed{\frac{\partial v_{\perp}}{\partial s} + v_{ii} \frac{\partial \theta}{\partial s} - \frac{\partial \theta}{\partial t} = 0} \tag{39}$$

Summarizing, we now have four equations and four dependent variables, $v_{\perp}$, v_{ii} , θ, T and two independent variables, s and t. The line density, μ, is a variable, but it is dependent on the strain, E, and thence the tension, T, as will be shown next.

Referring to Fig. 4, the line density per foot, μ, at some time, t, is related to the initial line density, μ_o, by,

$$\mu = \frac{\mu_o L}{L + \Delta L} \tag{40}$$

or,

$$\mu = \mu_o \left(\frac{1}{1+\varepsilon} \right) \tag{41}$$

wherein, ε is the unit strain.

The part in parentheses can be expanded as a series. Saving the first two and most significant terms,

$$\mu = \mu_o (1 - \varepsilon) \tag{42}$$

and,

$$\frac{\partial \mu}{\partial t} = -\mu_o \frac{\partial \varepsilon}{\partial t} \tag{43}$$

As a mooring line expands and contracts, internal friction from the rubbing of the fibers will dissipate energy so that internal damping of dynamic action will exist. Very little is known about the true mathematical form of such damping except that if the model is as shown in either Fig. 5a or 5b, it is not correct according to Refs. (2) and (16). However, these models are frequently used because of their mathematical simplicity and the results give at least an approximate idea of the influence of damping. For this work it would seem reasonable to use a model similar to Fig. 5b since plastic lines continually deform under a constant load. However, the resulting equations were not convenient to introduce into the foregoing developments, so the model for the firmo-viscous condition of Fig. 5a was adopted, using a hysteretic damping coefficient, as will be explained. Thus the equation for stress in the line becomes (16),

$$\sigma = \sigma(\varepsilon) + q \frac{\partial \varepsilon}{\partial t} \tag{44}$$

wherein σ is the dynamic tension divided by the original cross-sectional area of the line and $\sigma(\varepsilon)$ is the statically loaded non-linear stress-strain diagram, typical of braided or twisted lines, and q is the viscous damping coefficient.

This work was divided into two investigations--one dealing with the internal damping where the problem was considerably simplified by assuming a linear stress- strain diagram and one which ignores the internal damping, but considers the non-linear stress-strain diagram. These approaches are exemplified by Eqs. (45) and (46) and the corresponding stress-strain diagrams are shown in Fig. 6.

Without damping:

$$\sigma = \sigma(\varepsilon) \tag{45}$$

With damping:

$$\sigma = E\varepsilon + q\frac{\partial \varepsilon}{\partial t} \tag{46}$$

wherein E is the modulus of elasticity.

Parallel developments will be presented for the damped and the undamped cases.

Without damping, from the σ-ε diagram constructed of straight line segments:

$$\sigma = \sigma_i + E_i\varepsilon \tag{47}$$

wherein i denotes the segment into which E falls.

Then

$$\frac{\partial \sigma}{\partial t} = E_i \frac{\partial \varepsilon}{\partial t} \tag{48}$$

or,

$$\frac{\partial \varepsilon}{\partial t} = \frac{1}{A E_i} \frac{\partial T}{\partial t} \tag{49}$$

where A is the original cross-sectional area of the line. With damping, from the displaced σ-ε diagram, see Fig. 6:

$$\frac{\partial \sigma}{\partial t} = E \frac{\partial \varepsilon}{\partial t} + q \frac{\partial^2 \varepsilon}{\partial t^2} \tag{50}$$

or,

$$\frac{\partial \varepsilon}{\partial t} = \frac{1}{AE} \frac{\partial T}{\partial t} - \frac{q}{E} \frac{\partial^2 \varepsilon}{\partial t^2} \tag{51}$$

By substitution of Eqs. (51) and (49) into Eq. (43) and thence into Eq. (35), and by assuming that the mass density does not greatly change, i. e. $\mu = \mu_o$, one obtains for the conservation of mass equation (it should be noted that up to this point μ has been treated as a variable and now is considered to be constant):

Without damping - conservation of mass

$$\boxed{\frac{\partial v_{\parallel}}{\partial s} - v_{\perp} \frac{\partial \theta}{\partial s} - \frac{1}{A E_i} \frac{\partial T}{\partial t} = 0} \tag{52}$$

With damping - conservation of mass

$$\frac{\partial v_{\parallel}}{\partial s} - v_{\perp} \frac{\partial \theta}{\partial s} - \frac{1}{AE} \frac{\partial T}{\partial t} = - \frac{q}{E} \frac{\partial^2 \varepsilon}{\partial t^2} \tag{53}$$

It will be convenient to consider the rhs of Eq. (53) as a forcing function by obtaining an estimate of $\partial^2 \varepsilon / \partial t^2$ from past strains.

The forcing function, $F_{\perp}$ (pounds per foot) in Eq. (32) now needs to be determined. The external hydrodynamic force on the line is determined from the Morison equation, which states that the total force is the sum of a drag component and an inertia component. The drag component is proportional to the square of the relative velocity between the water and the line. The inertia component is due to the total effects from the pressure field set up by the accelerating fluid and the effects from the disturbance of the acceleration field set up by the presence of the cylinder. The former is equal to the mass of the displaced fluid times the fluid acceleration and the latter is proportional to the difference in acceleration between the fluid and the cylinder. Thus,

$$F_{\perp} = \frac{C_D D m}{2} V_r \left| V_r \right| + \frac{\pi D^2}{4} m A_w + \frac{C_I \pi D^2}{4} m A_r \tag{54}$$

wherein C_D is a drag coefficient, taken as 1.4 for this work, which includes a consideration for flutter, D is the line diameter, m is the mass density of the water, V_r is the relative velocity, A_w is the acceleration of the water, C_I is an inertia coefficient which is commonly taken as 1.0 for a cylinder and A_r is the relative acceleration.

But, $\rho = \pi D^2 m/4$ and $Dm = 4\rho/\pi D$.

Thus Eq. (54) becomes:

$$F_{\perp} = \frac{2\, C_D\, \rho\, V_r |V_r|}{\pi D} + \rho A_w + C_I \rho A_r \tag{55}$$

Also,

$$V_r = V_z \cos\theta - V_x \sin\theta - v_{\perp} \tag{56}$$

where V_z and V_x are the vertical and horizontal water velocities as functions of x and z, and,

$$A_r = A_z \cos\theta - A_x \sin\theta - \left(\frac{\partial v}{\partial t}\right)_{\perp} \tag{57}$$

Recall that,

$$\left(\frac{\partial v}{\partial t}\right)_{\perp} = \frac{\partial v_{\perp}}{\partial t} + v_{\parallel} \frac{\partial \theta}{\partial t} \tag{24}$$

Now by combining Eqs. (24), (57), (55) and (32), it is seen that,

$$(\mu+C_I\rho)\ \frac{\partial v_\perp}{\partial t} + v_{//}\ \frac{\partial\theta}{\partial t} - T\frac{\partial\theta}{\partial s} = \frac{2C_D\rho}{\pi D}\ V_r|V_r| +$$

$$+ (\rho+C_I\rho)\ (A_z\cos\theta - A_x\sin\theta) - \mu g\ (1 - \frac{1}{s.g.})\cos\theta \qquad (58)$$

Letting $\mu + C_I\rho = M$, Eq. (58) becomes,

Conservation of momentum, perpendicular direction:

$$\frac{\partial v_\perp}{\partial t} + v_{//}\ \frac{\partial\theta}{\partial t} - \frac{T}{M}\ \frac{\partial\theta}{\partial s} = \frac{C_D}{\pi D}\left(\frac{2}{C_I + s.g.}\right) V_r|V_r| +$$

$$+\left(\frac{1+C_I}{s.g.+C_I}\right)(A_z\cos\theta - A_x\sin\theta) - \left(\frac{s.g.-1}{s.g.+1}\right) g\cos\theta \qquad (59)$$

Repeating other governing equations for convenience of reference:

Conservation of momentum, parallel direction:

$$\frac{\partial v_{//}}{\partial t} - v_\perp\ \frac{\partial\theta}{\partial t} - \frac{1}{\mu}\ \frac{\partial T}{\partial s} = -g\ (1 - \frac{1}{s.g.})\sin\theta \qquad (60)$$

Continuity of line filament:

$$\frac{\partial v_\perp}{\partial s} + v_{//}\ \frac{\partial\theta}{\partial s} - \frac{\partial\theta}{\partial t} = 0 \qquad (61)$$

Conservation of mass without damping:

$$\frac{\partial v_{\parallel}}{\partial s} - v_{\perp} \frac{\partial \theta}{\partial s} - \frac{1}{AE_i} \frac{\partial T}{\partial t} = 0 \tag{52}$$

Conservation of mass with damping:

$$\frac{\partial v_{\parallel}}{\partial s} - v_{\perp} \frac{\partial \theta}{\partial s} - \frac{1}{AE} \frac{\partial T}{\partial t} = \frac{q}{E} \frac{\partial^2 \varepsilon}{\partial t^2} \tag{53}$$

Perhaps the reader should be reminded that at this point μ is considered to be constant.

Solution by the Method of Characteristics

Wilson and Garbaccio (19) show that the above set of hyperbolic partial differential equations are quasi-linear because the derivative terms never appear as products. They can be solved, therefore, by the method of characteristics.

There are at least two methods to transform the equations to total differentials for solution, but perhaps that shown by Lister (6) is as easy to follow as any. Since the equations are quasi-linear, useful linear combinations of them can be formed as follows. Multiply Eq. (52) by $+C_{\parallel}$ and add to Eq. (30). The result is,

$$\frac{\partial v_{\parallel}}{\partial t} + C_{\parallel} \frac{\partial v_{\parallel}}{\partial s} - v_{\perp} \frac{\partial \theta}{\partial t} - C_{\parallel} v_{\perp} \frac{\partial \theta}{\partial s} - \frac{C_{\parallel}}{AE_i} \frac{\partial T}{\partial t} -$$

$$- \frac{1}{\mu} \frac{\partial T}{\partial s} = - g \left(1 - \frac{1}{s.g.}\right) \sin\theta \qquad (60)$$

Now, if $C_{\parallel} \mu = AE_i / C_{\parallel}$, then equation (60) can be written,

$$\boxed{\frac{Dv_{\parallel}}{Dt} - v_{\perp} \frac{D\theta}{Dt} - \frac{1}{C_{\parallel} \mu} \frac{DT}{Dt} = -g \left(1 - \frac{1}{s.g.}\right) \sin\theta} \qquad (61)$$

Where,

$$\frac{D}{Dt} = \frac{\partial}{\partial t} + C_{\parallel} \frac{\partial}{\partial s} \qquad (62)$$

$$C_{\parallel} = \left(\frac{AE_i}{\mu}\right)^{1/2} \qquad (63)$$

Eq. (63) is the celerity of a longitudinal elastic wave along the line. Eq. (61) is a total differential equation expressing the activity of the four dependent variables, $v_{\perp}$, $v_{\parallel}$, θ and T, with respect to time along the characteristic curve,

$$\frac{ds}{dt} = +\left(\frac{AE_i}{\mu}\right)^{1/2} \tag{64}$$

A similar total differential equation can be generated by multiplying Eq. (52) by $-C_{II}$ and adding to Eq. (30). The result is:

$$\boxed{\frac{Dv_{II}}{Dt} - v_{\perp}\frac{D\theta}{Dt} + \frac{1}{\mu C_{II}}\frac{DT}{Dt} = -g\left(1-\frac{1}{s.g}\right)\sin\theta} \tag{65}$$

where,

$$\frac{D}{Dt} = \frac{\partial}{\partial t} - C_{II}\frac{\partial}{\partial s} \tag{66}$$

$$C_{II} = \left(\frac{AE_i}{\mu}\right)^{1/2} \tag{63}$$

and

$$\frac{ds}{dt} = -\left(\frac{AE_i}{\mu}\right) \tag{67}$$

The only changes to the above, by considering Eq. (53) instead of (52) would be in Eqs. (61) and (65), such as,

$$\frac{Dv_{\parallel}}{Dt} - v_{\perp} \frac{D\theta}{Dt} - \frac{1}{\mu C_{\parallel}} \frac{DT}{Dt} = -g \left(1 - \frac{1}{s.g.}\right) \sin\theta - \frac{C_{\parallel} q}{E} \frac{\partial^2 \varepsilon}{\partial t^2} \tag{68}$$

and,

$$\frac{Dv_{\parallel}}{Dt} - v_{\perp} \frac{D\theta}{Dt} + \frac{1}{\mu C_{\parallel}} \frac{DT}{Dt} = -g \left(1 - \frac{1}{s.g.}\right) \sin\theta + \frac{C_{\parallel} q}{E} \frac{\partial^2 \varepsilon}{\partial t^2} \tag{69}$$

Now, two additional total differential equations can be formed by multiplying Eq. (39) by $+C_{\perp}$ and $-C_{\perp}$ and adding to Eq. (59), respectively, to obtain,

$$\boxed{\frac{Dv_{\perp}}{Dt} + (v_{\parallel} - C_{\perp}) \frac{D\theta}{Dt} = \text{rhs } 59} \tag{70}$$

where,

$$\frac{D}{Dt} = \frac{\partial}{\partial t} + C_{\perp} \frac{\partial}{\partial s} \tag{71}$$

$$C_{\perp} = \left(\frac{T}{M}\right)^{1/2} \tag{72}$$

and it should be noted that $C_{\perp}$ is the celerity of a transverse wave moving along the line. The solution is executed on the characteristic,

$$\frac{ds}{dt} = + \left(\frac{T}{M}\right)^{1/2} \tag{73}$$

Also,

$$\boxed{\frac{Dv_{\perp}}{Dt} + (v_{\parallel} + C_{\perp}) \frac{D\theta}{Dt} = \text{rhs} \quad 59} \tag{74}$$

where

$$\frac{D}{Dt} = \frac{\partial}{\partial t} - C_{\perp} \frac{\partial}{\partial s} \tag{75}$$

$$C_{\perp} = \left(\frac{T}{M}\right)^{1/2} \tag{72}$$

$$\frac{ds}{dt} = -\left(\frac{T}{M}\right)^{1/2} \tag{76}$$

Fig. 7 shows the s-t plane with which one can visualize the mode of solution, using the fixed time interval procedure with the method of characteristics. The procedure for this work was as follows. Assume that all the unknowns are determined at the s intersection points at some time, t. Then the four slopes of the four characteristic curves, Eqs. (64, 67, 72 and 76) were determined at each grid point and applied at the $t + \Delta t$ grid points. Take point (s, t) for example. The four total differential equations, (61, 65, 70 and 74) are then presented as difference equations and the values of the four dependent variables, $v_{\perp}$, $v_{\parallel}$, θ and T, are determined at the grid intersection point, $(s, t + \Delta t)$.

In the above procedure it is assumed that the characteristic curves can be approximated as straight lines over the interval, Δt. A second order correction can be made to this assumption, but it was found not necessary to do so if Δt was kept sufficiently small.

It should be kept in mind that point s on the line at time t does not represent the same tagged point at $t + \Delta t$. That is, if one were to imagine a painted point on the physical line near point s, then the painted spot will shift with respect to point s on the s-t grid as the line length extends and contract. In this respect the s-t grid is analagous to the Eulerian coordinate system in fluid mechanics. The s-t grid is fixed in space and time and the line moves with respect to the grid. Referring to Fig. 7, grid point (NR, 0) represents the upper end of the line at time 0 and grid point (1, 0) represents the anchor end of the line. The heavy dots near grid NR represent the upper end of the line when the line is shorter than at time 0 and the circles represent the upper end when the line is longer. The computer program that was assembled to accomplish the above calculations took into account the change in line length. The addition or deletion of grid points at the upper end of the line was accomplished.

The boundary and initial conditions were established such that $v_{\parallel}$ and $v_{\perp}$ were always zero at the anchor and were zero at all points on the line at $t=0$. At the anchor the four equations reduce to two, so

that we have a system of two equations and two unknowns. At the top of the line it is specified that the coordinates and velocities must be equal to those of the attachement point of the buoy.

The tension at the top of the line was determined by taking the computed coordinates of point NP and the known coordinates of the attachment point, (from the buoy subroutine) and calculating the residual strain in the end piece. Then the tension was calculated with the aid of either Eq. (46) or (47).

Final Equations for Numerical Solution

The finite differences form of the equations will be shown for the condition without internal damping in the line.

Using Eq. (61) as the example:

$$\frac{\Delta v_{\parallel}}{\Delta t} - v_{\perp} \frac{\Delta \theta}{\Delta t} - \frac{1}{C_{\parallel} \mu} \frac{\Delta T}{\Delta t} = - g \left(1 - \frac{1}{s.g.}\right) \sin\theta \qquad (77)$$

Using the superscript (1) to denote conditions at the present time and the superscript (2) to denote conditions at the end of the next time increment:

$$\frac{v_{\parallel}^{(2)} - v_{\parallel}^{(1)}}{\Delta t} - v_{\perp}^{(1)} \frac{\theta^{(2)} - \theta^{(1)}}{\Delta t} - \frac{1}{C_{\parallel} \mu} \frac{T^{(2)} - T^{(1)}}{\Delta t} =$$

$$= -g \left(1 - \frac{1}{s.g.}\right) \sin\theta^{(1)} \qquad (78)$$

In the second term of the lhs of Eq. (77) $v_\perp$ appears and could be considered as the average value during the time increment. However, non-linearities then appear in the products with the angle, θ. It was felt that if Δt were kept sufficiently small that the value of $v_\perp$ for the present time, or (1) conditions, would give good results. Therefore, matters were simplified in all the total differential equations by using the (1) value of all variables except where they appear in the derivatives. Thus, Eq. (78) becomes:

$$v_{\parallel}^{(2)} - v_\perp^{(1)}\ \theta^{(2)} - \frac{1}{C_{\parallel}\mu}\ T^{(2)} = -\Delta t\ g\left(1 - \frac{1}{s.g.}\right) \sin\theta^{(1)} + \tag{79}$$

$$+ v_{\parallel}^{(1)} - v_\perp^{(1)}\ \theta^{(1)} - \frac{1}{C_{\parallel}\mu}\ T^{(1)}$$

The (1) conditions were interpolated from the grid intersection in the s-t plane. Similar operations were performed on Eqs. (65), (70) and (74). Thus four equations with four unknowns ($v_{\parallel}^{(2)}$, $v_\perp^{(2)}$, $\theta^{(2)}$, $T^{(2)}$) result.

A matrix representation of the equations was made.

$$\begin{bmatrix} 1 & 0 & -v_{\perp}^{(1)} & -\frac{1}{C_{\parallel}\mu} \\ 1 & 0 & -v_{\perp}^{(1)} & +\frac{1}{C_{\parallel}\mu} \\ 0 & 1 & (v_{\parallel}^{(1)} - C_{\perp}) & 0 \\ 0 & 1 & (v_{\parallel}^{(1)} + C_{\perp}) & 0 \end{bmatrix} \begin{bmatrix} v_{\parallel}^{(2)} \\ v_{\perp}^{(2)} \\ \theta^{(2)} \\ T^{(2)} \end{bmatrix} = \begin{bmatrix} f_1 \\ f_2 \\ f_3 \\ f_4 \end{bmatrix} \quad \begin{array}{l} \text{On} \\ \frac{ds}{dt} = \\ \left(\frac{AE}{\mu}\right)^{1/2} \\ -\left(\frac{AE}{\mu}\right)^{1/2} \\ \left(\frac{T}{M}\right)^{1/2} \\ -\left(\frac{T}{M}\right)^{1/2} \end{array} \tag{80}$$

Note that the value of $v_{\perp}^{(1)}$ in the first row is different from the value of $v_{\perp}^{(1)}$ in the second row because they are interpolated to different positions in the s-t plane. That is, one starts from $+ (AE/\mu)^{1/2}$ and the other starts from $- (AE/\mu)^{1/2}$. The forcing equations, f, will be listed below.

$$f_1 = - \Delta t g \left(1 - \frac{1}{s.g.}\right) \sin\theta^{(1)} + v_{\parallel}^{(1)} - v_{\perp}^{(1)} \theta^{(1)} - \frac{1}{C_{\parallel}\mu} T^{(1)} \tag{81}$$

$$f_2 = - \Delta t g \left(1 - \frac{1}{s.g.}\right) \sin\theta^{(1)} + v_{\parallel}^{(1)} - v_{\perp}^{(1)} \theta^{(1)} + \frac{1}{C_{\parallel}\mu} T^{(1)} \tag{82}$$

$$f_3 = \Delta t \left[\frac{C_D}{\pi D}\left(\frac{2}{C_I + s.g.}\right) V_r |V_r| + \left(\frac{1+C_I}{s.g.+C_I}\right)\left(A_z \cos\theta^{(1)} - A_x \sin\theta^{(1)}\right) - \left(\frac{s.g.-1}{s.g.+1}\right) g \cos\theta^{(1)}\right] + v_{\perp}^{(1)} + (v_{\parallel}^{(1)} - C_{\perp}^{(1)})\,\theta^{(1)} \tag{83}$$

$$f_4 = \Delta t\left[\frac{C_D}{\pi D}\left(\frac{2}{C_I+s.g.}\right) V_r|V_r| + \left(\frac{1+C_I}{s.g.+C_I}\right)\left(A_z \cos\theta^{(1)} - A_x \sin\theta^{(1)}\right) - \right.$$
$$\left. - \left(\frac{s.g.-1}{s.g.+1}\right) g \cos\theta^{(1)}\right] + v_\perp^{(1)} + \left(v_{||}^{(1)} + C_\perp^{(1)}\right)\theta^{(1)} \qquad (84)$$

Special consideration was given at the boundaries in accordance with information presented in earlier parts of this report.

Coefficients for the Line

The drag coefficient, C_D, was assumed to have a value of 1.4, which was the value used by Wilson (18). This seems to be a reasonable value, accounting for low Reynolds number and possibly some additional drag due to line strumming. The drag forces acting longitudinally on the line were assumed to be negligible, as was determined with experimentation on the steady current part of the numerical model.

The inertia coefficient, C_I, was taken as 1.0 since the pressure distribution that exists due to the acceleration of the fluid had already been considered.

The saturated mass density of a 1-1/2" diameter dacron or nylon line was estimated to be 0.03 slugs per foot. Thus the saturated specific gravity was 1.23.

Motion of the Buoy

The Equations of Dynamics

The buoy was treated as a rigid body. At a given time, all the forces acting on the buoy were determined. Thence from applying Newton's second law of motion, the translation and rotational accelerations were determined. After having obtained the accelerations, the displacements and velocities at the next time increment were determined from recurrence formulae.

It is not possible at present to predict the pressure distribution on a floating object subjected to waves. It was felt that an approximate approach to representing the forces acting on the buoy would suffice providing the qualifying coefficients involved were evaluated with real information from either a laboratory study or a prototype study. Thus, the forces acting on the buoy were considered to be those from wave pressure (considering hydrostatics and water particle acceleration due to wave motion), viscous drag, added mass effects (water acceleration due to the presence of the buoy), wind drag, gravity and mooring line tension.

It was found necessary to consider three coordinate systems while working with the forces acting on the buoy. The primary coordinate system has been illustrated in Fig. 1. The secondary coordinate system is oriented to the buoy and moves with the buoy. The tertiary coordinate system is one of cylindrical coordinates and describes all points on the buoy in three-dimensional space. All coordinate systems are illustrated in Fig. 8.

Consider Fig. 9 which shows the buoy as a free body diagram with the above forces acting on it. Fig. 10 shows the important dimensions of the buoy. In order to approximate the force distributions as they occur in nature, it was necessary to develop a strip theory technique. For this study, it was decided to divide the buoy into several pie-shaped pieces as shown in Fig. 11. Since it was not known how the hydrodynamic forces were distributed on the surfaces of the buoy, the drag and inertia forces in the z2 direction were assumed to act at the lower chine as shown in Fig. 9. The drag and inertia forces in the x2 direction were assumed to act at a point one-half way from the attachment point to where the water surface intersects the buoy center line. The pressure forces were evaluated by using the Airy wave theory except right near the surface of the water as explained later.

The forces were first computed for the x3, z3 coordinate system and then converted to the secondary system. The forces in Fig. 9 will now be developed in more detail.

In the x2 direction the total drag force was assumed to be primarily dependent on the buoy surface area and was:

$$F_{Dx2} = C_{DRAD} \frac{\pi(40)^2}{4} \rho_T V_{x2} |V_{x2}| \tag{85}$$

wherein ρ_T is the mass density of the water per cubic foot, C_{DRAD} is the drag coefficient of the buoy in the radial direction and V_{x2} is the relative velocity between the water and the buoy, evaluated at the mid-point between the attachment point and the intersection of the water surface with the buoy center line. The water velocity is due to wave action and water current. Also,

$$F_{Ix2} = C_{IRAD} \rho_T \forall_T A_{x2} \tag{86}$$

where C_{IRAD} is the inertia coefficient of the buoy in the radial direction (which should not include an accomodation for the pressure gradient in the fluid), $\forall_T$ is the total submerged volume of the buoy and A_{x2} is the relative acceleration between the water and the buoy, evaluated at the same point as the above relative velocity.

The wind force was calculated as,

$$F_{WIND} = C_{DW} \frac{\rho_a V_{WI} \left| V_{WI} \right|}{2} \tag{87}$$

where C_{DW} is the wind drag coefficient and has dimensions of ft.^{2}, ρ_a is the mass density of the air and V_{WI} is the wind velocity. As a simplification, the velocity of the buoy, or the relative velocity, was ignored.

In the z2 direction, as previously stated, the drag and inertia forces were assumed to act at the lower chine. The drag and inertia forces were calculated for each pie piece and later summed. In order to make the dynamic action of the numerical model match that of an early hydraulic model, it was necessary to adjust not only the drag and inertia coefficients but the basic form of the drag expression itself. It was desired to create a pitch decay curve that had considerably more damping for small magnitudes of pitch than for large magnitudes of pitch. The final expression for drag was thus,

$$F_{Dz2} = C_{DAXL} \frac{\pi(40)^2}{4} \frac{1}{12} \frac{\rho_T}{2} V_{z2} \left| V_{z2} \right|^{-.6} \tag{88}$$

where C_{DAXL} is the drag force in the z2 direction and V_{z2} is the relative velocity between the water and the buoy evaluated at the lower chine. Likewise,

$$F_{Iz2} = C_{IAXL} \rho_T \forall A_{z2} \tag{89}$$

where C_{IAXL} is the inertia coefficient in the axial direction, $\forall$ is the submerged volume of the individual pie piece and A_{z2} is the relative acceleration evaluated at the lower chine. Thus, the equations of motion become:

In the x2 direction:

$$\Sigma \text{ Forces} = \text{Mass} \cdot \text{Acceleration}$$

$$\text{Wt. } \sin\theta + W_{x2} - T_{x2} + \Sigma(\text{Pres. Forces})_{x2} + F_{Dx2} + F_{Ix2} = \frac{Wt}{g} \ddot{x}_2 \tag{90}$$

and,

$$F_{Ix2} = C_{IRAD} \rho_T \forall_T \left[A_{wx} - (\ddot{x}_2 + Z21 \cdot \ddot{\theta})\right] \tag{91}$$

where A_{wx} is the acceleration of the water at the point a distance z21 from the center of gravity. Thus, Eq. 90 becomes:

$$\text{Wt. } \sin\theta + W_{x2} - T_{x2} + \Sigma(\text{Pres. Forces})_{x2} + F_{Dx2} + C_{IRAD} \rho_T \forall_T A_{wx}$$

$$= (\frac{Wt}{g} + C_{IRAD} \rho_T \forall_T) \ddot{x}_2 + C_{IRAD} \rho_T \forall_T z21 \cdot \ddot{\theta} \tag{92}$$

For the numerical program as developed, the last term was inadvertently ignored, but should have small influence.

In the z2 direction:

$$\Sigma \text{Forces} = \text{Mass} \cdot \text{Acceleration}$$

$$\text{Wt.} \cos\theta - W_{z2} - T_{z2} + \Sigma(\text{Pres. Forces})_{z2} + \Sigma F_{Dz2} + \Sigma F_{Iz2} = \frac{Wt}{g} \ddot{z}_2 \tag{93}$$

and

$$F_{Iz2} = C_{IAXL} \rho_T \forall \left[A_{wz} - (\ddot{z}_2 - xCH \cdot \ddot{\theta}) \right] \tag{94}$$

Thus Eq. (93) becomes,

$$\text{Wt} \cos\theta - W_{z2} - T_{z2} + \Sigma(\text{Pres. Forces})_{z2} + \Sigma F_{Dz2} + C_{IAXL} \rho_T \Sigma \forall A_{wz} = (\frac{Wt}{g} + C_{IAXL} \rho_T \Sigma \forall) \ddot{z}_2 - C_{IAXL} \rho_T xCH \ddot{\theta} \Sigma \forall \tag{95}$$

For the numerical program as developed, the last term was inadvertently ignored, but once again, it should have small influence.

For the Summation of Moments:

$$\Sigma \text{Moments abut the c. g.} = \bar{I} \ddot{\theta}$$

$$W_{x2} \cdot z22 - (F_D + F_I)_{x2} \cdot z21 + T_{x2} \cdot z23 + \Sigma(\text{Pres. Forces}) \cdot \text{Mom.Arms} - \Sigma(F_D + F_I)_{z2} \cdot xCH = \bar{I} \ddot{\theta} \tag{96}$$

or,

$$W_{x2} \cdot z22 - F_{Dx2} \cdot z21 + Tx2 \cdot z23 + \Sigma(\text{Pres. Forces}) \cdot \text{Mom. Arm}$$
$$- \Sigma F_{Dz2} \cdot xCH - C_{IRAD} \rho_T \forall_T \left[A_{wx} - (\ddot{x}_2 + z21 \cdot \ddot{\theta})\right] \cdot z21 - C_{IAXL} \rho_T \Sigma$$
$$\Sigma\forall \left[Awz - (\ddot{z}_2 - xCH \cdot \ddot{\theta})\right] xCH = \bar{I}\, \ddot{\theta} \qquad (97)$$

or,

$$W_{x2} \cdot z22 - F_{Dx2} \cdot z21 + T_{x2} \cdot z23 + \Sigma\,(\text{Pres. Forces}) \cdot \text{Mom. Arm}$$
$$- F_{Dx2} \cdot xCH - C_{IRAD} \rho_T \forall_T A_{wx} \cdot z21 - C_{IAxL} \rho_T \Sigma\forall A_{wz} xCH$$
$$= (\bar{I} + C_{IRAD} \rho_T \forall_T z21^2 + C_{IAXL} \rho_T \Sigma\forall xCH^2)\, \ddot{\theta}$$
$$+ C_{IRAD} \rho_T \forall_T \cdot z21 \cdot \ddot{x}_2 - C_{IAXL} \rho_T (\Sigma\forall XCH) \ddot{z}_2 \qquad (98)$$

In Eq. (98) the solidly underlined term was inadvertently deleted from the numerical model. The terms that are underlined with dashed lines were evaluated with the previous values of acceleration from the time increment in question. The three Eqs. (92), (95) and (98) should be solved simultaneously. All the foregoing errors were realized during the writing of this report and will be rectified in the future. However, of utmost importance for any numerical model is how well it matches experimental results. The RESULTS section of this report shows that the match was very good.

Integration of the Equations by Recurrence

The accelerations were obtained in the secondary coordinate system and converted to the primary system. Then the displacements and velocities of the buoy in the primary system were determined for the next time increment by the use of recurrence formulae.

It is necessary to get started properly and for this work it was considered that the acceleration was constant during the first time interval. Thus the displacements, rotations, and velocities for the first time interval were obtained from the basic equations:

At t = o,

$$x_1 = \frac{1}{2} \ddot{x}_o (\Delta t)^2 + x_o \tag{99}$$

$$\dot{x}_1 = x_o \Delta t \tag{100}$$

For time greater than zero, it was assumed for each time increment that the velocity and acceleration was constant during the interval and equal to the average values. Thus

$$x_{s+1} = 2 x_s - x_{s-1} + x_s (\Delta t)^2 \tag{101}$$

$$x_{s+1} = \dot{x}_s + \frac{\Delta t}{2} (3 x_s - x_{s-1}) \tag{102}$$

wherein the subscript s+1 represents the value at the next time increment, s is the present time increment, etc., and x represents any displacement or rotation.

During the time increment, Δt, the water surface changes position as well as the buoy so that a new set of forces act on the buoy. With the new forces, new accelerations are obtained and the work proceeds from one time increment to the next.

Coefficients for the Buoy

The drag coefficient, C_{DRAD}, was given a value of 0.036 for simplicity. This was a value obtained from drag tests on a model buoy in a wave-towing basin. It is realized, however, that the drag on the buoy is due to viscous skin friction drag and bow wave drag and is thus dependent on Reynolds number and Froude number. Therefore, the assumed constant coefficient represents an average value for the likely ranges of relative surface current velocity. A more exact, and variable, value of C_{DRAD} can be easily inserted into the program.

The drag coefficient, C_{DAXL}, was taken to be 9.64 (ft./sec.) as explained further in RESULTS. This is a dimensional drag coefficient because of the unconventional form of the drag expression. It is realized that this is an extremely crude and empirical approach and needs refinement. However, the results show good agreement between the hydraulic model and the numerical model.

The inertia coefficient, C_{IRAD}, was taken to be 0.4. The value was assumed from best judgement. No information exists on experimental determination of this coefficient. There is information on other floating shapes, such as Lewis forms, a cylinder, sphere, etc., but it is known that this coefficient depends a great deal on the shape of the object. Ref. 3, gives some information on two-dimensional forms. Laboratory experimentation is sorely needed to determine the inertia, or added mass, coefficients for floating buoys.

The inertial coefficient, C_{IAXL}, was taken to be 1.4 and was adjusted to help force the pitch drag curve of the numerical model to

agree with the hydraulic model. It is shown in Ref.10, how this inertia coefficient can greatly influence the natural period of the buoy in pitch. This was experienced when experimenting with the value of C_{IAXL}. It is not generally known, however, that the inertia coefficient has a small influence on relative damping. This is also reviewed in Ref.10. As pointed out in Refs.11, and 13, it is most important to adjust any model, whether it be a numerical model or a hydraulic model, so that the natural or resonant frequency of model motion falls into the same position on the modeled wave spectrum as does the prototype condition.

The wind drag coefficient, C_{DW}, was taken to be 100 ft^2, and it was assumed that the center of application of the wind force was 28.2' above the center of gravity, as shown on Fig.9 . This coefficient also needs verification by laboratory experimentation.

Wave Equations

The equations which define the wave activity will now be summarized.

The pressures acting on the buoy were evaluated by using the Airy wave theory except near the surface of the water.

The classically derived expression for the water pressure is,

$$p = \gamma \left[\eta \frac{\cosh kz}{\cosh kh} + (h - z) \right] \tag{103}$$

with

$$\eta = H/2 \sin (kx - wt) \tag{104}$$

where γ is the unit weight of sea water, k is the wave number, $2\pi / \lambda$ with λ the wave length.

Eq. (103) gives erroneous values for pressure for points on the buoy hull near the water surface because as z approaches η, Eq. (103) does not approach zero. Therefore, the pressure was determined arbitrarily from the following equations.

$$p = \gamma (h + \eta - z) \qquad (\eta \geq o,\ z \geq h) \tag{105}$$

$$p = \gamma \left[\eta \frac{\cosh kz}{\cosh kh} + (h - z) \right] \quad (\eta \geq o,\ z < h) \tag{106}$$

$$p = \gamma \left[\eta \frac{\cosh kz}{\cosh kh} + (h - z) \right] \left[1 - \frac{1}{e^{(h+\eta - z)}} \right] \quad (\eta < o) \tag{107}$$

A Stokes finite amplitude wave of third or fifth order could have been used but it was felt that the small increase in accuracy, if any, was not worth the effort. A trochoidal wave was considered but not used because the water particles orbit in directions opposite to those which are observed.

The remaining equations are for the horizontal and vertical water particle velocities and the horizontal and vertical water particle temporal accelerations. It was assumed that effects from convective acceleration could be ignored. The equations, in the above order, are,

$$u = \frac{H}{2} \omega \sin (kx - \omega t) \frac{\cosh kz}{\sinh kh} \tag{108}$$

$$w = - \frac{H}{2} \omega \cos (kx - \omega t) \frac{\sinh kz}{\sinh kh} \tag{109}$$

$$\dot{u} = - \frac{H}{2} \omega^2 \cos (kx - \omega t) \frac{\cosh kz}{\sinh kh} \tag{110}$$

$$\dot{w} = - \frac{H}{2} \omega^2 \sin (kx - \omega t) \frac{\sinh kz}{\sinh kh} \tag{111}$$

RESULTS

Line Motion

Directly after the Conclusions of this report is a sample output from the computer program for the simulated Bermuda mooring discussed later in this section. It was included in order to illustrate the different output formats for the steady state current case and the dynamic wave case. At time 9.83 seconds one can detect an elastic, or longitudinal wave forming in the line as well as a transverse wave.

A listing of the entire program was not included as it is felt that such lengthy listings in publications are of value only to the authors. Instead, fairly detailed flow charts are included which explain the dynamic portion of this work. It was intended to use only a few symbols in the flow charts so that one need not be familiar with notation to be able to follow them.

In Ref. 15 are displayed the results of measurements of mooring line tension and vertical buoy acceleration for a single point mooring of the forty foot diameter ONR buoy in 13,000 feet of water near Bermuda. The vertical accelerations were converted to water surface elevations by double integration and spectra were calculated for the accelerations, the water surface, and the mooring line tension fluctuations.

One case was selected for study and an attempt was made to compare results from the numerical model with the actual measurements, with good results. The November 5, 1966, information was used because a distinct spectrum existed for the line tension at 590 feet and 3590 feet down the line. Experimental transfer functions were determined

for this study by dividing the ordinates of the tension spectra (after the noise level was subtracted out) by the ordinates of the wave spectrum and taking the square root of the result. Fig. 25 shows the result.

Unfortunately, the wind and surface current was not recorded for the selected day, but on October 26 a wind speed of 6. 1 kt. and a surface current of 0. 7 kt. were recorded. The condition used for input to this program were a wind of 11. 8 kt., or 20 fps and a surface current of 2. 9 kt. or 5 fps, with a distribution according to depth as shown in the Sample Output.

Transfer functions were obtained from the numerical model by subjecting the mooring to a number of wave trains, each of a particular frequency. It was intended to continue each wave until steady state dynamic response was achieved. Then, assuming that the range in line tension is linearly related to wave height, the transfer function for the given particular frequency can be obtained by dividing the range in line tension by the wave height.

Figs. 12 through 23 show the results by plotting the water surface at the buoy and the line tensions with respect to time. It can be seen that in most of the cases, steady state response was not truly achieved. The cases were not continued, however, because of lack of funds. The figures also show that more than one frequency existed in the response. The source of this other frequency or frequencies has not as yet been determined. One possible source would be the time required for an elastic wave to traverse the line to the anchor and back. Possible other sources would be the pitch or heave frequencies of the buoy.

The degree of linearity was checked for at least one case -- that for a wave length of 260 feet and heights of 2, 5, 10, and 20 feet. The sparse results as shown in Fig. 24 indicate that linearity in line tension is strongest at the deeper position on the line. This possibility is also indicated in Ref. 15 where the probability density distributions of line tension are more normally distributed with depth.

The comparisons between the prototype spectra and the spectra obtained with the numerical model is shown in Fig. 25. It is felt that the results show good agreement, considering that the prototype system was actually loaded in a three dimensional manner while all the forces in the numerical model are co-planar. Other differences were in the steady state current loading and the fact that the prototype was excited by a truly random wave while the numerical model was excited by a number of discrete wave frequencies, which only works when linearity exists. Besides, the numerical model had not reached truly steady state and it was thus difficult to select the proper tension range. It was felt that a peak tension followed by a minimum was more representative of what the steady state range would be than vice-versa.

Fig. 26 shows a plot of line tension contours on the s-t plane for the same mooring as shown in Fig. 14.

Buoy Motion

Some hydraulic model information exists at General Dynamics-Convair on the decay curves, among other things, of a 1:53.5 scale ratio model. Coefficients and drag expressions were adjusted in the numerical model so that the results matched as shown in Fig. 27. It should be noted that the drag coefficient in the axial direction is dimensional since the drag force in that direction was taken proportional to $V/|V|^{-.6}$. Thus, in the prototype the drag coefficient needs to be 9.64 when one considers Froude modeling.

Fig. 28 shows the decay curve in heave of the 1:53.5 scale ratio model. The decay curves in pitch and in heave were determined for the buoy in the free floating, or unmoored condition.

Fig. 29 shows the response curve in pitch of the unmoored prototype buoy when a 150 kt. wind is suddenly applied to it. The steady state motion of the buoy under such a circumstance is a constant speed, which the program predicted, but was not shown here.

The remainder of the displayed results are for the buoy at the modeled Bermuda mooring. Fig. 30 shows the attitude of the buoy as predicted by the program on the surface of a wave 200 feet long by 20 feet high. The motion appears to be quite realistic.

Frequency response curves for the prototype buoy at the Bermuda mooring in pitch and heave were also constructed. Linearity of pitch and heave with respect to wave height was seen to exist for the 260 feet long wave. Fig. 31 shows that the frequency response curves are quite flat and nearly equal to 1.0 up to a frequency of 0.28. The largest value was 1.05 to 1.07. This indicates that the wave spectra as computed

from the buoy vertical acceleration are probably quite good for wave frequencies below 0.28. Another conclusion indicated by these curves is that the buoy is nearly perfectly a surface follower (although some lag, or phase shift, may exist) for waves longer than 65 feet, and is stable, or motionless, for waves shorter than about 35 feet.

The results obtained from including internal line damping, or structural damping, were inconclusive and erratic. Therefore, they are not included in this report. It is hoped that this topic will be pursued vigorously in the future.

CONCLUSIONS

From the results it can be concluded that the numerical model as developed, without internal line damping, does a reasonable job of modeling the actions of a prototype mooring for both the line and the buoy. However, only sparse data exists from prototype moorings or model studies and it cannot be assumed that the numerical model is good for all ranges of water depths, wave conditions, etc. Primarily, more laboratory information is needed so that the large number of coefficients used can be properly evaluated.

The transfer function generated had good agreement with prototype information.

The influence of internal line damping on the propagation of disturbances down the line should be investigated in the future.

The numerical model is operational and fairly economical to run. Now more sophisticated expressions for the forcing functions can be introduced. However, since coefficients need to be evaluated by experimental methods even with the more sophisticated expressions, it is felt that the influence on the results from the program will be small.

SAMPLE OUTPUT

The following pages are shown in order to illustrate the type of output printed from the program.

DACRON LINE 1.5 INCH DIAMETER SCOPE = 1.33

GR	RHO	CDN	CDT	CDS	WIF	UTEN
32.20	1.990	1.400	.035	.036	48.0	60000.0

VELOCITY GRADE CHANGES	CORRESPONDING DEPTH CHANGES
5.000	0.00
2.925	200.00
2.085	400.00
1.250	800.00
.420	1800.00
0.000	4000.00
0.000	40000.00

STRESS GRADE CHANGES	CORRESPONDING STRAINS
0.0	0.000
408000.0	.190
1630000.0	.280
3060000.0	.330
4900000.0	.380

D	DMU	DP	BD	WI	NS	NP	CRIT	IN PLACE SCOPE
.125	2.440	13100.000	40.000	20.000	1	30	26.2	1.359

SEGMENT LENGTHS IN FEET ARE 17800.0

WEIGHTS, STARTING FROM BOTTOM ARE 0 0
TOTAL DRAG ON BUOY = 1173.3 LB

NO. OF ITERATIONS	BOTTOM ANGLE	SURFACE ANGLE	BOTTOM TENSION	SURFACE TENSION
25	.55875	1.32609	2528.2	4843.0

SEGMENT NO.	INCREMENT NO.	S/STOTAL (IN PLACE)	TEN/UTEN	XI/DP	ZETA/DP
1	1	.0245	.04284	.028009	.018022
1	2	.0498	.04359	.056496	.037400
1	3	.0761	.04440	.085497	.058233
1	4	.1034	.04526	.115051	.080631
1	5	.1318	.04620	.145200	.104718
1	6	.1614	.04720	.175987	.130635
1	7	.1923	.04829	.207463	.158537
1	8	.2247	.04945	.239680	.188604
1	9	.2588	.05071	.272695	.221036
1	10	.2946	.05207	.306574	.256064
1	11	.3324	.05354	.341384	.293949
1	12	.3725	.05513	.377203	.334993
1	13	.4151	.05686	.414117	.379543
1	14	.4604	.05874	.452219	.428001
1	15	.5089	.06078	.491616	.480835
1	16	.5609	.06302	.532427	.538593
1	17	.6169	.06548	.574785	.601922
1	18	.6776	.06818	.618843	.671588
1	19	.7426	.07112	.664184	.747491
1	20	.8082	.07413	.707985	.825149
1	21	.8619	.07663	.742378	.889601
1	22	.8960	.07822	.763163	.930970
1	23	.9153	.07911	.774348	.954715
1	24	.9269	.07965	.780697	.969189
1	25	.9347	.08001	.784718	.979026
1	26	.9401	.08025	.787287	.985814
1	27	.9439	.08042	.788994	.990694
1	28	.9466	.08054	.790148	.994295
1	29	.9489	.08064	.791005	.997627
1	30	.9508	.08073	.791667	.999733

SEGMENT NO.	IN PLACE LENGTH	ON SHORE LENGTH	IN PLACE/ON SHORE	SCOPE
1	17800.0000	15408.0868	1.1552	
TOTAL	16924.0172	15408.0868	1.1552	1.177

T(1, 31) = 4.84296730E+03, TEN(1, 30) = 4.84371699E+03

TSHORES = 14895.347

RADIUS TO UPPER CHINE =	20.000	RADIUS TO LOWER CHINE =	13.070
HEIGHT TO UPPER CHINE =	4.000	HEIGHT TO LOWER CHINE =	0.000
TOTAL DEPTH OF BUOY =	7.500	WEIGHT OF BUOY IN POUNDS =	184609.59
INERTIA COEF. OF BUOY, RAD =	.400	INERTIA COEF. OF BUOY, AXL =	1.400
DRAG COEF. OF BUOY, AXL =	9.640	MOMENT OF INERTIA OF BUOY =	7.50E+05
DENSITY OF LINE, SLUGS/FT. =	.02992	INERTIA COEF. OF LINE, TRNS =	2.000
UNIT WEIGHT OF WATER =	64.000	DENSITY OF WATER, SLUGS/FT. =	.02439
WAVE LENGTH =	260.000	WAVE HEIGHT =	5.000
WAVE FREQUENCY =	.882	WAVE NUMBER =	.02417
PHASE SHIFT =	145.01632	WAVE PERIOD =	7.12277
DENSITY OF AIR, SLUGS/FT.3 =	.0024	DRAG COEF. OF WIND =	100.000
LINE LENGTH IN FEET =	16924.02	WATER DEPTH IN FEET =	12972.06

DS	DELTAT	CEL	SG	A14	A24
564.13	.1927	938.983	1.2269	0.0000	0.0000

TIME = 0.00

SEGMENT NO. 1

POINT NO.	COORDINATES X	Z	ANGLE RADIANS	TENSION	VELOCITIES PARALLEL	PERPENDICULAR
1	0.00	0.00	5.587E-01	2.528E+03	0.	0.
2	478.34	299.06	5.916E-01	2.583E+03	0.	0.
3	946.60	613.67	6.231E-01	2.640E+03	0.	0.
4	1404.72	942.87	6.533E-01	2.700E+03	0.	0.
5	1852.70	1285.75	6.821E-01	2.762E+03	0.	0.
6	2290.59	1641.41	7.097E-01	2.826E+03	0.	0.
7	2718.52	2009.01	7.360E-01	2.893E+03	0.	0.
8	3136.62	2387.74	7.611E-01	2.961E+03	0.	0.
9	3545.09	2776.83	7.850E-01	3.031E+03	0.	0.
10	3944.14	3175.59	8.078E-01	3.103E+03	0.	0.
11	4333.99	3583.35	8.296E-01	3.176E+03	0.	0.
12	4714.87	3999.50	8.504E-01	3.251E+03	0.	0.
13	5087.00	4423.48	8.704E-01	3.327E+03	0.	0.
14	5450.61	4854.80	8.894E-01	3.404E+03	0.	0.
15	5805.93	5292.97	9.074E-01	3.483E+03	0.	0.
16	6153.32	5737.46	9.247E-01	3.562E+03	0.	0.
17	6492.94	6187.91	9.415E-01	3.643E+03	0.	0.
18	6824.99	6643.97	9.571E-01	3.724E+03	0.	0.
19	7149.86	7105.17	9.724E-01	3.807E+03	0.	0.
20	7467.67	7571.26	9.868E-01	3.890E+03	0.	0.
21	7778.69	8041.91	1.001E+00	3.974E+03	0.	0.
22	8083.16	8516.83	1.014E+00	4.059E+03	0.	0.
23	8381.25	8995.78	1.027E+00	4.144E+03	0.	0.
24	8673.17	9478.51	1.039E+00	4.230E+03	0.	0.
25	8959.06	9964.83	1.052E+00	4.317E+03	0.	0.
26	9238.90	10454.67	1.064E+00	4.404E+03	0.	0.
27	9512.65	10947.93	1.078E+00	4.492E+03	0.	0.
28	9779.62	11444.90	1.093E+00	4.581E+03	0.	0.
29	10039.05	11945.84	1.115E+00	4.669E+03	0.	0.
30	10287.36	12452.39	1.155E+00	4.757E+03	0.	0.
31A	10514.98	12968.56	1.155E+00	4.843E+03	0.	0.

TOTAL LINE LENGTH = 16924.02

PITCH ANGLE	ANGULAR VELOCITY	CG COORDINATES X	Z
-6.042E-02	0.	0.00	0.00

ANGLE OF VELOCITY	BUOY VELOCITY	AP COORDINATES X	Z	AP VELOCITY X	Z
0.	0.	10514.98	12968.56	0.	0.

Z3WATR2= 3.49513E+00
TOTAL DISPLACED VOLUME= 2880.9956
SLOPE OF WATER SURF.= .0604 WATER SURFACE= 1.5060E-03

ANGULAR ACCELERATION	CG ACCELERATION X	Z	AP ACCELERATION X	Z
3.847E-02	-1.936E+00	-1.701E+00	-2.101E+00	-1.710E+00

ENDRMDR	SUMRUN	STRESSS	DELSNP	DS	ENDSTR	ESTRAIN	R
5.642E+02	1.692E+04	0.	3.437E+00	5.641E+02	8.998E+01	0.	1.011E-01

TIME = .19

SEGMENT NO. 1

POINT NO.	COORDINATES X	Z	ANGLE RADIANS	TENSION	VELOCITIES PARALLEL	PERPENDICULAR
1	0.00	0.00	5.587E-01	2.528E+03	0.	0.
2	478.36	299.03	5.915E-01	2.583E+03	-3.046E-04	-2.237E-03
3	946.63	613.62	6.231E-01	2.640E+03	-1.513E-03	-1.364E-03
4	1404.77	942.80	6.532E-01	2.700E+03	-2.161E-03	-8.57[illegible]E-
5	1852.76	1285.65	6.821E-01	2.762E+03	-2.365E-03	-6.905E-[illegible]
6	2290.67	1641.30	7.097E-01	2.82[illegible]E+03	-2.250E-03	-8.090E-[illegible]
7	2718.61	2008.88	7.360E-01	2.893E+03	-1.951E-03	-1.127E-03
8	3136.73	2387.59	7.611E-01	2.961E+03	-1.604E-03	-1.529E-[illegible]
9	3545.22	2776.67	7.850E-01	3.031E+03	-1.352E-03	-1.865E-[illegible]
10	3944.29	3175.41	8.078E-01	3.103E+03	-1.340E-03	-1.957E-03
11	4334.15	3583.15	8.296E-01	3.176E+03	-1.711E-03	-1.595E-03
12	4715.04	3999.28	8.504E-01	3.251E+03	-2.612E-03	-5.395E-04
13	5087.19	4423.26	8.703E-01	3.327E+03	-3.285E-03	2.940E-04
14	5450.81	4854.56	8.894E-01	3.404E+03	-1.760E-03	-1.818E-03
15	5806.16	5292.72	9.074E-01	3.483E+03	-1.283E-03	-2.555E-03
16	6153.55	5737.20	9.247E-01	3.562E+03	-3.629E-03	7.601E-04
17	6493.19	6187.63	9.414E-01	3.643E+03	-2.224E-03	-1.433E-03
18	6825.26	6643.68	9.571E-01	3.724E+03	-1.672E-03	-2.340E-03
19	7150.14	7104.87	9.723E-01	3.807E+03	-2.840E-03	-5.877E-04
20	7467.96	7570.96	9.868E-01	3.890E+03	-2.090E-03	-1.902E-03
21	7779.00	8041.60	1.001E+00	3.974E+03	-2.830E-03	-7.346E-04
22	8083.47	8516.52	1.014E+00	4.059E+03	-2.575E-03	-1.658E-05
23	8381.57	8995.46	1.027E+00	4.144E+03	-2.656E-03	2.097E-03
24	8673.50	9478.18	1.039E+00	4.230E+03	-3.035E-03	6.073E-03
25	8959.39	9964.51	1.052E+00	4.317E+03	-2.998E-03	5.805E-03
26	9239.23	10454.34	1.064E+00	4.404E+03	-4.050E-03	1.660E-02
27	9512.96	10947.62	1.078E+00	4.492E+03	-5.711E-03	3.957E-02
28	9779.89	11444.60	1.093E+00	4.581E+03	-1.003E-02	4.065E-02
29	10039.20	11945.61	1.116E+00	4.669E+03	-2.272E-02	7.711E-02
30	10287.11	12452.35	1.153E+00	4.757E+03	-5.485E-02	1.567E-01
31A	10514.94	12968.53	1.153E+00	5.255E+03	-4.656E-01	2.362E-01

TOTAL LINE LENGTH = 16924.11

PITCH ANGLE	ANGULAR VELOCITY	CG COORDINATES X	Z
-5.970E-02	7.414E-03	10514.69	12972.82

ANGLE OF VELOCITY	BUOY VELOCITY	AP COORDINATES X	Z	AP VELOCITY x	Z
3.825E+00	5.221E-01	10514.94	12968.53	-4.049E-01	-3.296E-01

Z3WATR2= 3.10251E+00
TOTAL DISPLACED VOLUME= 2460.4551
SLOPE OF WATER SURF.= .0595 WATER SURFACE= -4.2376E-01

ANGULAR ACCELERATION	CG ACCELERATION X	Z	AP ACCELERATION x	Z
2.885E-02	-1.288E+00	-3.868E+00	-1.412E+00	-3.874E+00

ENDRMOR	SUMRUN	STRESSS	DELSNP	DS	ENDSTR	ESTRAIN	R
5.642E+02	1.692E+04	0.	3.438E+00	5.641E+02	8.941E+01	0.	1.011E-01

TIME = 9.83

SEGMENT NO. 1

POINT NO.	COORDINATES X	Z	ANGLE RADIANS	TENSION	VELOCITIES PARALLEL	PERPENDICULAR
1	0.00	0.00	5.560E-01	2.532E+03	0.	0.
2	479.17	297.73	5.890E-01	2.587E+03	-1.573E-02	-8.129E-03
3	948.24	611.13	6.206E-01	2.644E+03	-2.826E-02	-1.460E-02
4	1407.18	939.19	6.509E-01	2.704E+03	-3.926E-02	-1.962E-02
5	1855.98	1280.99	6.798E-01	2.766E+03	-4.748E-02	-2.292E-02
6	2294.72	1635.61	7.074E-01	2.830E+03	-5.096E-02	-2.461E-02
7	2723.50	2002.21	7.337E-01	2.897E+03	-4.699E-02	-2.503E-02
8	3142.47	2379.98	7.589E-01	2.966E+03	-3.256E-02	-2.452E-02
9	3551.80	2768.18	7.829E-01	3.037E+03	-5.268E-03	-2.329E-02
10	3951.68	3166.09	8.059E-01	3.110E+03	3.555E-02	-2.154E-02
11	4342.34	3573.08	8.278E-01	3.185E+03	8.828E-02	-1.933E-02
12	4723.99	3988.52	8.487E-01	3.261E+03	1.503E-01	-1.647E-02
13	5096.88	4411.84	8.686E-01	3.340E+03	2.214E-01	-1.277E-02
14	5461.25	4842.51	8.877E-01	3.419E+03	3.085E-01	-8.289E-03
15	5817.35	5280.05	9.059E-01	3.501E+03	4.276E-01	-2.968E-03
16	6165.42	5724.00	9.233E-01	3.586E+03	5.999E-01	4.527E-03
17	6505.70	6173.95	9.400E-01	3.673E+03	8.403E-01	1.649E-02
18	6838.44	6629.51	9.559E-01	3.763E+03	1.142E+00	3.398E-02
19	7163.86	7090.32	9.712E-01	3.854E+03	1.464E+00	5.550E-02
20	7482.19	7556.06	9.859E-01	3.945E+03	1.735E+00	7.828E-02
21	7793.65	8026.42	1.000E+00	4.033E+03	1.862E+00	1.005E-01
22	8098.45	8501.13	1.014E+00	4.115E+03	1.768E+00	1.222E-01
23	8396.78	8979.92	1.027E+00	4.190E+03	1.414E+00	1.432E-01
24	8688.82	9462.59	1.040E+00	4.260E+03	8.327E-01	1.229E-01
25	8974.62	9948.96	1.052E+00	4.327E+03	1.317E-01	8.278E-02
26	9254.15	10438.97	1.065E+00	4.396E+03	-5.177E-01	-2.182E-03
27	9527.45	10932.49	1.077E+00	4.473E+03	-9.170E-01	-1.951E-01
28	9794.92	11429.18	1.087E+00	4.562E+03	-8.920E-01	-7.106E-01
29	10057.39	11928.54	1.095E+00	4.666E+03	-3.478E-01	-1.469E+00
30	10316.01	12429.90	1.087E+00	4.785E+03	6.999E-01	4.342E-01
31A	10509.14	12967.02	1.087E+00	4.948E+03	8.292E-01	2.337E+00

TOTAL LINE LENGTH = 16930.67

PITCH ANGLE	ANGULAR VELOCITY	CG COORDINATES X	Z
4.490E-02	3.806E-02	10509.34	12971.32

ANGLE OF VELOCITY	BUOY VELOCITY	AP COORDINATES X	Z	AP VELOCITY X	Z
2.317E+00	2.480E+00	10509.14	12967.02	-1.684E+00	1.821E+00

Z3WATR2= 3.59126E+00
TOTAL DISPLACED VOLUME= 3053.1992
SLOPE OF WATER SURF.= -.0493 WATER SURFACE= -1.4423E+00

ANGULAR ACCELERATION	CG ACCELERATION X	Z	AP ACCELERATION X	Z
-3.508E-02	1.150E+00	1.221E+00	1.300E+00	1.217E+00

ENDRMDR	SUMRUN	STRESSS	DELSNP	DS	ENDSTR	ESTRAIN	R
5.713E+02	1.693E+04	0.	3.451E+00	5.641E+02	8.918E+01	0.	1.002E-01

FLOW CHARTS

The flow charts that appear on the following pages were constructed almost completely with phrases instead of symbols. The purpose was to present the form of the computer program as clearly as possible.

DRIVING PROGRAM

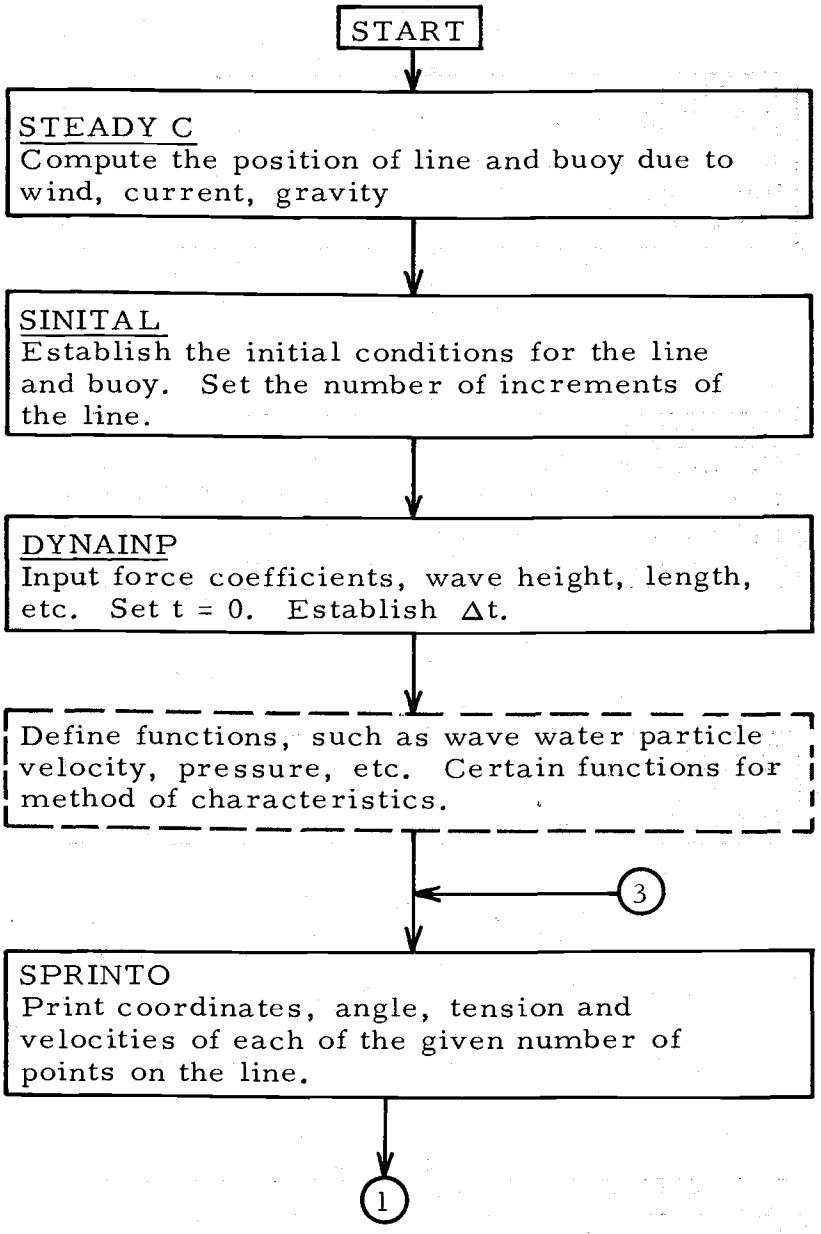

DRIVING PROGRAM - CONT.

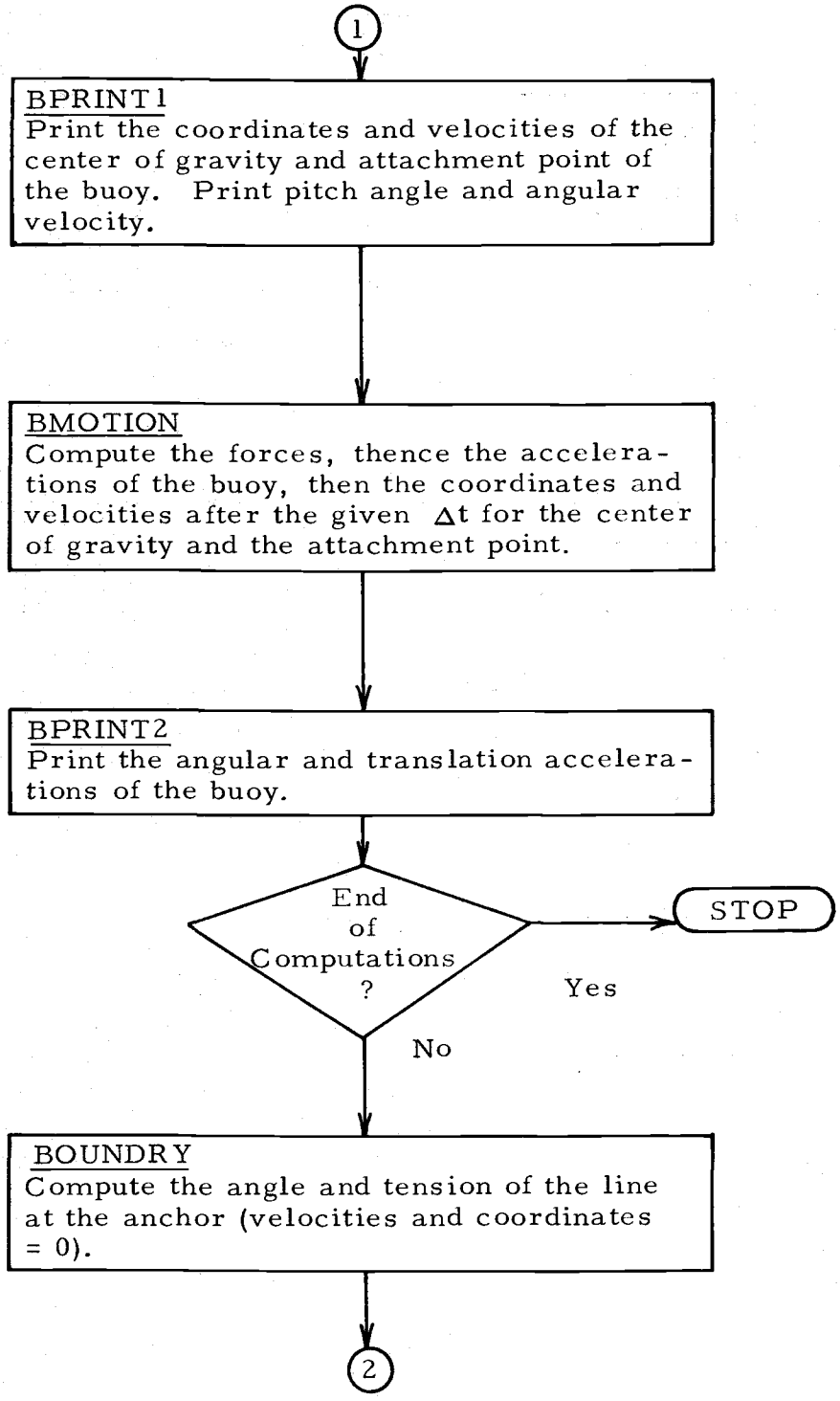

DRIVING PROGRAM - CONT.

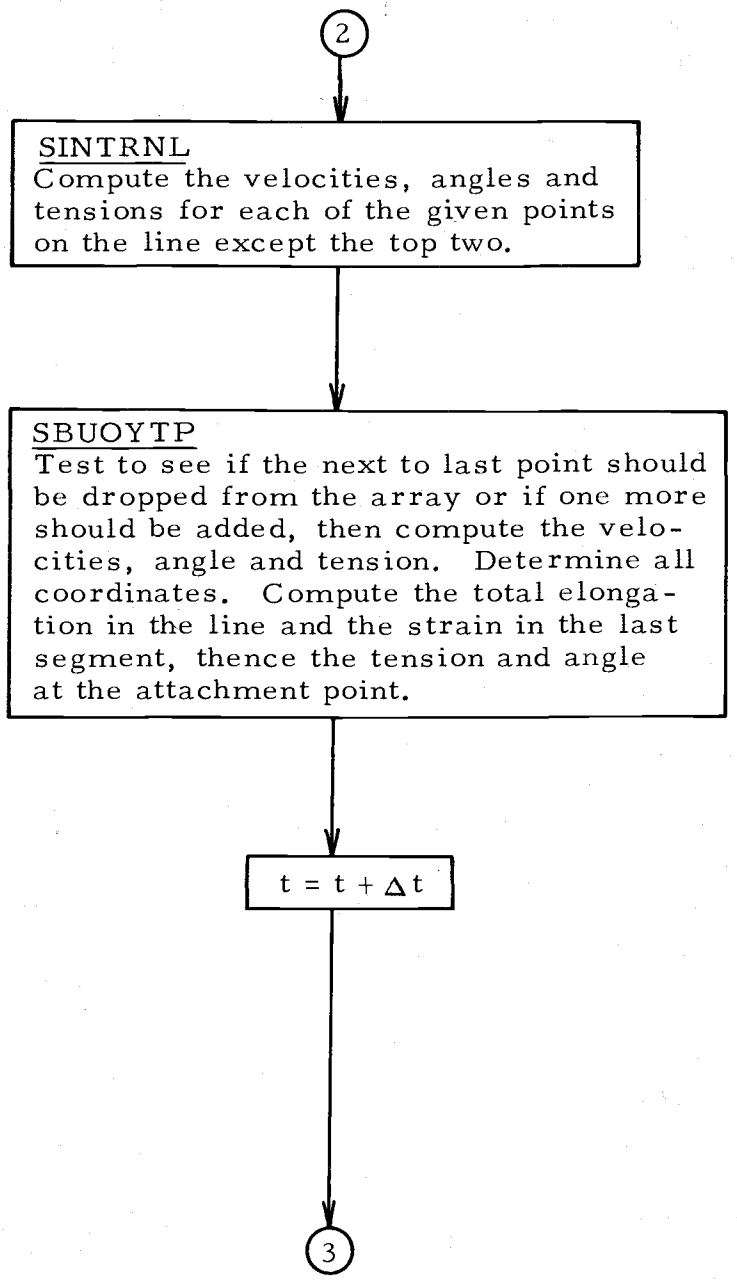

DYNAINP

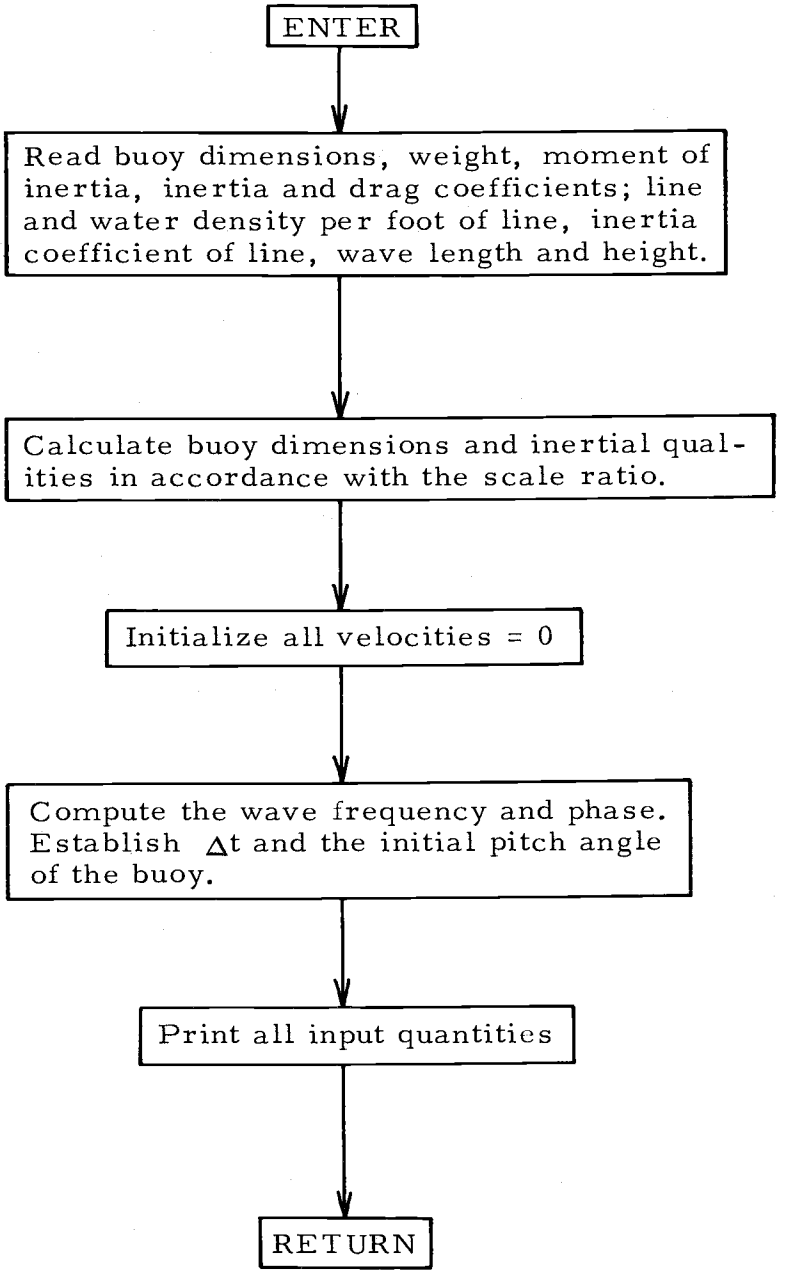
ENTER
Read buoy dimensions, weight, moment of inertia, inertia and drag coefficients; line and water density per foot of line, inertia coefficient of line, wave length and height.
Calculate buoy dimensions and inertial qualities in accordance with the scale ratio.
Initialize all velocities = 0
Compute the wave frequency and phase. Establish Δt and the initial pitch angle of the buoy.
Print all input quantities
RETURN

FUNCTIONS

Several functions are now established:

Water surface elevation from still water surface

Slope of the water surface

Horizontal wave water particle velocity

Vertical wave water particle velocity

Horizontal wave water particle acceleration

Vertical wave water particle acceleration

Wave pressure

Current velocity at a point - from the velocity profile

Other functions pertaining to the method of characteristics solution for line motion.

SPRINTO

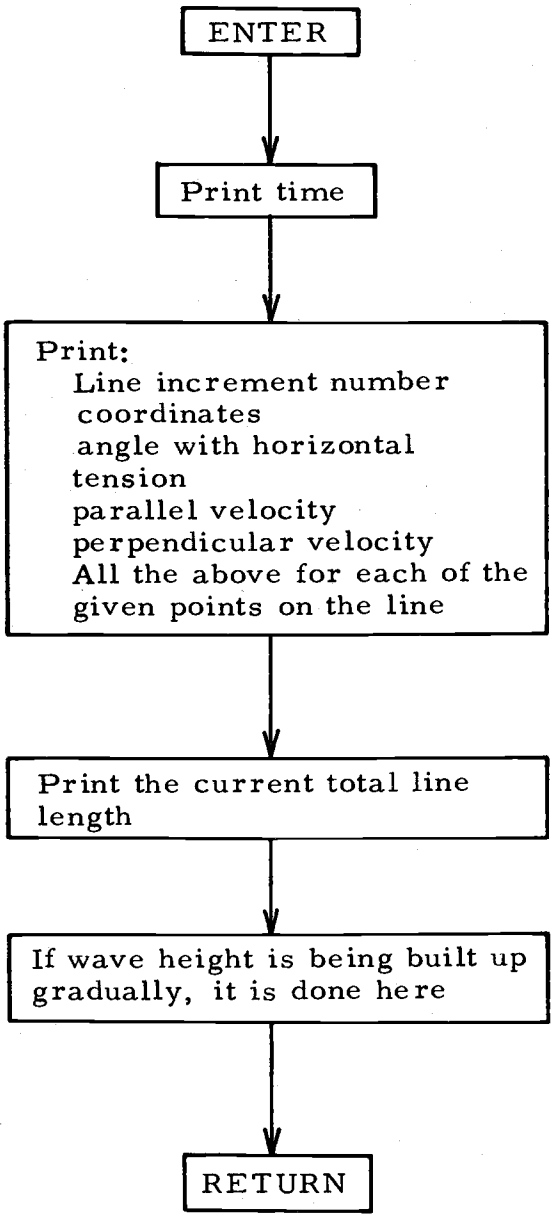
ENTER
Print time
Print:
Line increment number
coordinates
angle with horizontal
tension
parallel velocity
perpendicular velocity
All the above for each of the given points on the line
Print the current total line length
If wave height is being built up gradually, it is done here
RETURN

BMOTION

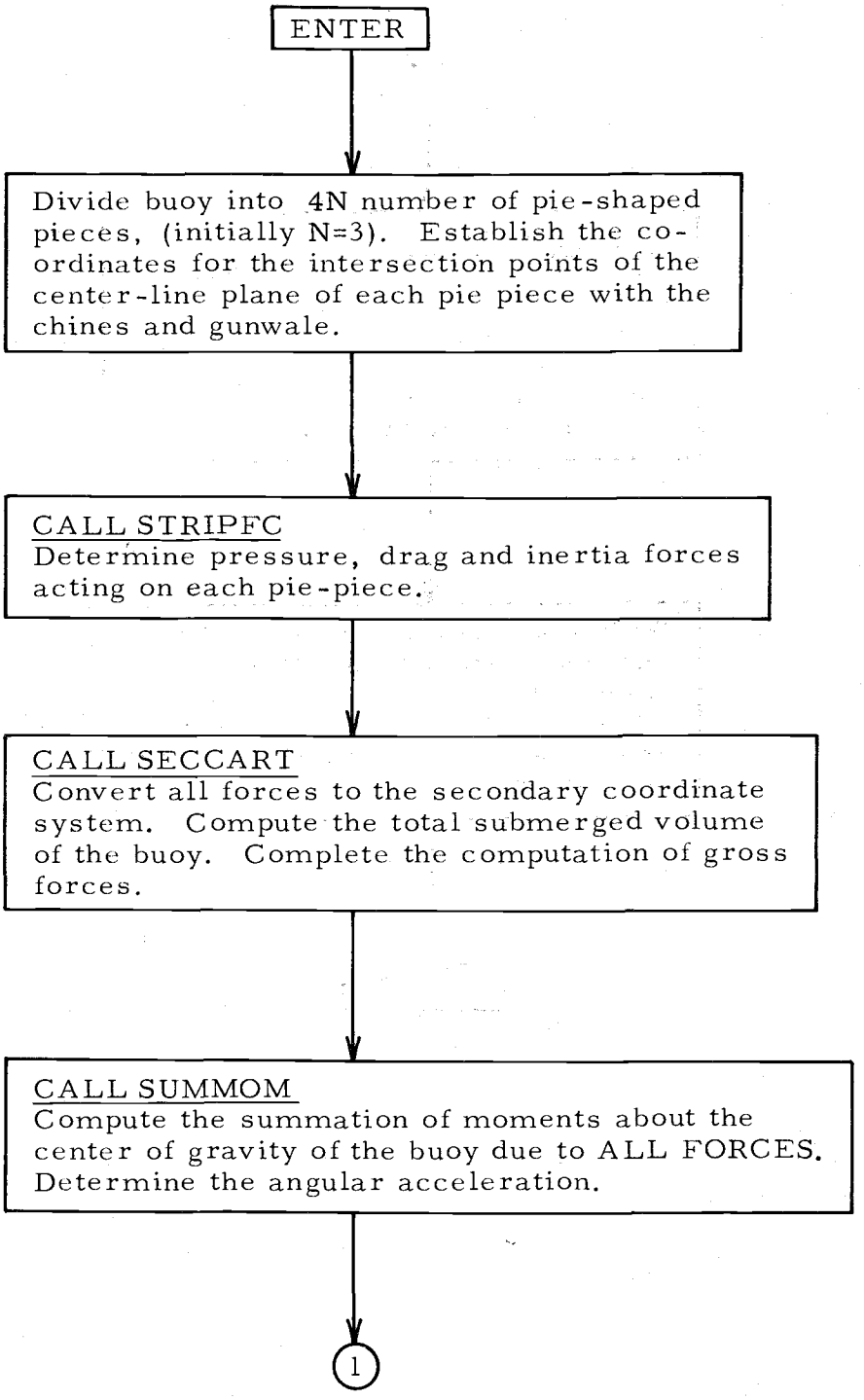
ENTER
Divide buoy into 4N number of pie-shaped pieces, (initially N=3). Establish the co-ordinates for the intersection points of the center-line plane of each pie piece with the chines and gunwale.
CALL STRIPFC
Determine pressure, drag and inertia forces acting on each pie-piece.
CALL SECCART
Convert all forces to the secondary coordinate system. Compute the total submerged volume of the buoy. Complete the computation of gross forces.
CALL SUMMOM
Compute the summation of moments about the center of gravity of the buoy due to ALL FORCES. Determine the angular acceleration.
1

BMOTION - CONT.

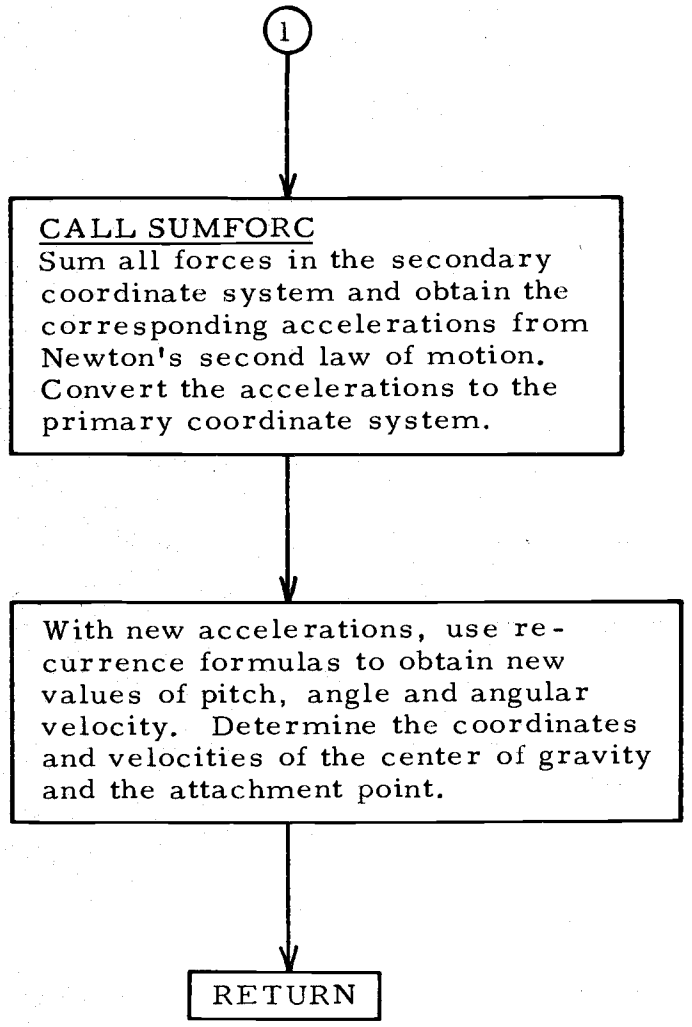

STRIPFC

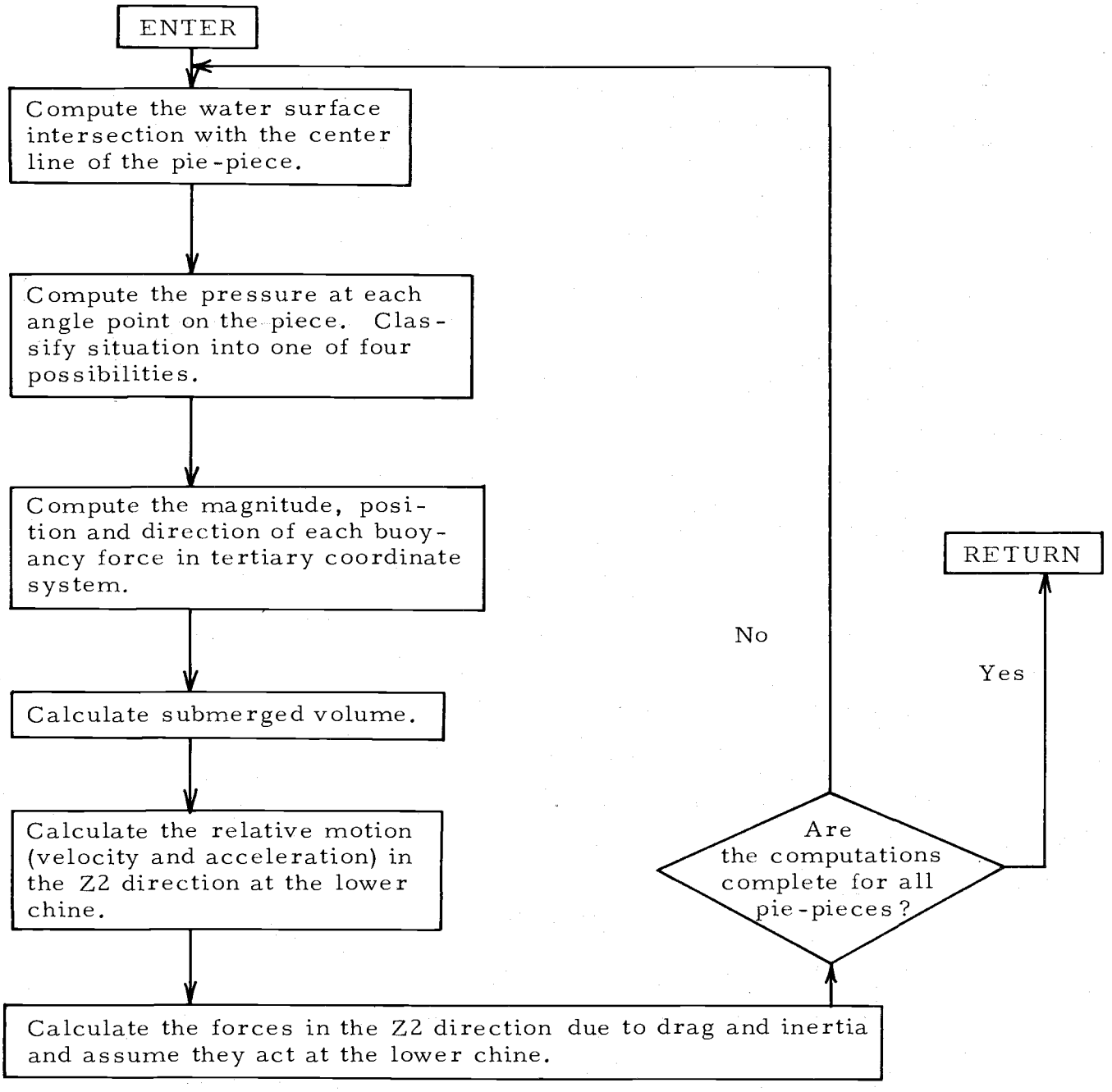
ENTER
Compute the water surface intersection with the center line of the pie-piece.
Compute the pressure at each angle point on the piece. Classify situation into one of four possibilities.
Compute the magnitude, position and direction of each buoyancy force in tertiary coordinate system.
Calculate submerged volume.
Calculate the relative motion (velocity and acceleration) in the Z2 direction at the lower chine.
Calculate the forces in the Z2 direction due to drag and inertia and assume they act at the lower chine.
Are the computations complete for all pie-pieces?
No
Yes
RETURN

BOUNDRY

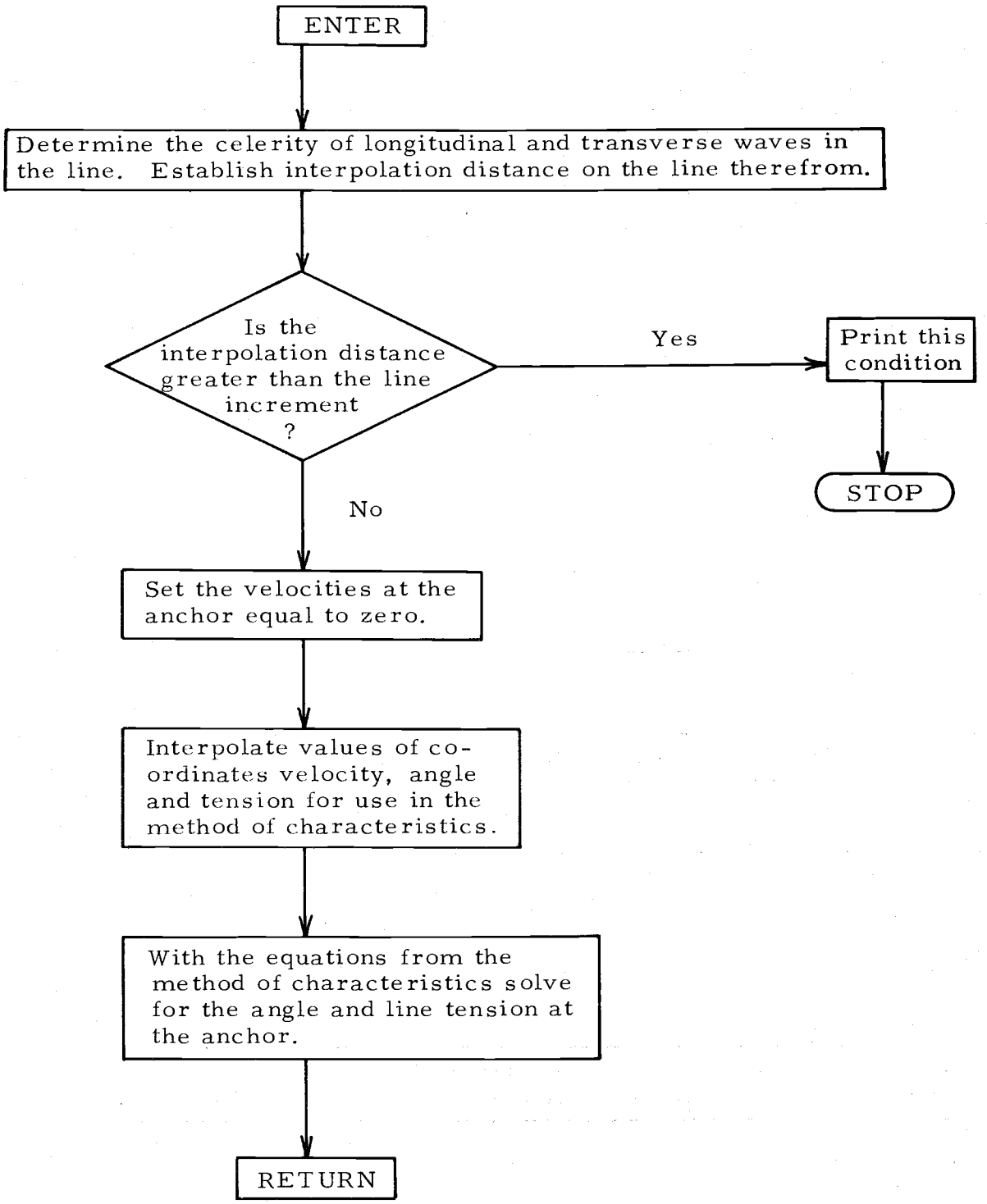
ENTER
Determine the celerity of longitudinal and transverse waves in the line. Establish interpolation distance on the line therefrom.
Is the interpolation distance greater than the line increment ?
Yes
Print this condition
STOP
No
Set the velocities at the anchor equal to zero.
Interpolate values of co-ordinates velocity, angle and tension for use in the method of characteristics.
With the equations from the method of characteristics solve for the angle and line tension at the anchor.
RETURN

SINTRNL

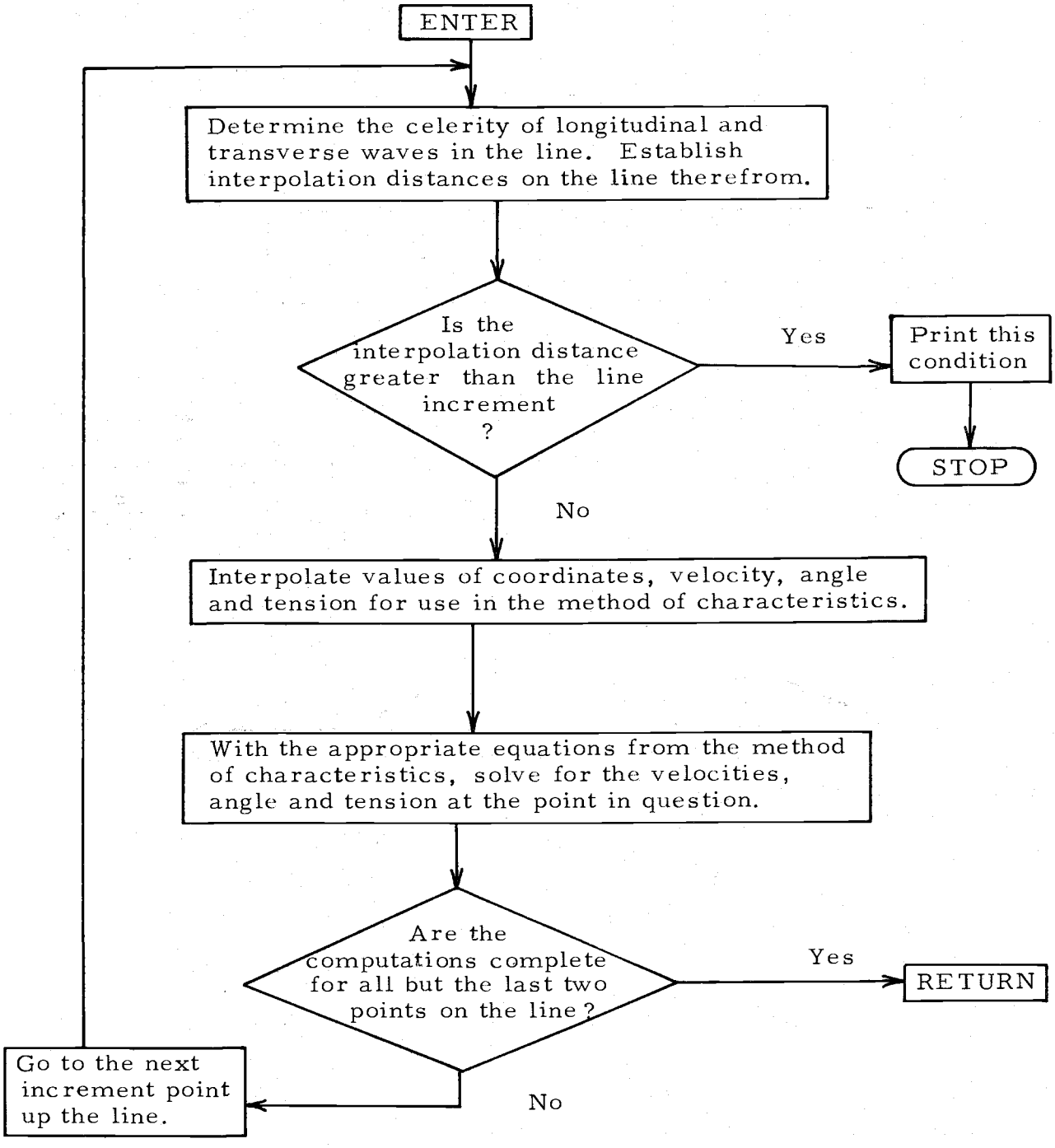
ENTER
Determine the celerity of longitudinal and transverse waves in the line. Establish interpolation distances on the line therefrom.
Is the interpolation distance greater than the line increment ?
Yes
Print this condition
STOP
No
Interpolate values of coordinates, velocity, angle and tension for use in the method of characteristics.
With the appropriate equations from the method of characteristics, solve for the velocities, angle and tension at the point in question.
Are the computations complete for all but the last two points on the line ?
Yes
RETURN
No
Go to the next increment point up the line.

SBUOYTP

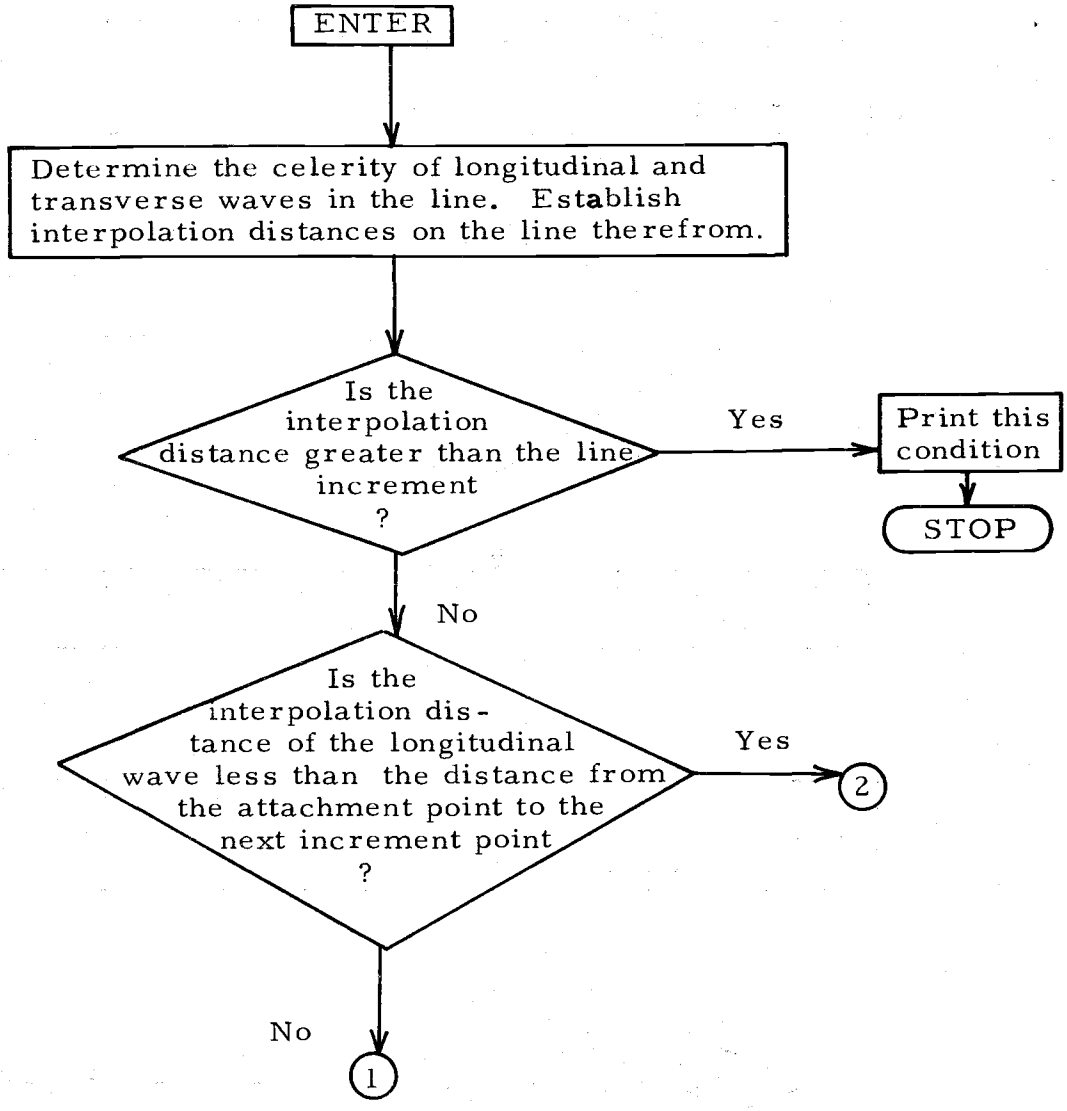
ENTER
Determine the celerity of longitudinal and transverse waves in the line. Establish interpolation distances on the line therefrom.
Is the interpolation distance greater than the line increment ?
Yes
Print this condition
STOP
No
Is the interpolation distance of the longitudinal wave less than the distance from the attachment point to the next increment point ?
Yes
2
No
1

SBUOYTP - CON'T.

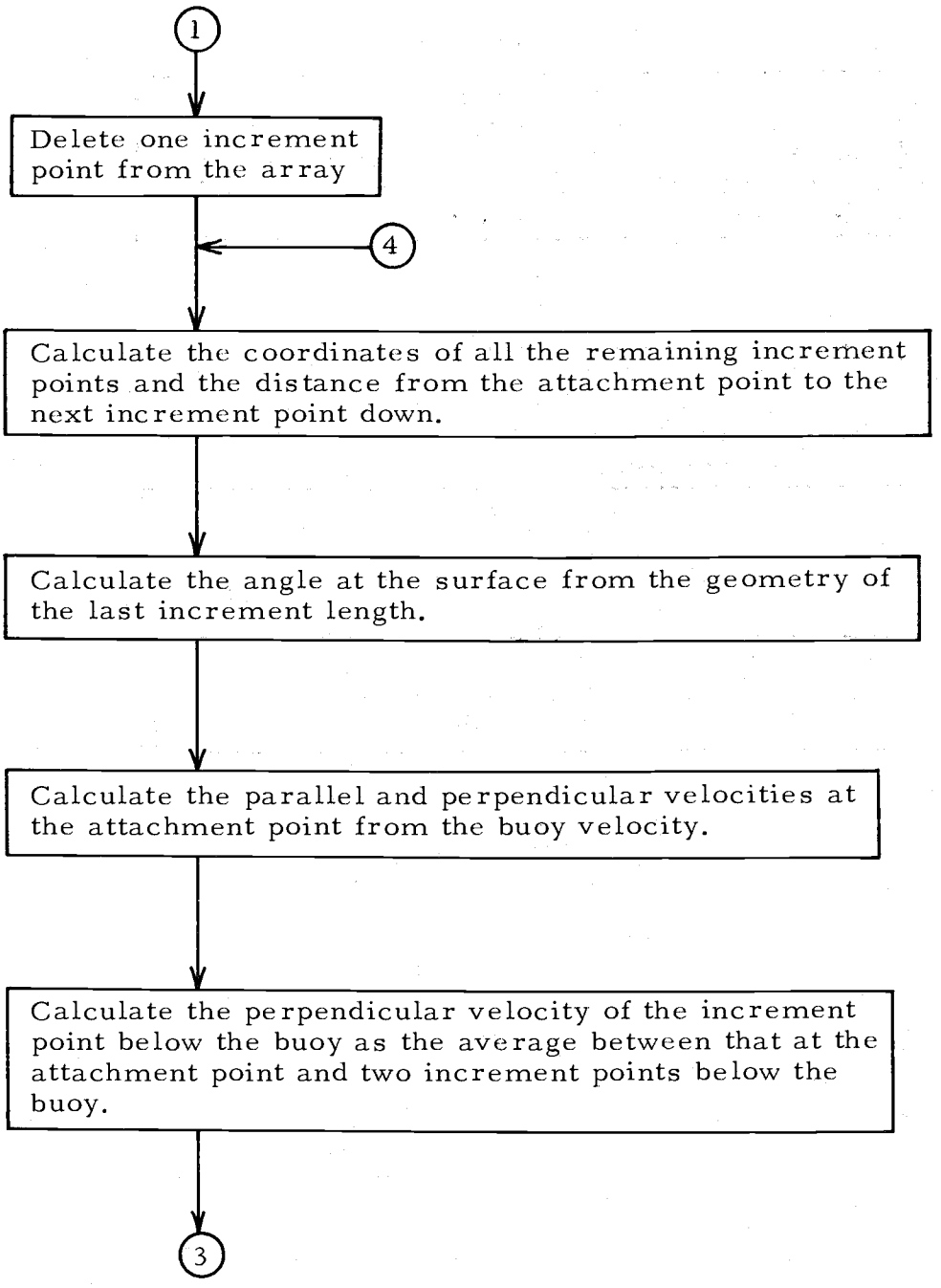

SBUOYTP - CON'T.

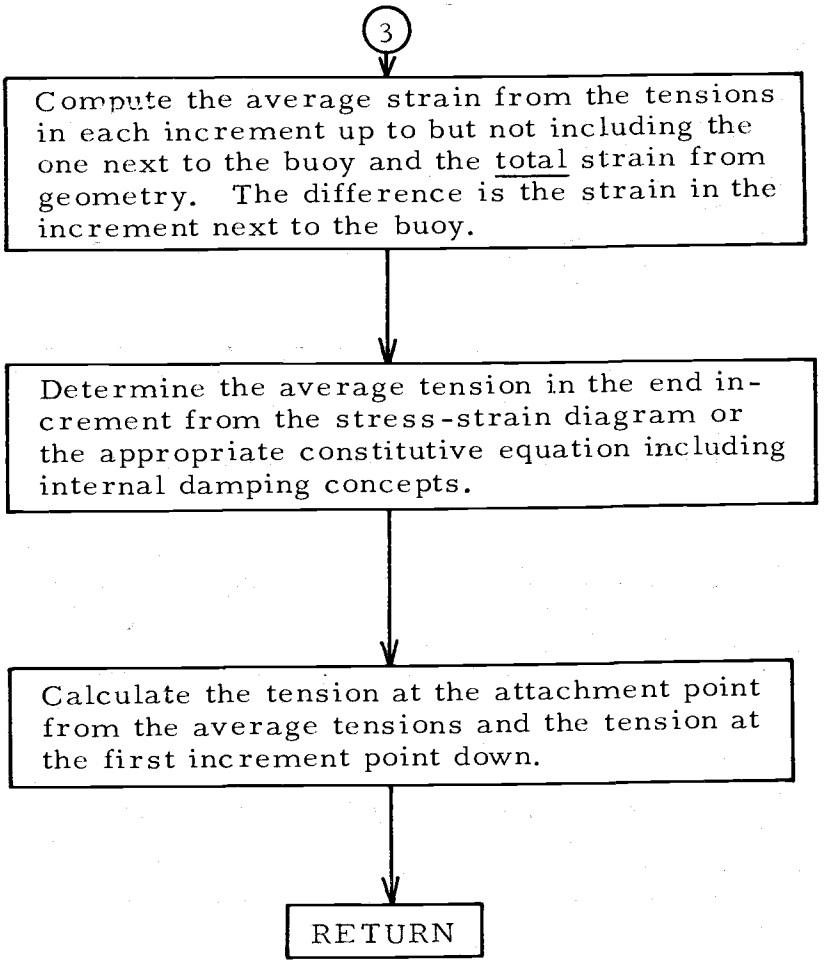

SBUOYTP - CON'T.

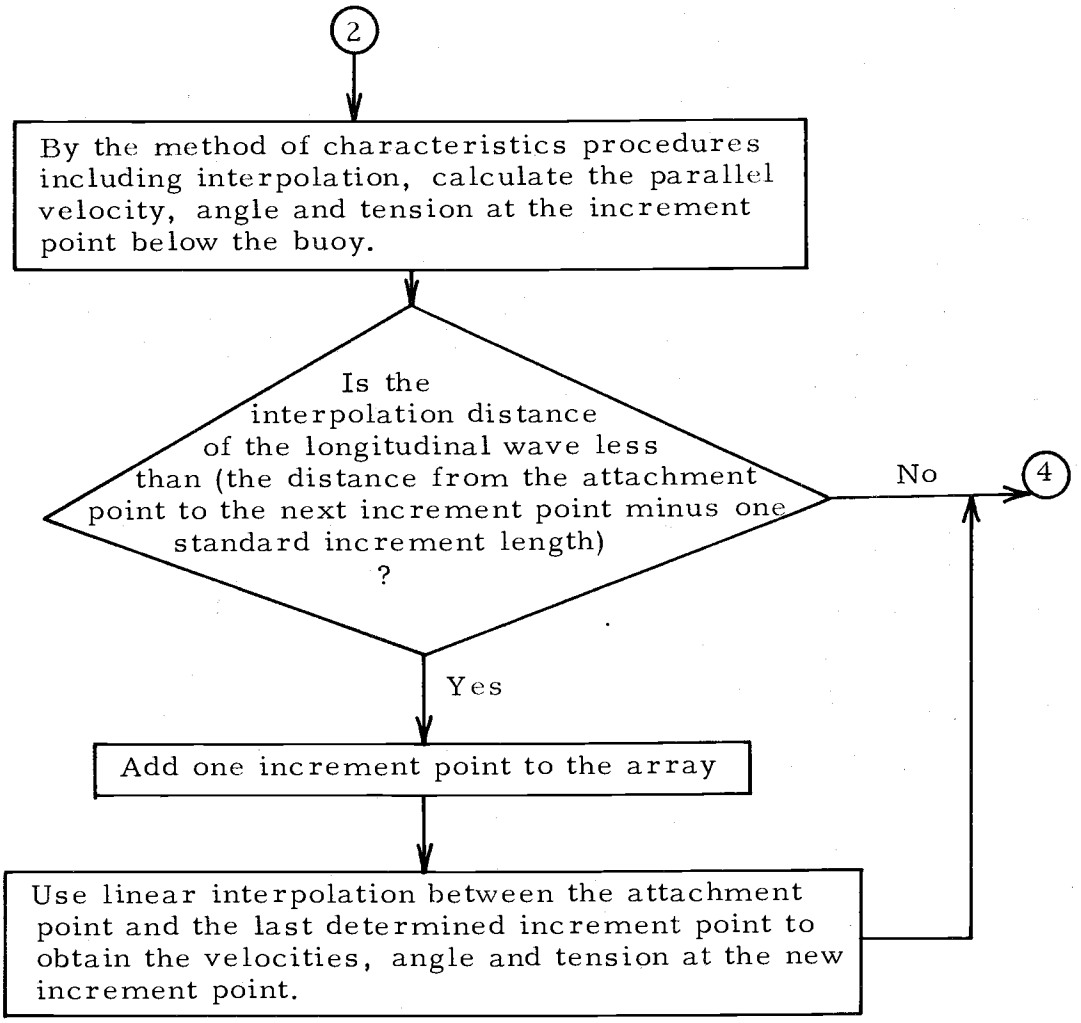

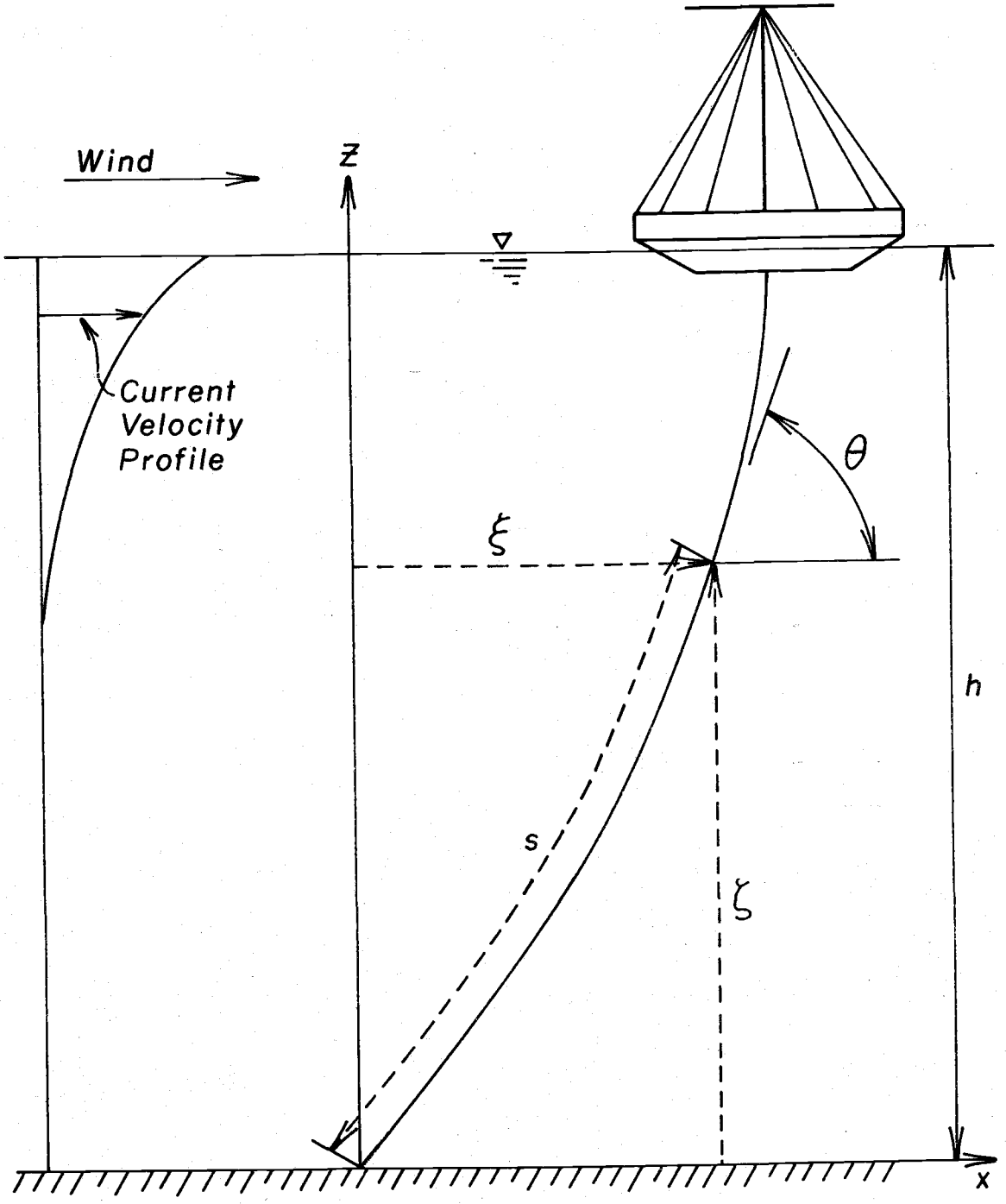

FIG. 1. DEFINITION SKETCH OF THE STATIC PROBLEM

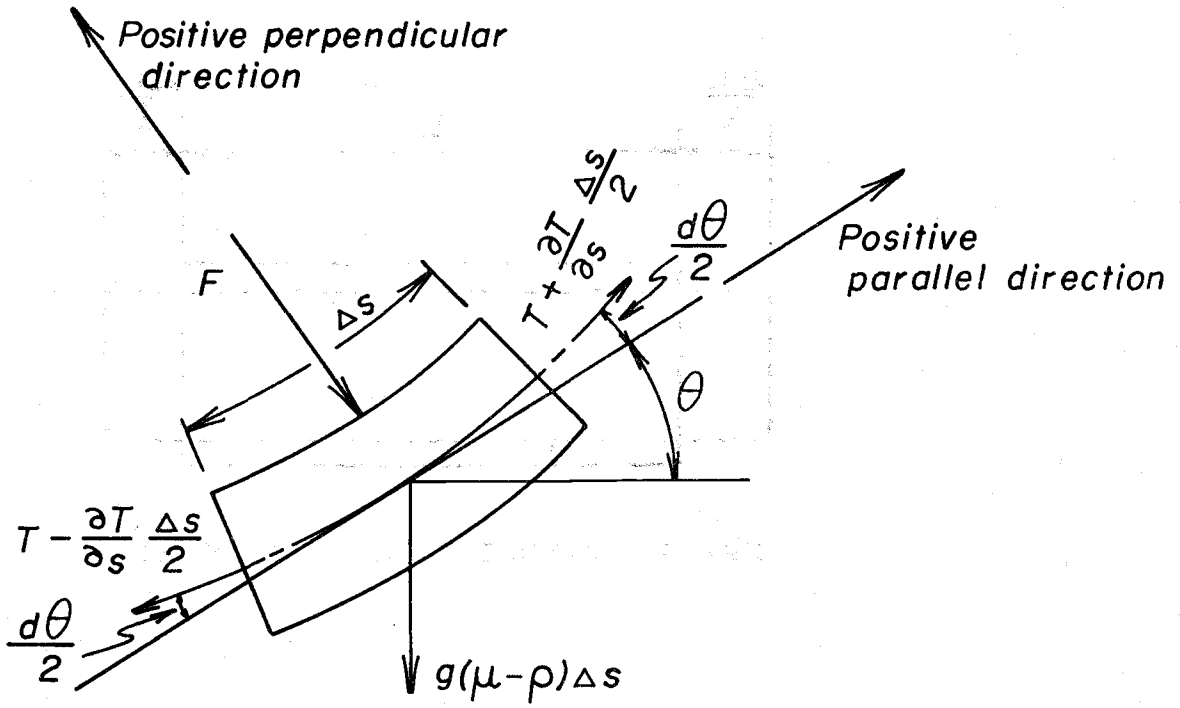

FIG. 2. FREE-BODY DIAGRAM OF A SMALL ELEMENT OF THE MOORING LINE.

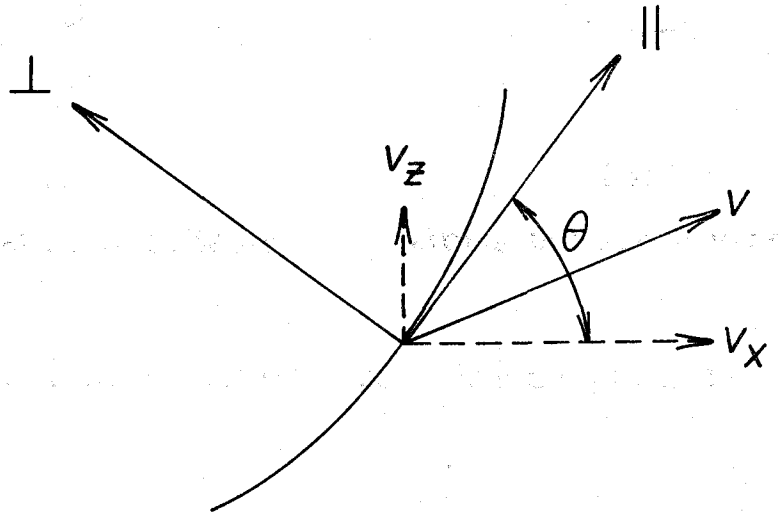

FIG. 3. THE VECTOR, V, AND THE MOORING LINE

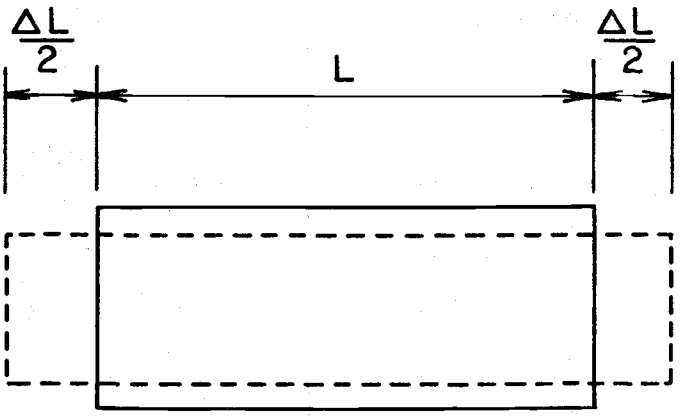

FIG. 4. CHANGE IN LINE DIAMETER

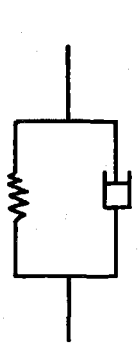

(a)

Firmo-viscous materials

(b)

Elastico-viscous materials

FIG. 5. SPRING AND DASHPOT MODELS OF LINE RESISTANCE

NOTE: There is a great deal of scatter in laboratory results of stress-strain diagrams for both Dacron and Nylon plaited lines. The diagram used below is fairly representative for either Dacron or Nylon.

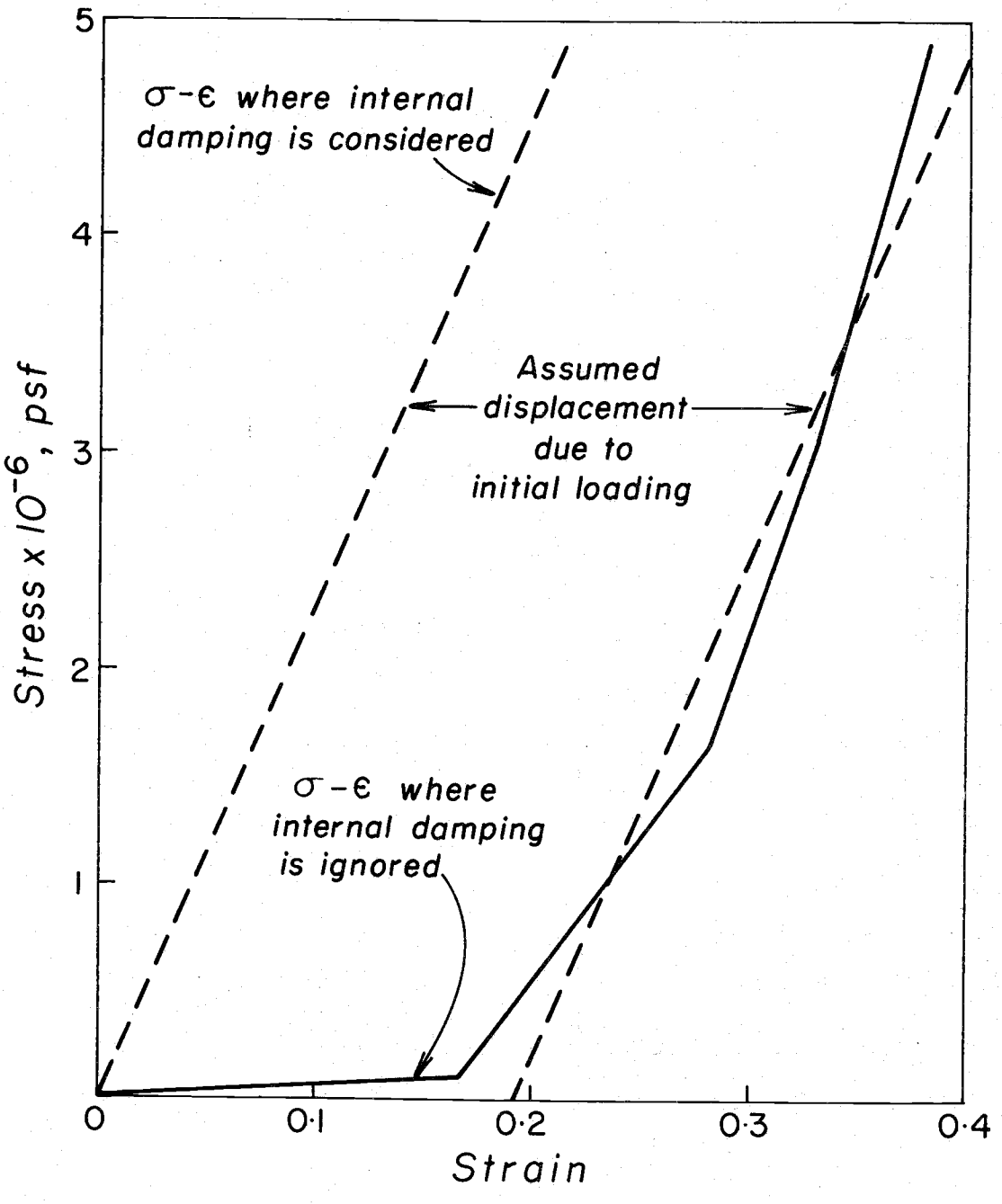

FIG. 6. STRESS-STRAIN DIAGRAMS USED FOR THIS STUDY

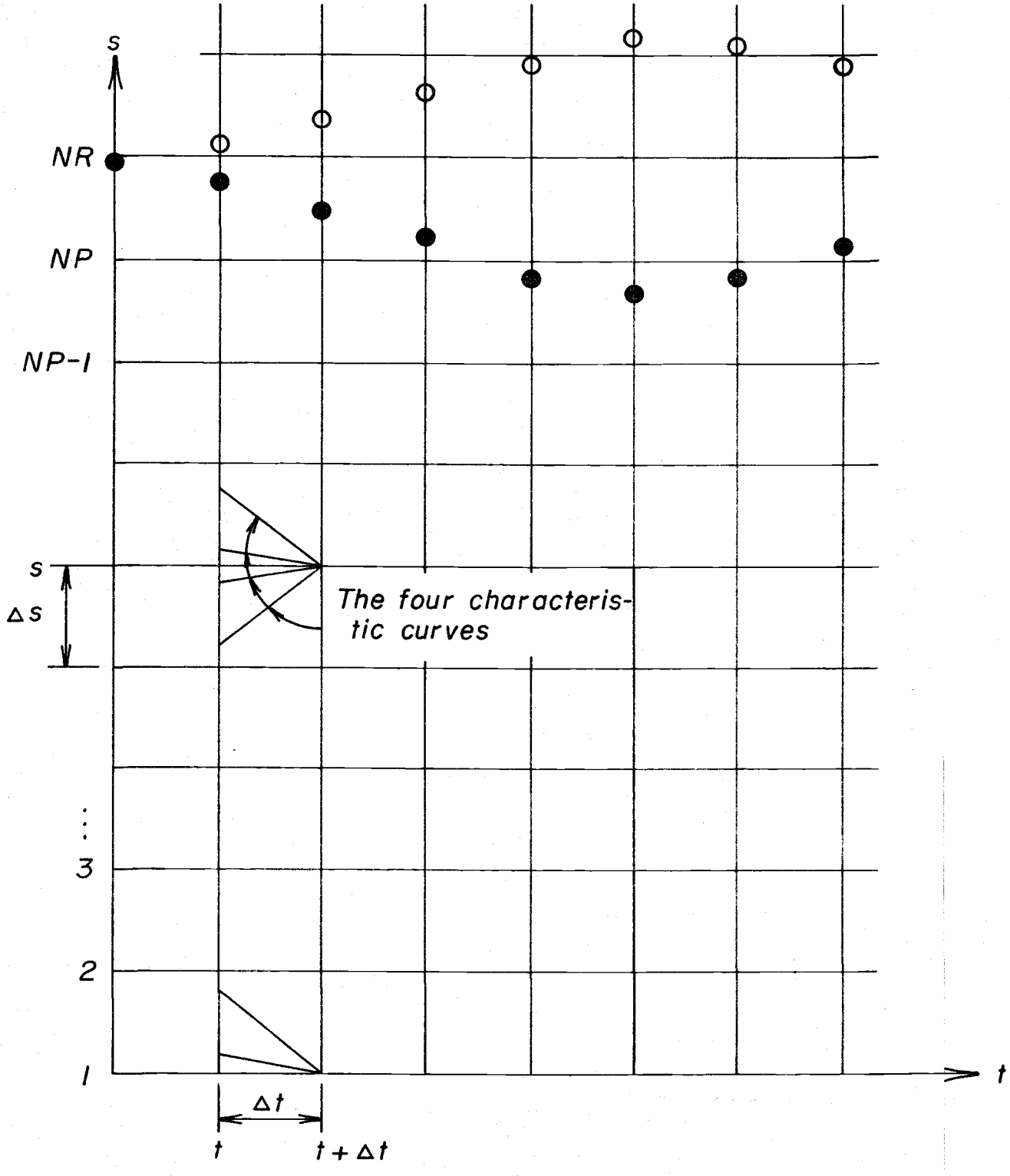

FIG. 7. THE s-t GRID

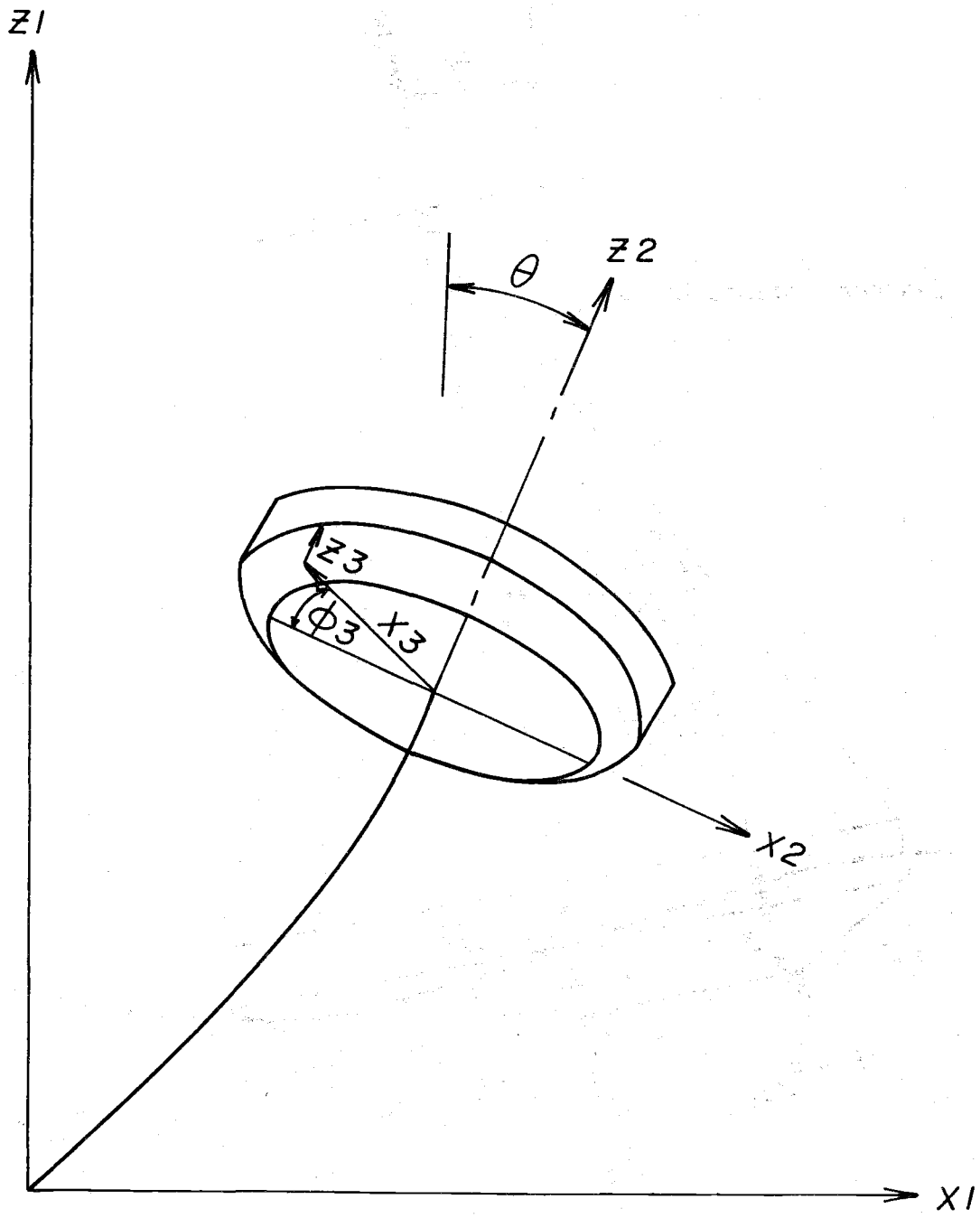

FIG. 8. THE THREE COORDINATE SYSTEMS USED FOR THE BUOY ANALYSIS

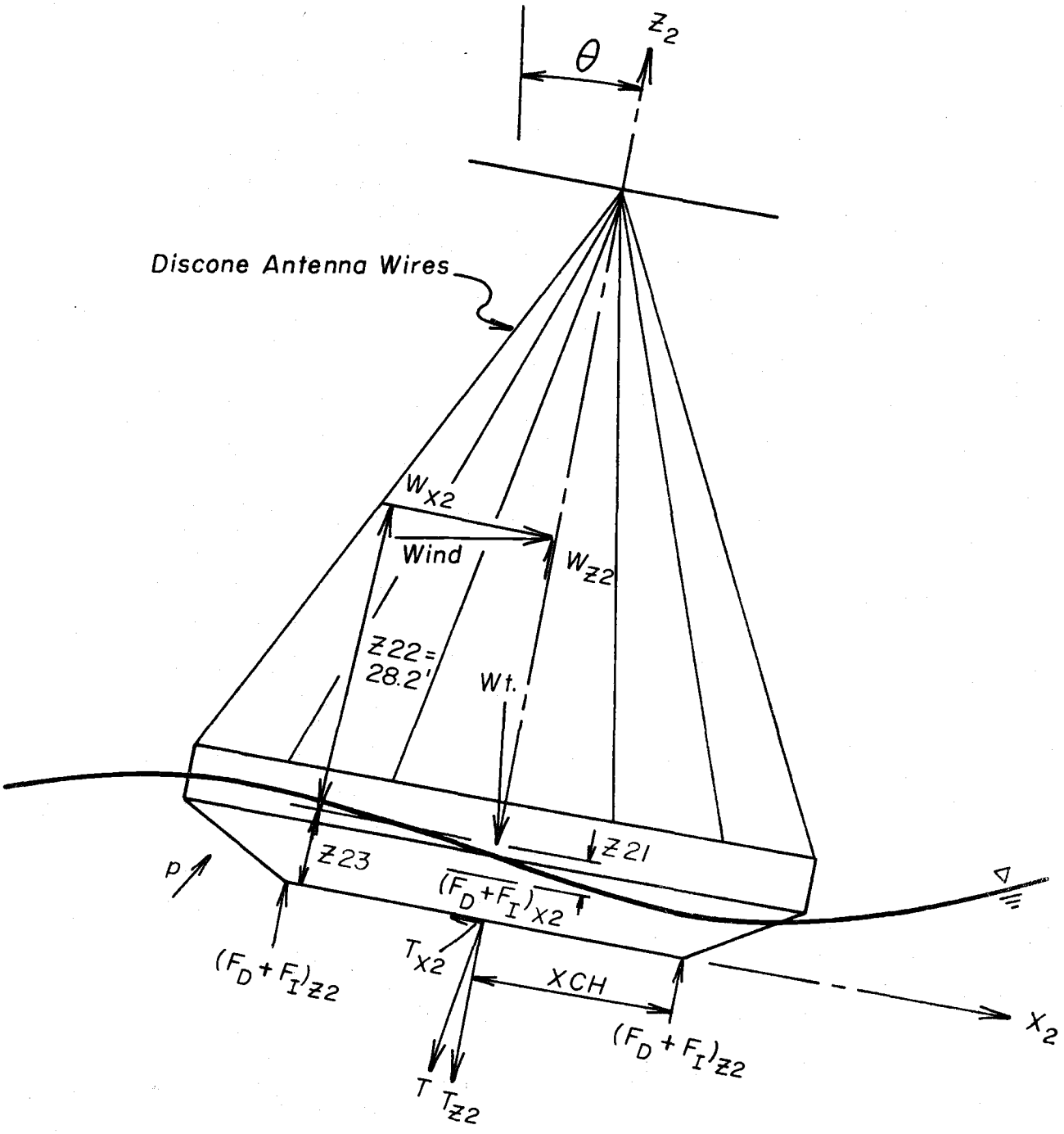

FIG. 9. FREE-BODY DIAGRAM OF THE BUOY WITH ALL FORCES SHOWN SCHEMATICALLY

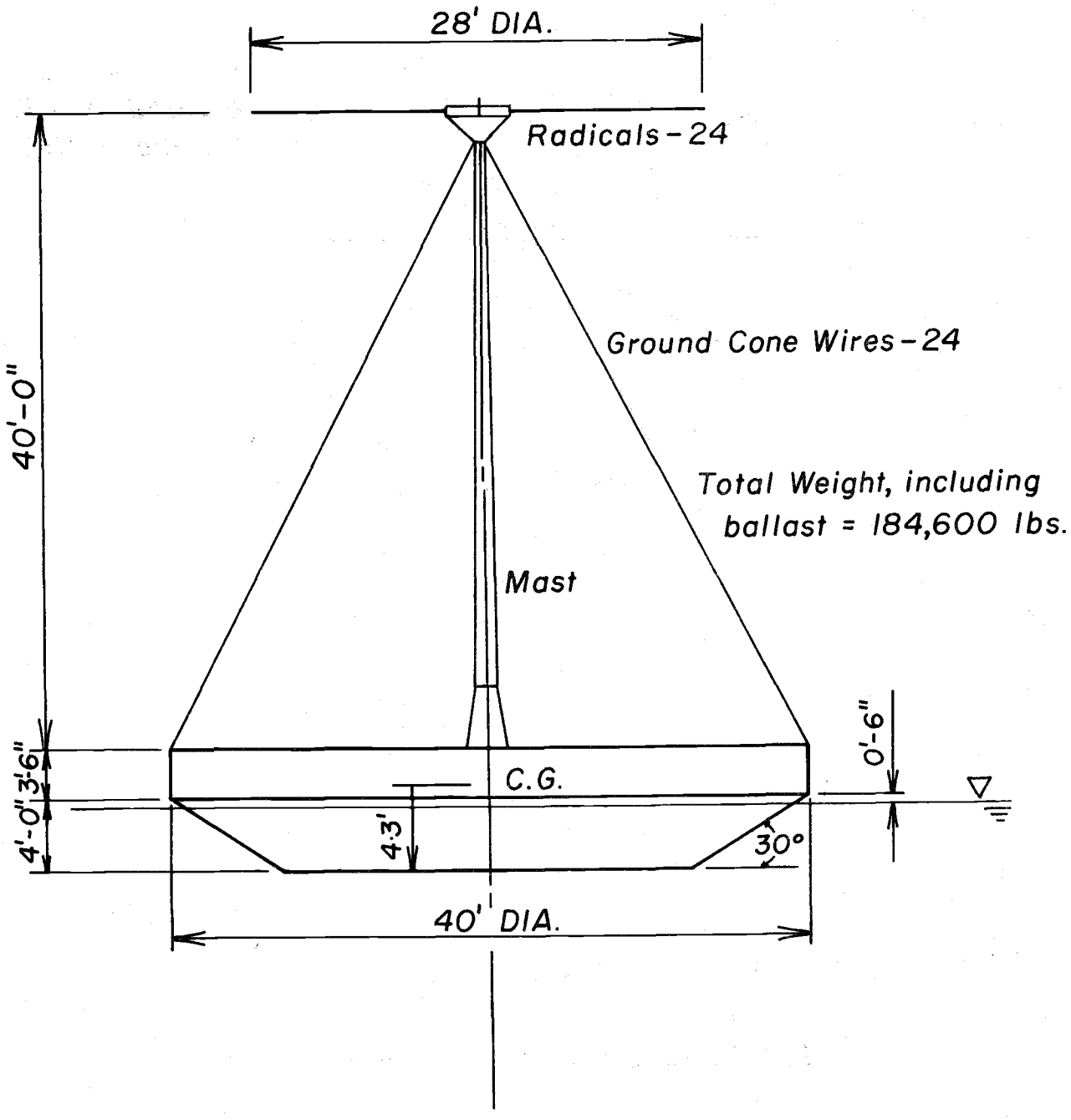

FIG. 10. DIMENSIONS OF THE ONR BUOY USED IN THIS STUDY

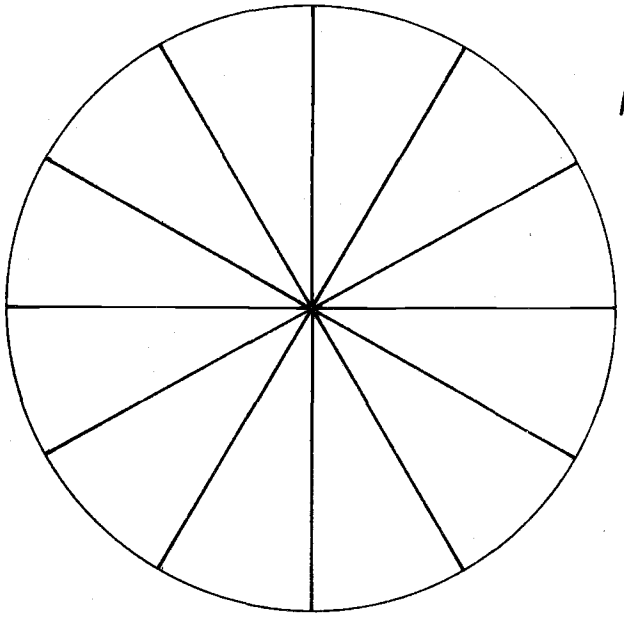

Note: The buoy was divided into 12 pieces for the initial work

a) Plan

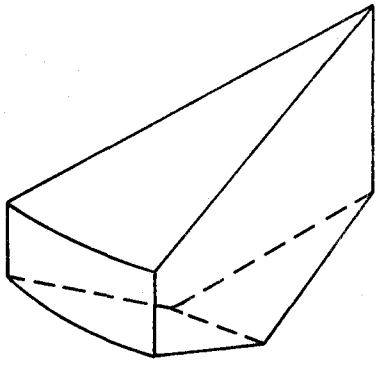

b) Perspective of one segment

FIG. 11. DIVISION OF THE BUOY FOR CALCULATION OF FORCES.

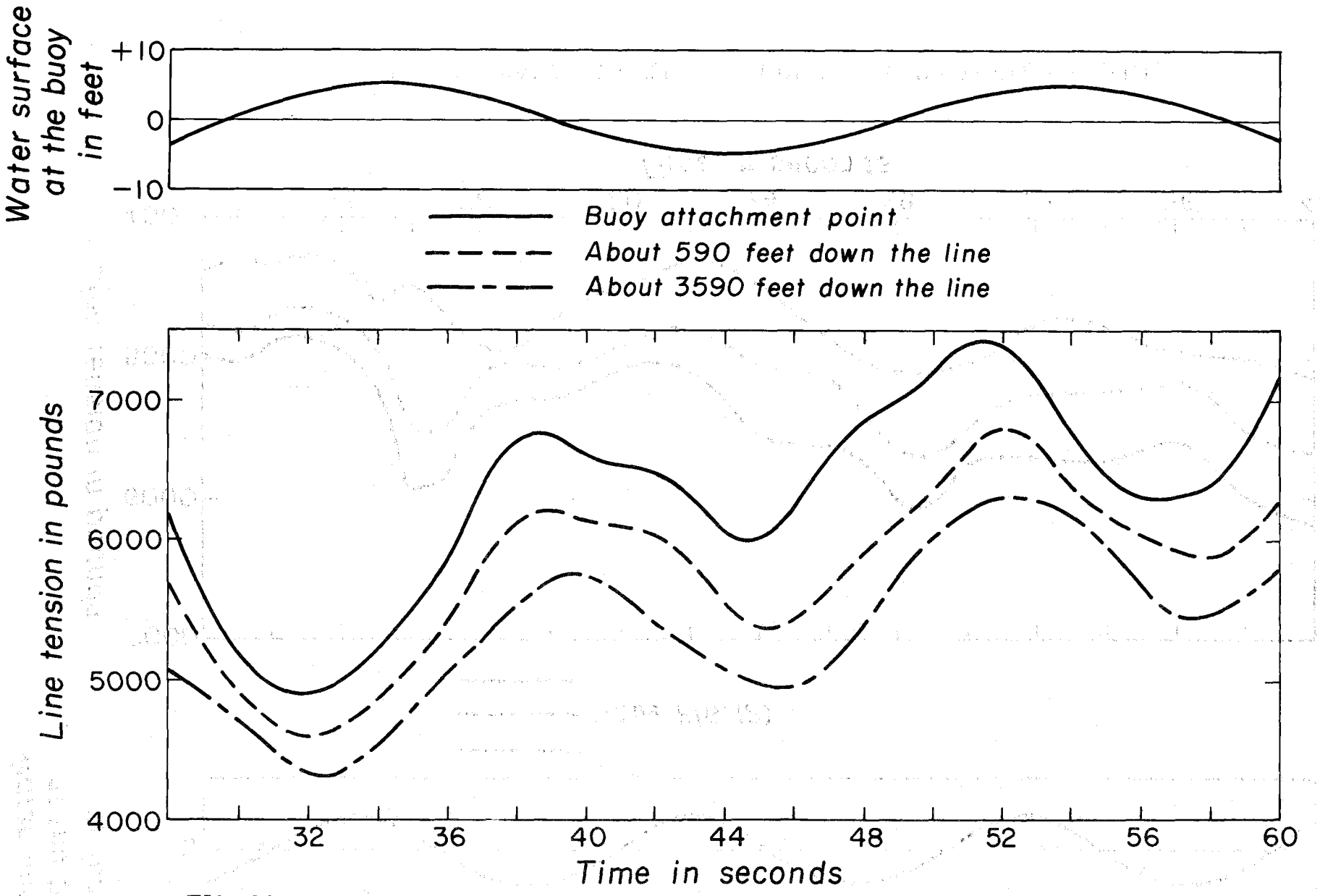

FIG. 12. MOORING LINE TENSIONS AT VARIOUS POSITIONS AND WATER SURFACE ELEVATION AT THE BUOY VS. TIME. WAVE LENGTH = 2000 FEET. WAVE HEIGHT = 20 FEET.

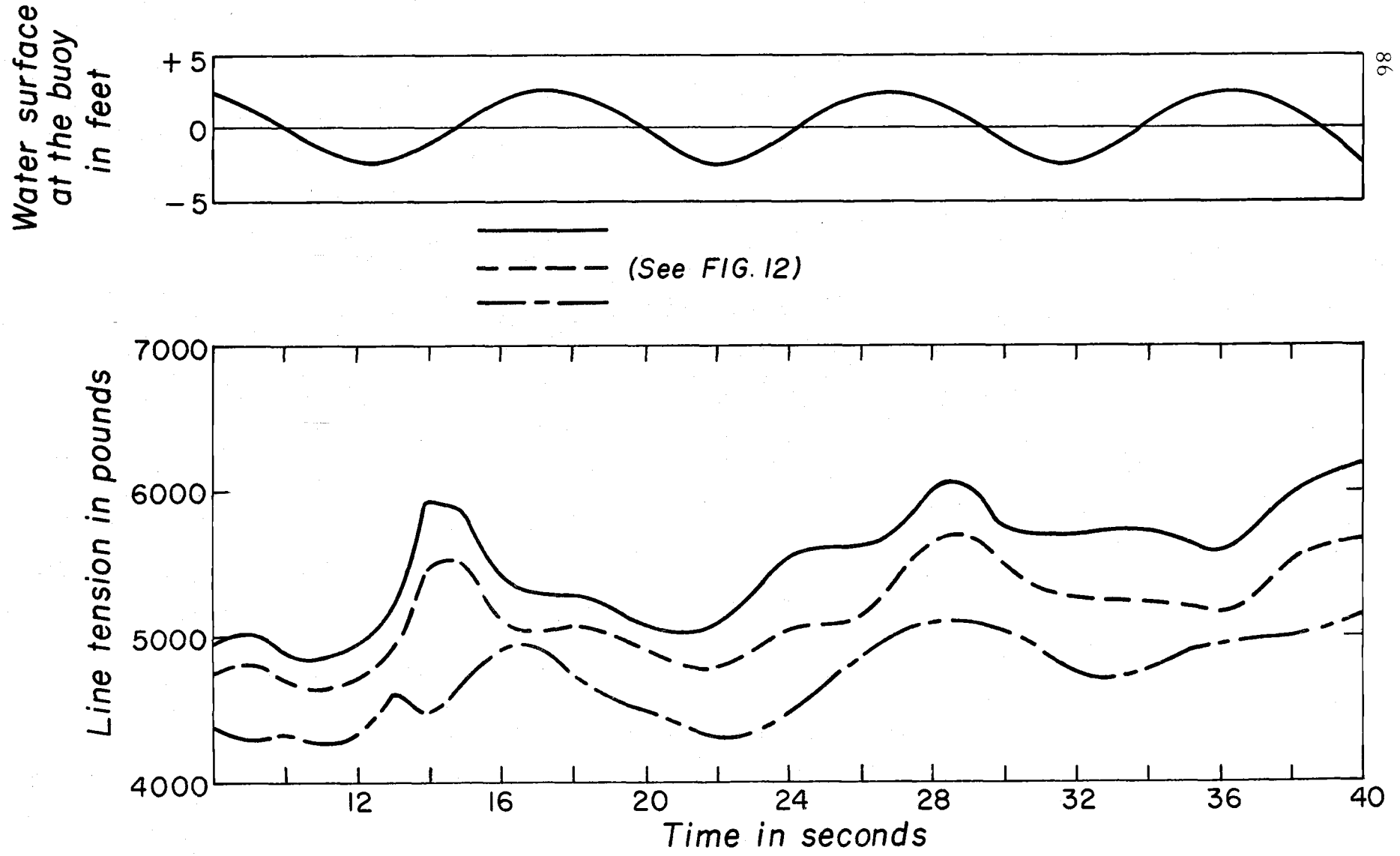

FIG. 13. WAVE LENGTH = 500 FEET. WAVE HEIGHT = 5 FEET.

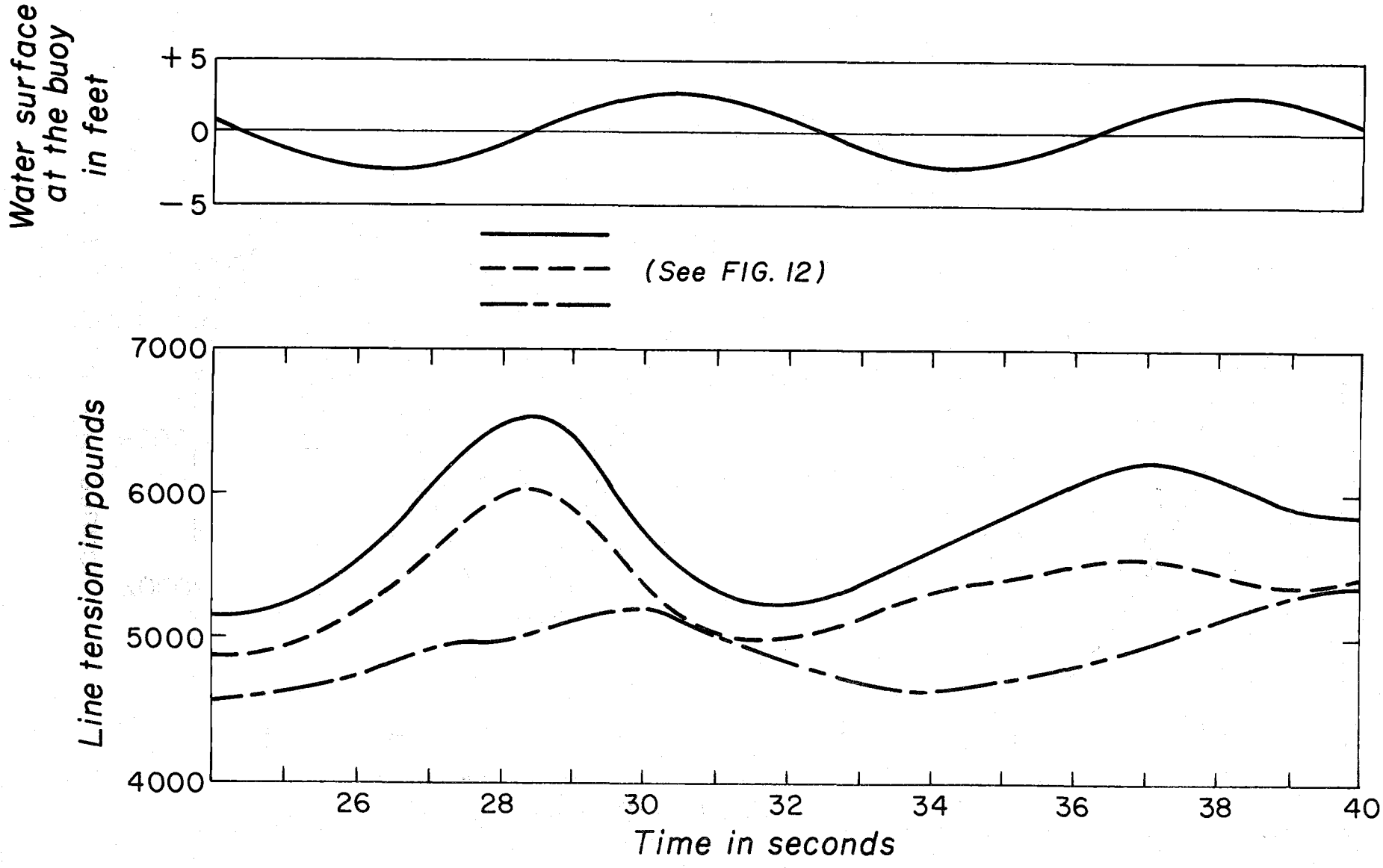

FIG. 14. WAVE LENGTH = 350 FEET. WAVE HEIGHT = 5 FEET.

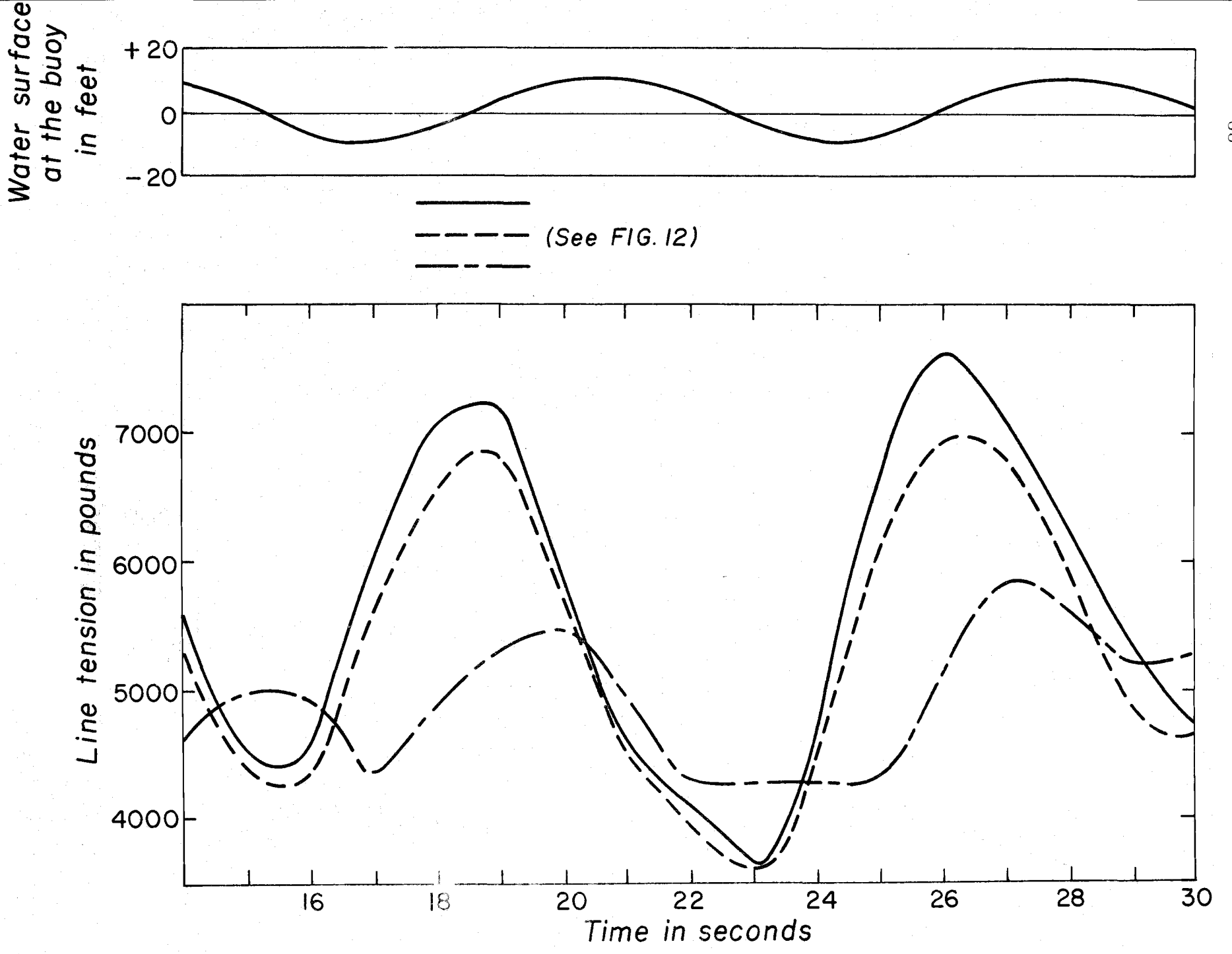

FIG. 15. WAVE LENGTH = 260 FEET. WAVE HEIGHT = 20 FEET.

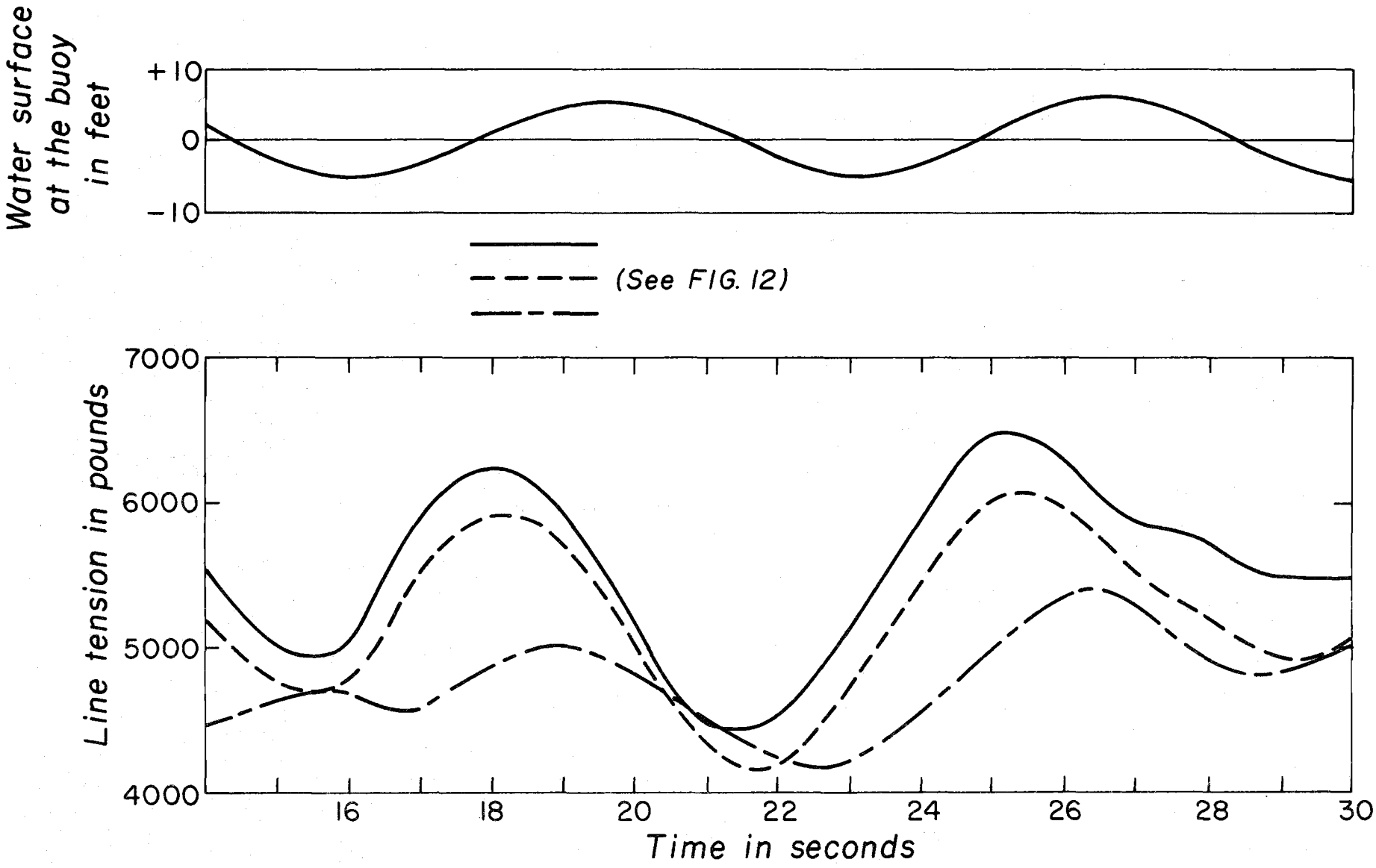

FIG. 16. WAVE LENGTH = 260 FEET. WAVE HEIGHT = 10 FEET.

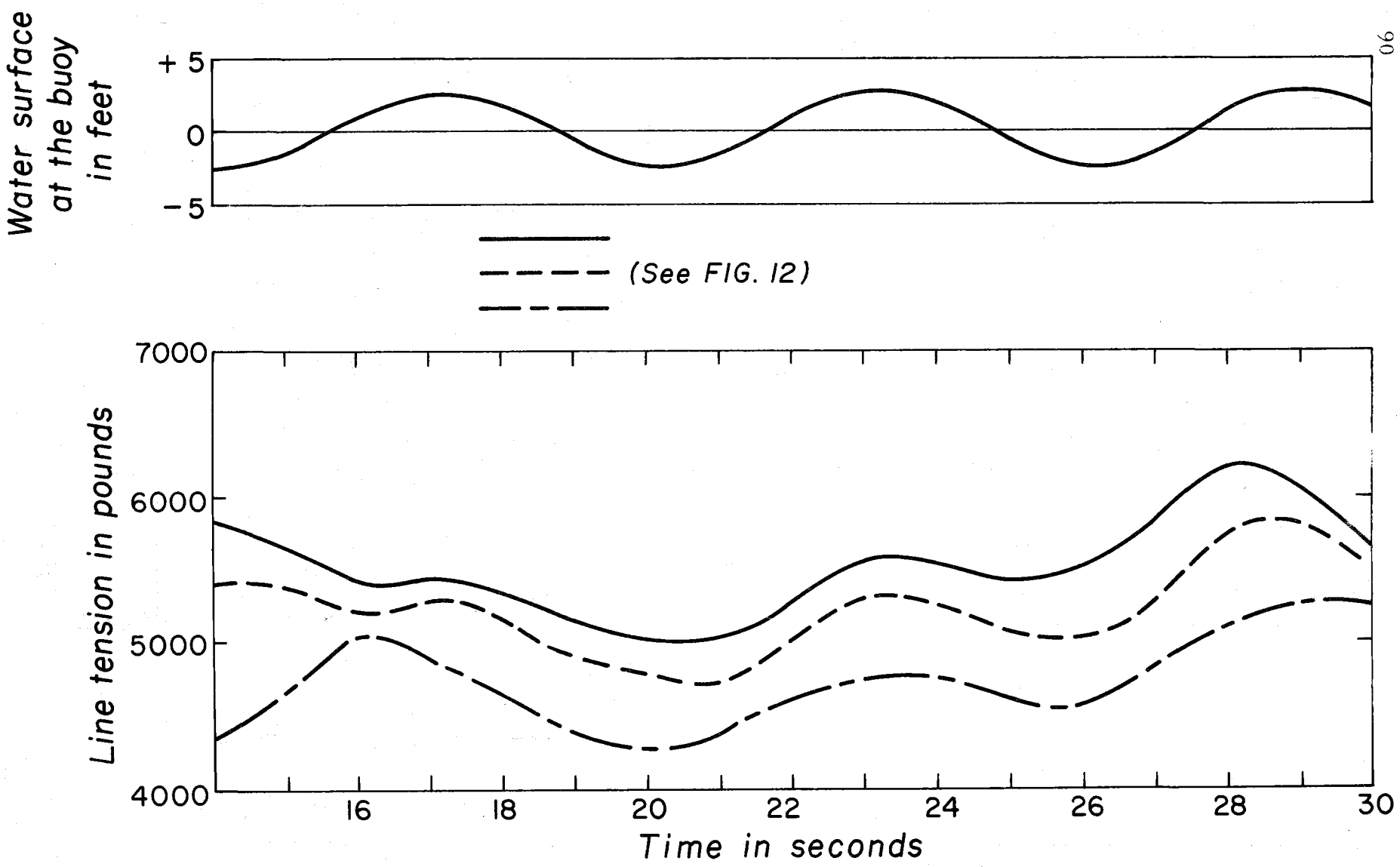

FIG. 17. WAVE LENGTH = 260 FEET. WAVE HEIGHT = 5 FEET.

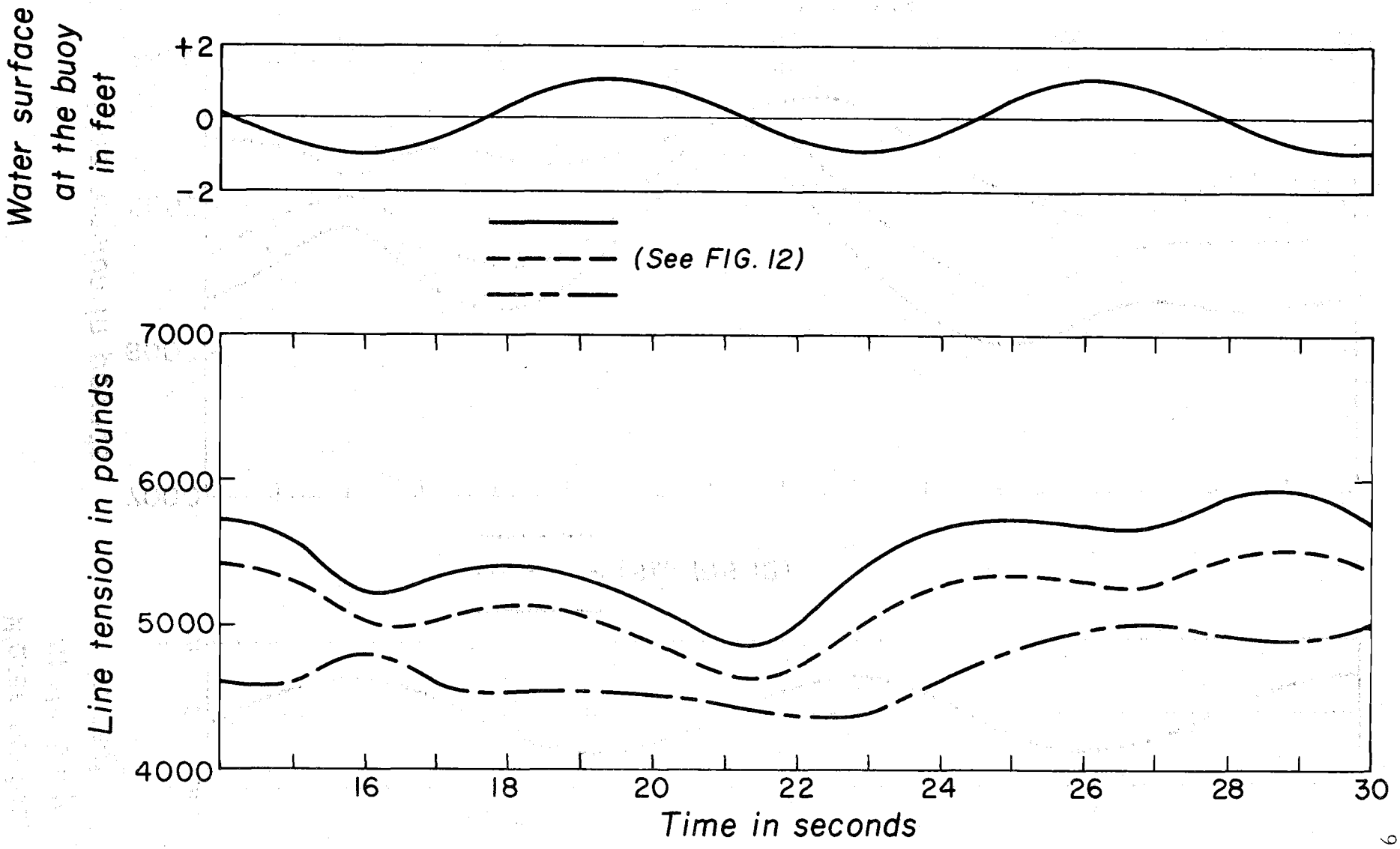

FIG. 18. WAVE LENGTH = 260 FEET. WAVE HEIGHT = 2 FEET.

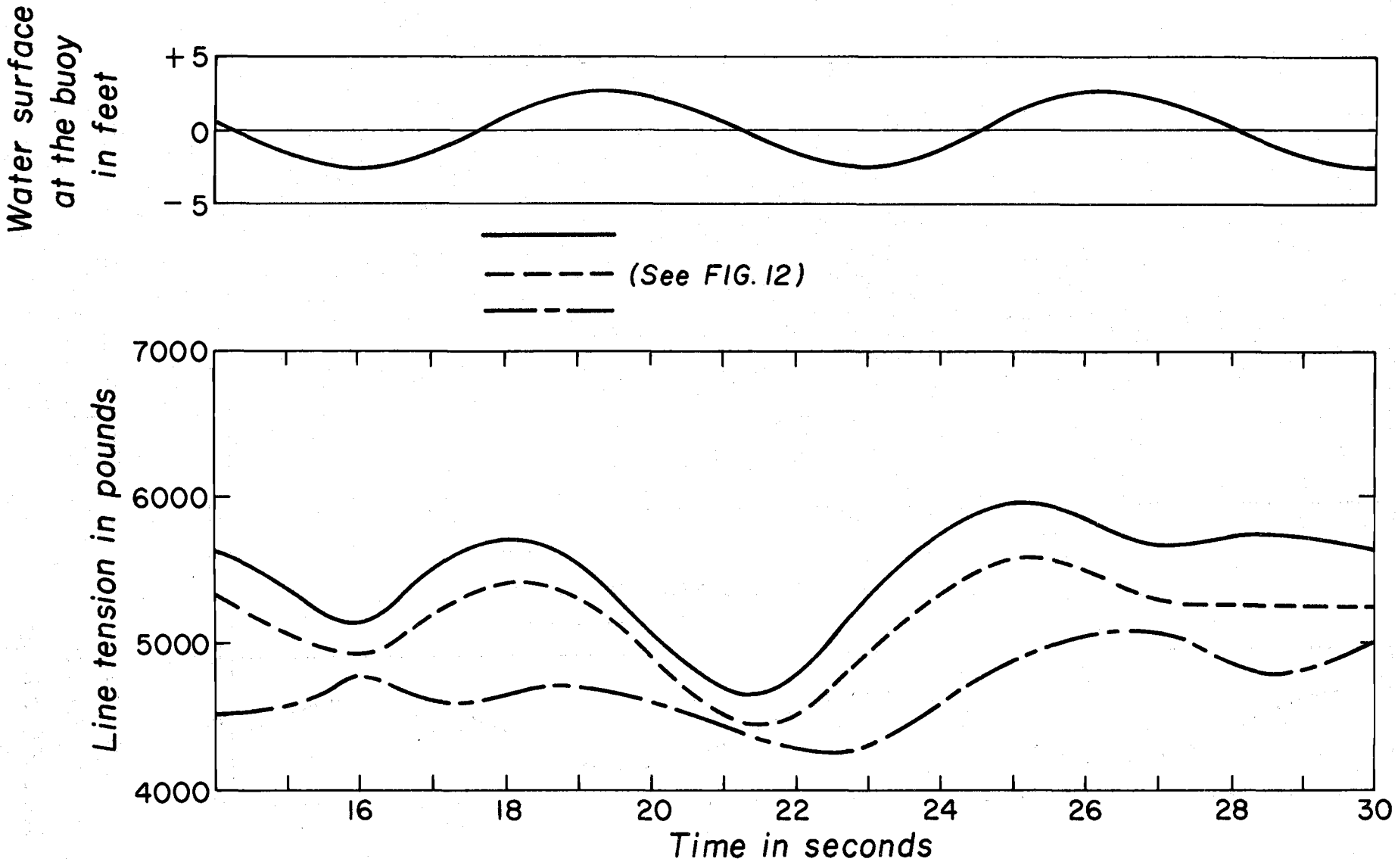

FIG. 19. WAVE LENGTH = 200 FEET. WAVE HEIGHT = 5 FEET.

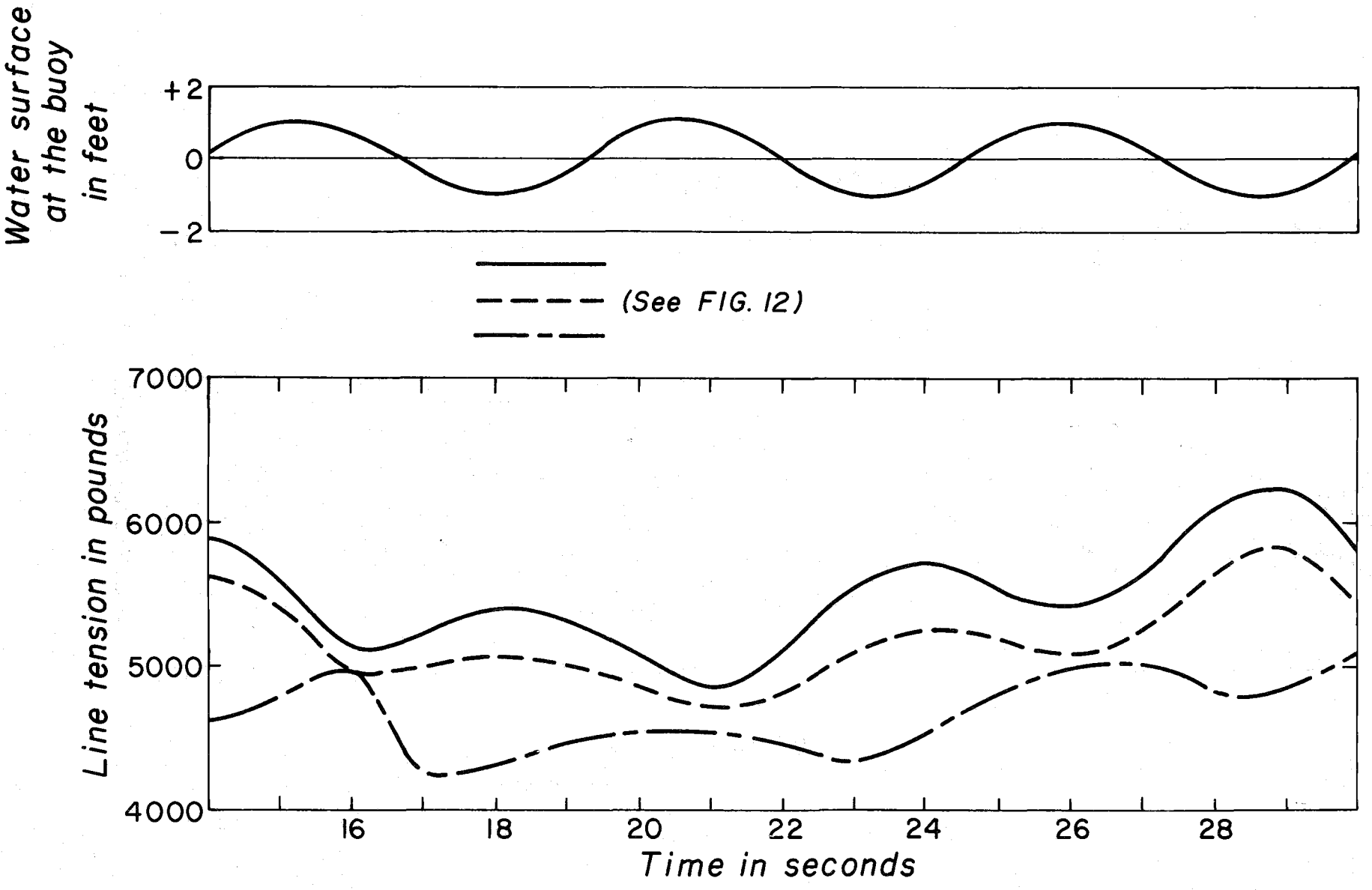

FIG. 20. WAVE LENGTH = 160 FEET. WAVE HEIGHT = 2 FEET.

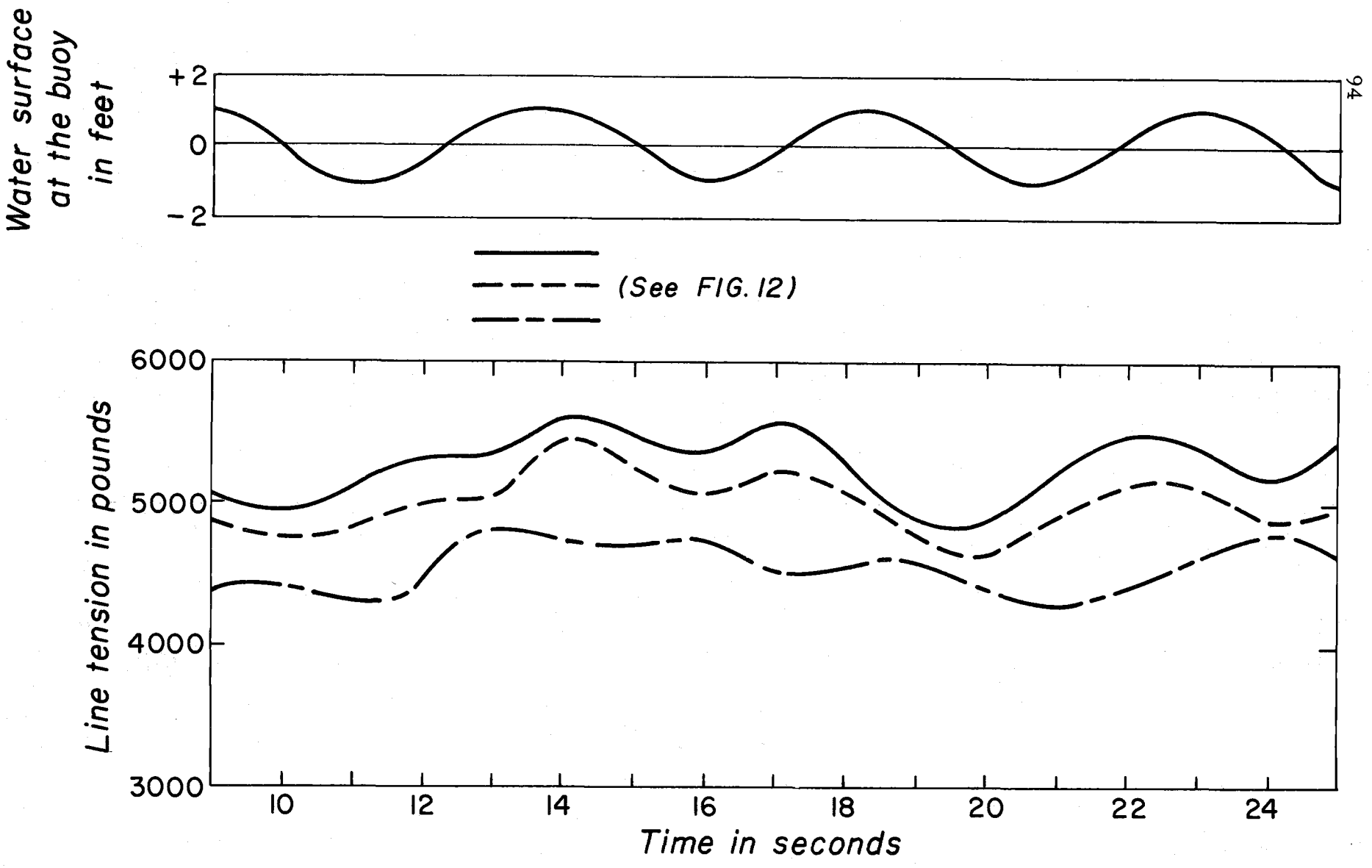

FIG. 21. WAVE LENGTH = 125 FEET. WAVE HEIGHT = 2 FEET.

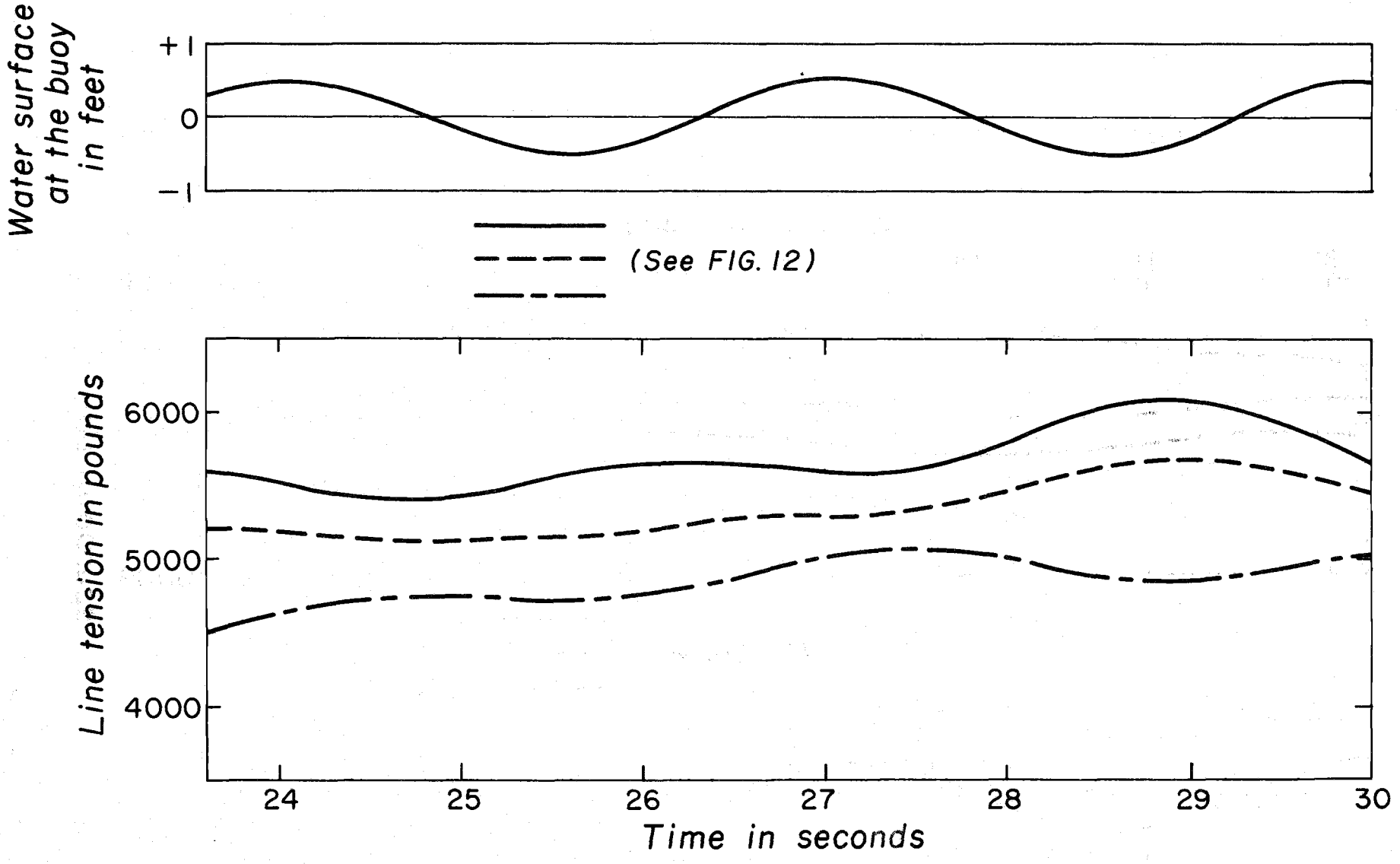

FIG. 22. WAVE LENGTH = 52 FEET. WAVE HEIGHT = 1 FOOT.

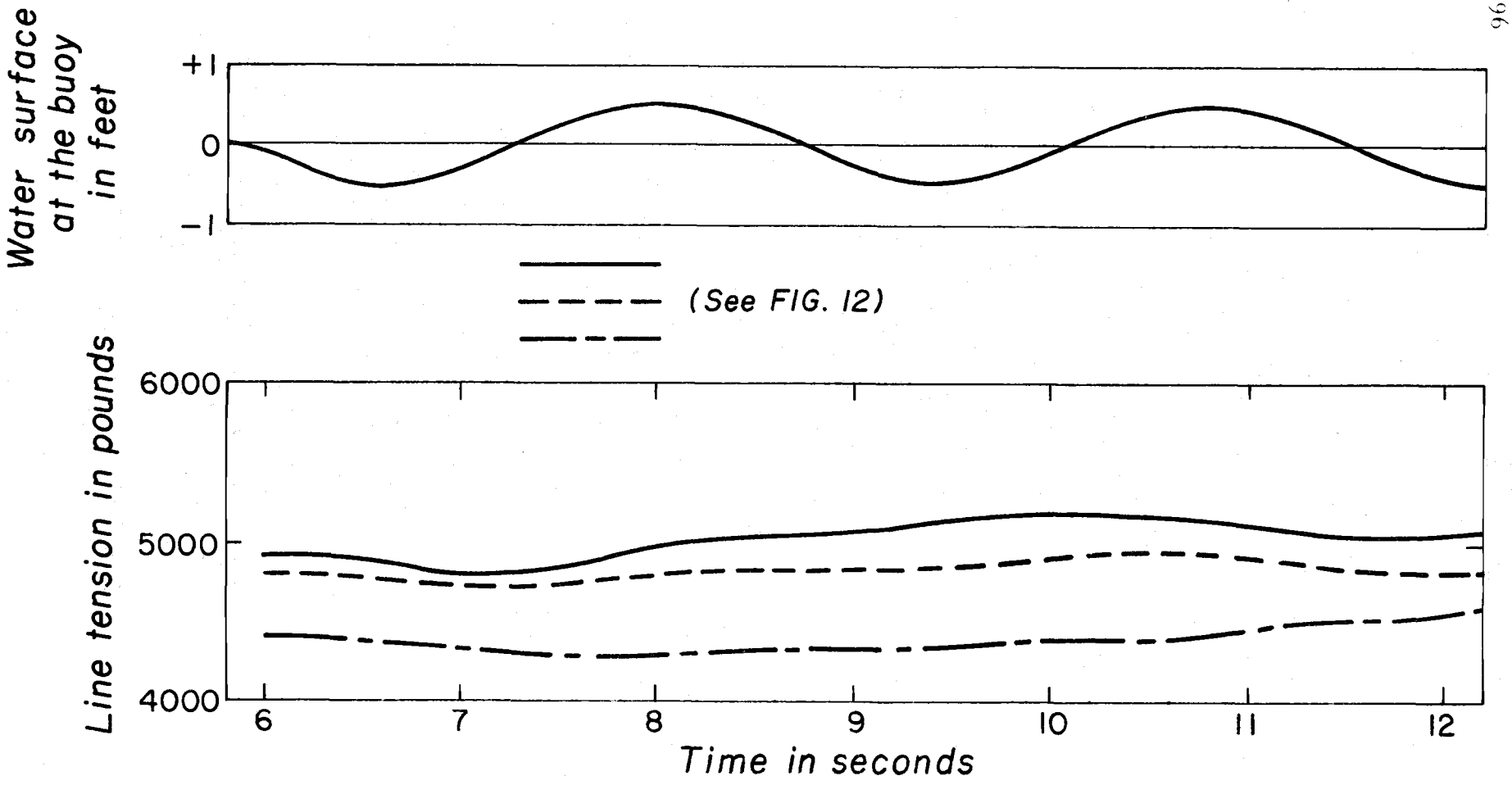

FIG. 23. WAVE LENGTH 42 FEET. WAVE HEIGHT = 1 FOOT.

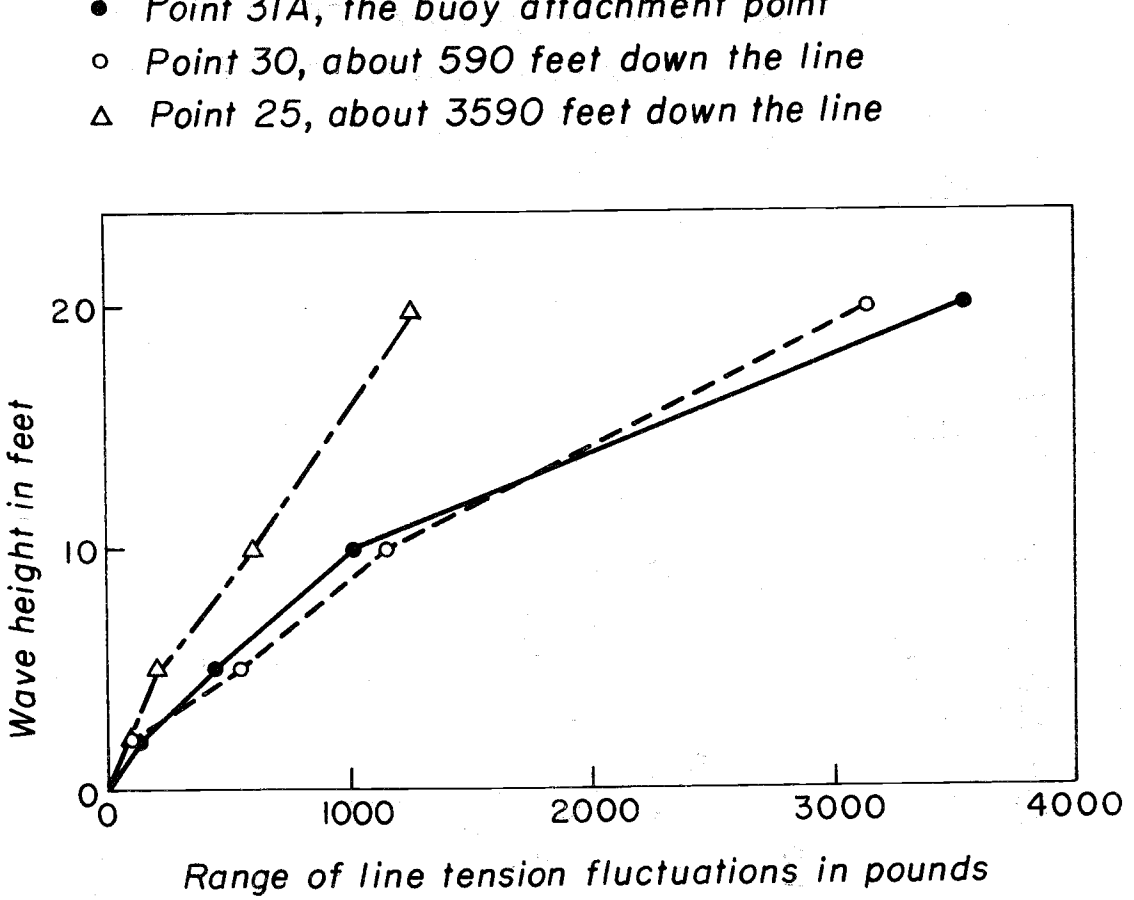

FIG. 24. WAVE HEIGHT VS. LINE TENSION FLUCTUATIONS FOR WAVE LENGTH OF 260 FEET, FREQUENCY OF 0.14 CPS.

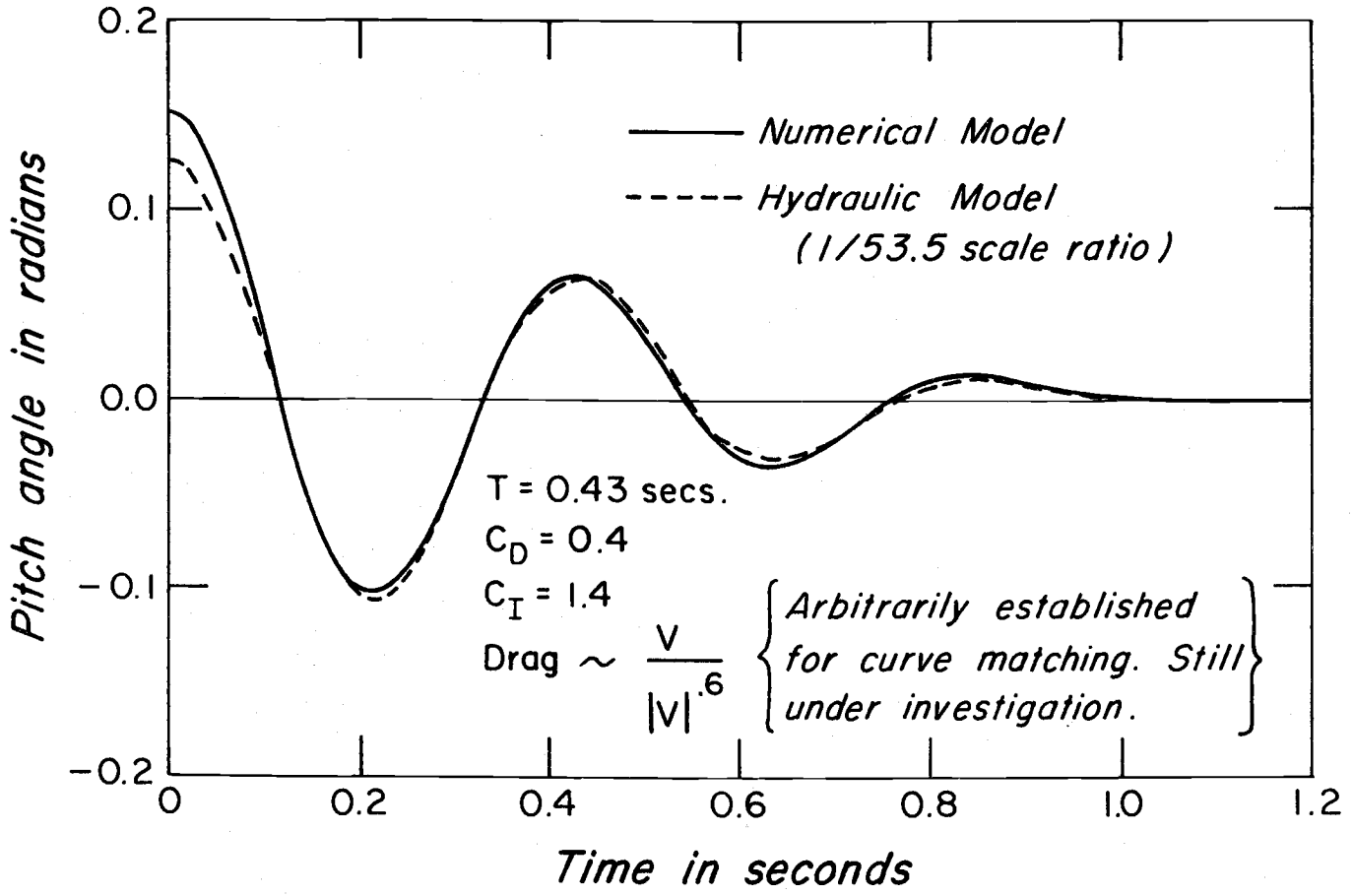

FIG. 27. DECAY OF UNFORCED PITCH MOTION - HYDRAULIC MODEL VS. NUMERICAL MODEL.

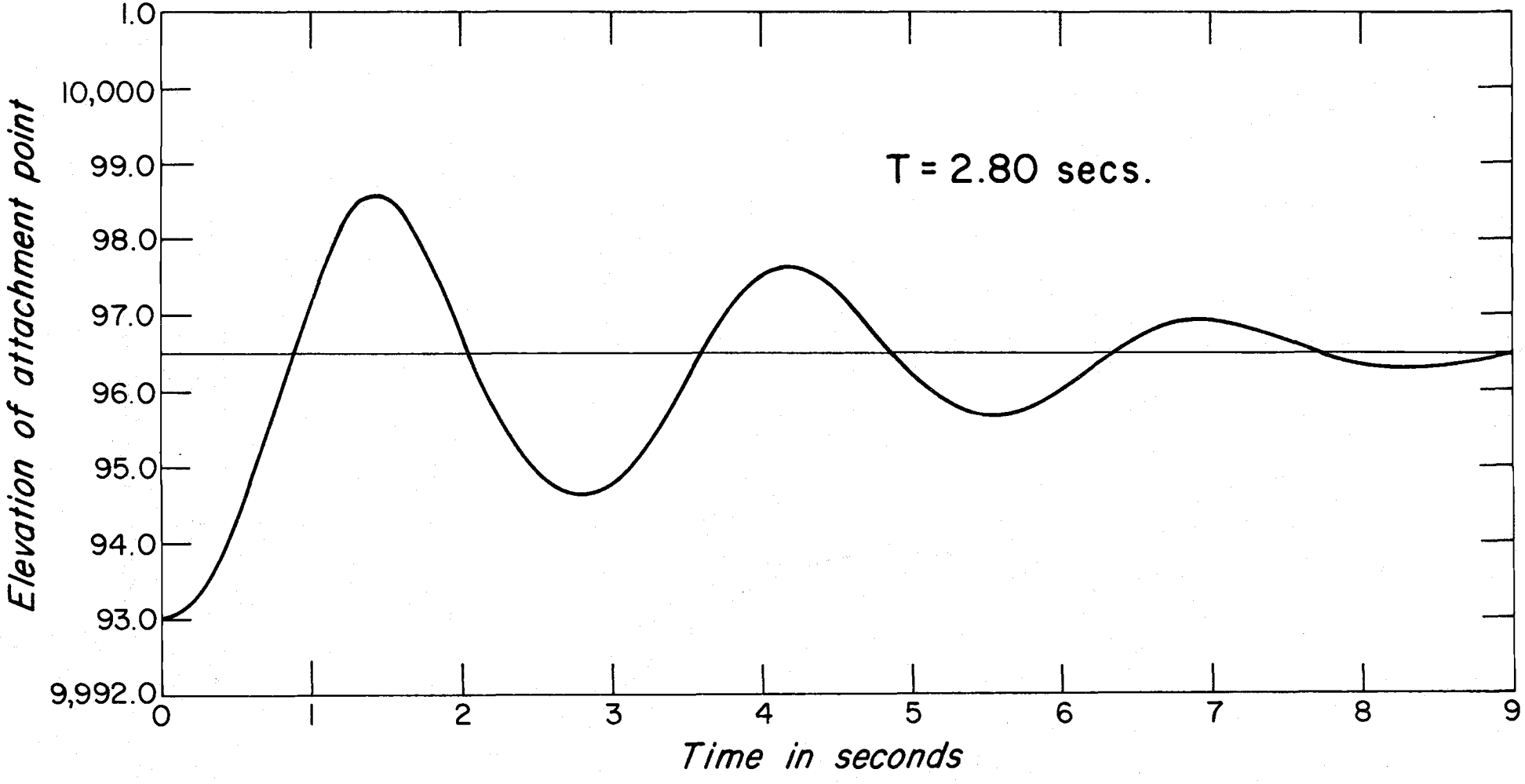

FIG. 28. DECAY OF UNFORCED HEAVE MOTION - NUMERICAL MODEL.

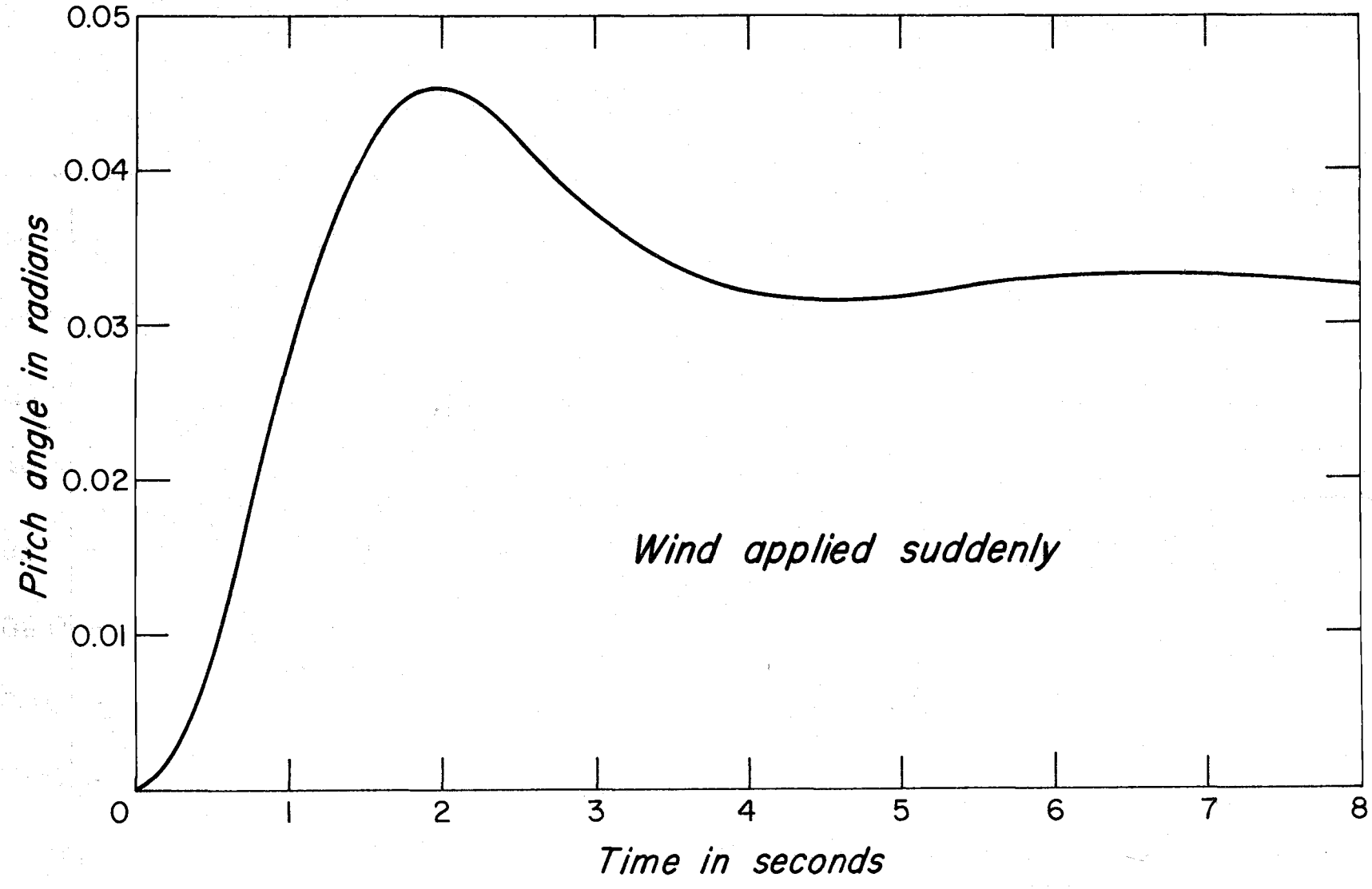

FIG. 29. PITCH OF UNMOORED BUOY WITH 150 KNOT WIND.

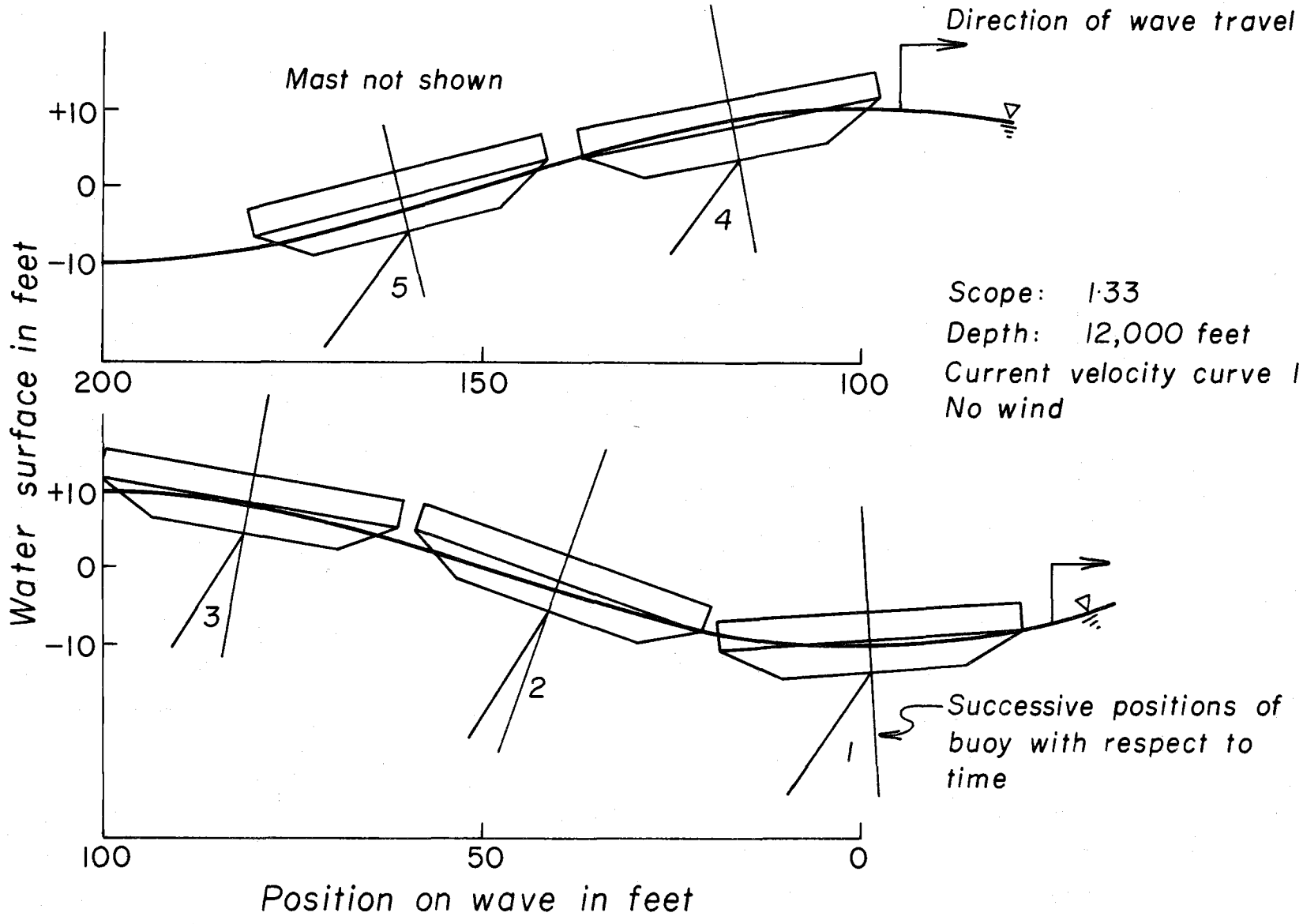

FIG. 30. SUCCESSIVE POSITIONS OF THE BUOY ON A WAVE WITH LENGTH OF 200 FEET AND HEIGHT OF 20 FEET: AS DETERMINED FROM THE NUMERICAL MODEL.

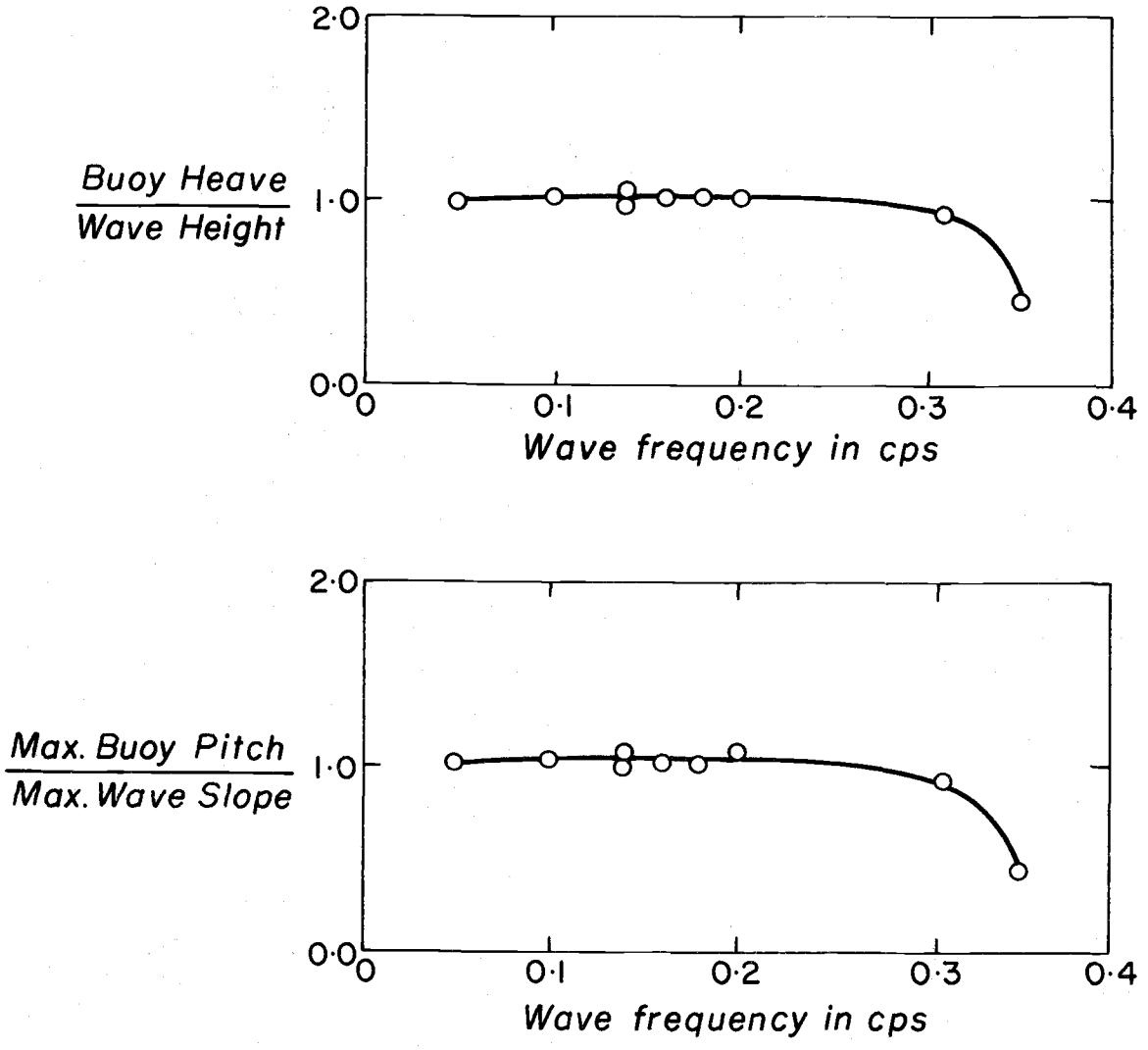

FIG. 31. FREQUENCY RESPONSE CURVES OF THE ONR BUOY WHILE MOORED IN 13,000 FEET OF WATER. FROM THE NUMERICAL MODEL.

REFERENCES

1. Berteaux, H. O., "Statics of Single Point Mooring Systems," Notes from 1968 Summer Course on Ocean Engineering, Joint Program by M. I. T. and W. H. O. I., Chapter 1.4, June - August, 1968.

2. Bishop, R. E. D. and D. C. Johnson, The Mechanics of Vibration, Cambridge at the University Press, 1960.

3. Landueber, L. and M. Macagno, "Added Mass of Two-Dimensional Forms Oscillating in a Free Surface," Journal of Ship Research, Vol. 1, November, 1957.

4. Landueber, L. and M. Macagno, "Added Mass of a Three-Parameter Family of Two-Dimensional Forces Oscillating in a Free Surface," Journal of Ship Research, Vol. 2, No. 4, March 1959.

5. Langer, R. M., "The Catenary in Space - Free Motions of Flexible Lines," J. R. M. Bege Company, Arlington, Mass. or AD 611429, Defense Documentation Center, December 1964.

6. Lister, M., "The Numerical Solution of Hyperbolic Partial Differential Equations," Mathematical Methods for Digital Computers, A. Ralston and H. Wilf eds., John Wiley & Sons, 1960.

7. Morrow, B. W. and W. F. Chang, "Determination of the Optimum Scope of a Moored Buoy," Journal of Ocean Technology, Vol. 2, No. 1, pp. 37-42, 1967.

8. Nath, J. H. and M. P. Felix, "A Numerical Model to Simulate Buoy and Mooring Line Motion in the Ocean Environment," General Dynamics Corporation Report No. AAX68-007, Convair Division of General Dynamics, San Diego, California, August 1968.

9. Nath, J. H. and M. P. Felix, "A Report on a Study of the Hull and Mooring Line Dynamics for the Convair Ocean Data Station Telemetering Buoy," General Dynamics Corporation, Engineering Research Report AN-1108, Convair Division of General Dynamics, San Diego, California, December 1, 1967.

10. Nath, J. H. and D. R. F. Harleman, "Response of a Vertical Cylinder to Random Waves," Proceedings of the National Meeting on Water Resources Engineering, American Society of Civil Engineers, New Orleans, La., February 1969.

11. Nath, J. H. and D. R. F. Harleman, "The Dynamics of Fixed Towers in Deep Water Random Waves," Proceedings of the Conference on Civil Engineering in the Oceans, American Society of Civil Engineers, San Francisco, September 1967.

12. Paquette, R. G. and B. E. Henderson, "The Dynamics of Simple Deep-Sea Buoy Moorings," General Motors Corporation Report to ONR Contract Nonr-4558(00) Project NR. 083-196, TR 65-79, GM Defense Research Laboratories, Santa Barbara, California, November 1965.

13. Plate, E. J. and J. H. Nath, "Modeling of Structures Subjected to Wind Generated Waves," Proceedings of the Conference on Ocean and Coastal Engineering, ASCE and Society of Civil Engineers, London, September 1968.

14. Reid, R. O., "Dynamics of Deep-Sea Mooring Lines," A and M Project 204, Reference 68-11F, Department of Oceanography, Texas A and M University, College Station, Texas, July 1968.

15. Uyeda, S. T., et al., "Two Experimental Moorings of a Large Oceanographic Buoy in 13,000 Feet of Water," Transactions of the Second International Buoy Technology Symposium, Marine Technology Society, September, 1967.

16. Van Santen, G. W., Introduction to a Study of Mechanical Vibration, Philips' Technical Library, Dist. by Elsevier Press, Inc., Houston, Texas, 1953.

17. Walton, T. S. and H. Polachek, "Calculations of Non-Linear Transient Motion of Cables," David Taylor Model Basin, Applied Math. Lab Report No. 1279, July 1959.

18. Wilson, B., "Characteristics of Deep Sea Anchor Cables in Strong Ocean Currents," Texas A and M Technical Report No. 203-3, Dept. of Oceanography and Meteorology, February 1961.

19. Wilson, B. W. and D. H. Garbaccio, "Dynamics of Ship Anchor Lines in Waves and Currents," Proceedings of the Conference on Civil Engineering in the Oceans, American Society of Civil Engineers, San Francisco, September 1967.

NOTATION

The following symbols are first defined where used.

A	An area; Acceleration
C	A coefficient for drag or inertia
$C_{\parallel}$	The celerity of a longitudinal wave in the mooring line
$C_{\perp}$	The celerity of a transverse wave in the mooring line
D	The line diameter
E	Modulus of elasticity of the line
F	The sum of the forces perpendicular to the line; Forces on the buoy
G	The sum of the forces acting longitudinally on the line
H	Wave height, trough to crest
I	Inertia; Moment of inertia
L	A length of the line
M	Total effective mass of the line in the perpendicular direction, $= \mu + C_I \rho$
P	Submerged weight of the line, per foot
S_o	Length of an elastic wave on the line
T	Line tension
T_o	Period of an elastic wave on the line
V	Any vector; Velocity
$\forall$	Volume

NOTATION - Cont'd

f	Forcing equation
g	Acceleration of gravity
h	Water depth
k	Wave number
m	Mass of the line; mass density of water
p	Water pressure
q	Coefficient of viscous damping, internal to the line
s	Distance on the line, measured from the anchor
s.g.	Specific gravity
t	Time
u	Horizontal water particle velocity
$\dot{u}$	Horizontal water particle acceleration
v	Velocity vector of the line at a point
w	Vertical water particle velocity
$\dot{w}$	Vertical water particle acceleration
x	Horizontal coordinate within the domain considered
z	Vertical coordinate within the domain considered
γ	Unit weight of sea water
ε	Unit strain
ζ	Vertical coordinate of a point on the mooring line
η	Water surface as measured from the still surface

NOTATION - Cont'd

θ Angle the mooring line makes with the horizon; pitch angle of the buoy

λ Wave length

μ Mass density of the line per foot

ν Creation or destruction of line mass; kinematic viscosity of sea water

ξ Horizontal coordinate of a point on the mooring line

ρ Mass density of sea water per foot of mooring line; volumetric mass density

σ Unit stress

ϕ Potential function

ω Radian frequency of a wave

$//$ The parallel, or tangential direction along the mooring line. Usually used as a subscript

$\perp$ The perpendicular, or transverse direction along the mooring line. Also usually a subscript.